

CAPITAL UNIVERSITY OF SCIENCE AND
TECHNOLOGY, ISLAMABAD



**Heat Transfer Analysis of MHD
Nanofluids over Stretching/
Shrinking Surfaces with Thermal
Radiation**

by

Irfan Rashid

A thesis submitted in partial fulfillment for the
degree of Doctor of Philosophy

in the

Faculty of Computing

Department of Mathematics

2021

Heat Transfer Analysis of MHD Nanofluids over Stretching/Shrinking Surfaces with Thermal Radiation

By

Irfan Rashid
(DMT 143020)

Dr. Annunziata D' Orazio, Associate Professor
Sapienza University of Rome Via Eudossiana, Italy
(Foreign Evaluator 1)

Dr. Muhammad Irfan Hameed, Professor
University of South Carolina Upstate, USA
(Foreign Evaluator 2)

Dr. Muhammad Sagheer
(Thesis Supervisor)

Dr. Muhammad Sagheer
(Head, Department of Mathematics)

Dr. Muhammad Abdul Qadir
(Dean, Faculty of Computing)

DEPARTMENT OF MATHEMATICS
CAPITAL UNIVERSITY OF SCIENCE AND TECHNOLOGY
ISLAMABAD

2021

Copyright © 2021 by Irfan Rashid

All rights reserved. No part of this thesis may be reproduced, distributed, or transmitted in any form or by any means, including photocopying, recording, or other electronic or mechanical methods, by any information storage and retrieval system without the prior written permission of the author.

Dedicated to
My Family,
My Teachers,
&
My Friends,

*Without whom none of my success
would be possible*



CAPITAL UNIVERSITY OF SCIENCE & TECHNOLOGY ISLAMABAD

Expressway, Kahuta Road, Zone-V, Islamabad
Phone: +92-51-111-555-666 Fax: +92-51-4486705
Email: info@cust.edu.pk Website: <https://www.cust.edu.pk>

CERTIFICATE OF APPROVAL

This is to certify that the research work presented in the thesis, entitled “**Heat Transfer Analysis of MHD Nanofluids over Stretching/ Shrinking Surfaces with Thermal Radiation**” was conducted under the supervision of **Dr. Muhammad Sagheer**. No part of this thesis has been submitted anywhere else for any other degree. This thesis is submitted to the **Department of Mathematics, Capital University of Science and Technology** in partial fulfillment of the requirements for the degree of Doctor in Philosophy in the field of **Mathematics**. The open defence of the thesis was conducted on **June 08, 2021**.

Student Name : Irfan Rashid (DMT143020)

The Examining Committee unanimously agrees to award PhD degree in the mentioned field.

Examination Committee :

(a) External Examiner 1: Dr. Tariq Javed
Professor
IIU, Islamabad

(b) External Examiner 2: Dr. Maryiam Javed,
Associate Professor
IST, Islamabad

(c) Internal Examiner : Dr. Muhammad Afzal
Assistant Professor
CUST, Islamabad

Supervisor Name : Dr. Muhammad Sagheer
Professor
CUST, Islamabad

Name of HoD : Dr. Muhammad Sagheer
Professor
CUST, Islamabad

Name of Dean : Dr. Muhammad Abdul Qadir
Professor
CUST, Islamabad

AUTHOR'S DECLARATION

I, **Irfan Rashid (Registration No. DMT-143020)**, hereby state that my PhD thesis entitled, '**Heat Transfer Analysis of MHD Nanofluids over Stretching/ Shrinking Surfaces with Thermal Radiation**' is my own work and has not been submitted previously by me for taking any degree from Capital University of Science and Technology, Islamabad or anywhere else in the country/ world.

At any time, if my statement is found to be incorrect even after my graduation, the University has the right to withdraw my PhD Degree.



(Irfan Rashid)

Dated: June, 2021

Registration No : DMT-143020

PLAGIARISM UNDERTAKING

I solemnly declare that research work presented in the thesis titled “**Heat Transfer Analysis of MHD Nanofluids over Stretching/ Shrinking Surfaces with Thermal Radiation**” is solely my research work with no significant contribution from any other person. Small contribution/ help wherever taken has been duly acknowledged and that complete thesis has been written by me.

I understand the zero tolerance policy of the HEC and Capital University of Science and Technology towards plagiarism. Therefore, I as an author of the above titled thesis declare that no portion of my thesis has been plagiarized and any material used as reference is properly referred/ cited.

I undertake that if I am found guilty of any formal plagiarism in the above titled thesis even after award of PhD Degree, the University reserves the right to withdraw/ revoke my PhD degree and that HEC and the University have the right to publish my name on the HEC/ University Website on which names of students are placed who submitted plagiarized thesis.



(Irfan Rashid)

Dated: June, 2021

Registration No : DMT-143020

List of Publications

It is certified that following publication(s) have been made out of the research work that has been carried out for this thesis:-

1. **I. Rashid**, M. Sagheer, and S. Hussain, “Entropy formation analysis of MHD boundary layer flow of nanofluid over a porous shrinking wall” *Physica A: Statistical Mechanics and its Applications*, vol. 536, p. 122608, 2019.
2. **I. Rashid**, M. Sagheer, and S. Hussain, “Exact solution of stagnation point flow of MHD $Cu - H_2O$ nanofluid induced by an exponential stretching sheet with thermal conductivity” *Physica Scripta*, vol. 95, p. 025207, 2020.
3. **I. Rashid**, M. Sagheer, and S. Hussain, “Magnetohydrodynamics nanofluid flow of shaped nanoparticles over a porous stretching wall and slip effect” *Numerical Methods for Partial Differential Equations*, pp. 1-24, 2021.
4. **I. Rashid**, R. Ul Haq, and Q. M. Al-Mdallal, “Aligned magnetic field effects on water based metallic nanoparticles over a stretching sheet with PST and thermal radiation effects” *Physica E: Low-dimensional Systems and Nanostructures*, vol. 89, pp. 33-42, 2017.

Irfan Rashid

(DMT 143020)

Acknowledgement

I bow my head before Him, who is worth of all praise, The Creator of the universe and offer countless Darood and Salaams to my beloved Holy Prophet **Hazrat Muhammad (PBUH)**, for Whom this universe has been manifested. I would like to thank **Allah** Almighty, whose benediction bestowed upon me talented teachers, provided me sufficient opportunities and enabled me to undertake and execute this research work.

My heartfelt appreciation goes to my affectionate, sincere, kind and most respected supervisor **Prof. Dr. Muhammad Sagheer** for so patiently bearing, guiding invaluable suggesting and continuously encouraging me with his precious contributions in completing this thesis. I am grateful for the constructive criticism as well as his encouraging comments. If not for his invaluable advice and guidance, this thesis would not have come to realization. He has been very kind in extending all possible help to make this work a success. His ideologies and concepts have a remarkable impact on my research contrivances. He genuinely facilitated me without which my objective would not have been obtained. I have learnt a lot from his abilities. He is my model as a teacher, a researcher, a supervisor and a mentor.

I extend my deepest gratitude to my teachers **Dr. Rashid Ali, Dr. Shafqat Hussain, Dr. Abdul Rehman Kashif, Dr. Muhammad Afzal, Dr. Rizwan-ul-Haq, Dr. Muhammad Awais, Dr. Dur-e-Shehwar** and **Dr. Samina Rashid**. I am grateful to all my teachers. They always guided me sincerely and honestly throughout my course work as well as research work.

It is a little sad that I could not spare time for my old parents; though their long-lasting prayers have opened new horizons for my success. I pay special thanks and tribute to my beloved parents who loved me a lot and have been taking since my childhood and I cannot pay the reward for such kind and care. The completion of my education was not possible without their prayers and supports. I am also thankful to my wife for her support and help in writing this thesis. I am also

mentioning the name of my lovely son (Abd ur Rehman), because I have not given much attention to him due to this thesis.

I pay regards to my caring and loving parents, my sisters, my brothers, whose sincere prayers and best wishes always would make me courageous and daring throughout my life. I am also grateful to friends for their guidance.

Irfan Rashid

(DMT 143020)

Abstract

In this thesis, it has been planned to study the fluid flow and heat transfer analysis of nanofluid over a stretching/shrinking sheet in the presence of different forces, e.g. surface and body forces. The considered nanofluid consist of three types of nanoparticles that are copper, alumina and magnetite, while water and engine oil are used as a base fluid. The flow is provoked due to the stretching/shrinking characteristics of the sheet. During the analysis, the flow is considered to be steady, incompressible, two dimensional, linear and viscous (Newtonian) fluid. The momentum analysis is executed under the influence of numerous body forces such as: normal and inclined magnetic field, stagnation point flow and porous media. Further, the energy analysis is carried out in the presence of Joule heating and thermal radiation phenomena. Moreover, the second law analysis of thermodynamics is also performed in order to compute the entropy generation due to the exchange of heat and momentum. Mathematical modeling is performed to convert the physical system into a set of partial differential equations which are further simplified as a system of nonlinear ordinary differential equations by using suitable similarity variables. The exact solutions are acquired from the transformed non-dimensional momentum and energy equations. The impact of various physical parameters on the velocity profile, temperature profile, local Nusselt number, skin friction coefficient and entropy generation profile are investigated via numeric tables and graphs. Further, flow behavior of the nanofluid is also portrayed via streamlines pattern for many emerging parameters. It is found that the velocity profile of nanofluid decreases with increasing values of solid volume fraction of nanoparticles in copper-water and shows opposite behavior for aluminum oxide-water, magnetite-engine oil and in shrinking case. It is figured out that the temperature profile increases for accelerating values of solid volume fraction of nanoparticles, Hartmann number, angle and velocity slip parameter in case of copper-water, aluminum oxide-water and magnetite-engine oil. The platelets nanoparticles have highest thermal conductivity and cylinders have least in case of magnetite-engine oil. It is noticed that the local Nusselt number is decreased by an increment in radiation parameter in case of stretching sheet.

Contents

Author's Declaration	v
Plagiarism Undertaking	vi
List of Publications	vii
Acknowledgement	viii
Abstract	x
List of Figures	xiii
List of Tables	xvi
Abbreviations	xvii
Symbols	xviii
1 Introduction	1
1.1 Background	1
1.2 Novelty in Thesis	8
1.3 Thesis Outcomes	9
1.4 Thesis Layout	9
2 Preliminaries	11
2.0.1 Applications of Nanofluid	18
3 Impact of Radiation on <i>Cu</i>-Water Based MHD Nanofluid	25
3.1 Mathematical Formulation	25
3.1.1 Continuity and Momentum Analysis	26
3.1.2 Heat Transfer Analysis	29
3.1.3 Second law analysis	32
3.2 Results and Discussion	33
3.3 Conclusion	44

4	Heat Transfer Analysis of Stagnation point flow past an Exponentially Stretching Surface	45
4.1	Mathematical Formulation	45
4.1.1	Continuity and Momentum Analysis	46
4.1.2	Heat Transfer Analysis	49
4.2	Results and Discussion	53
4.3	Conclusion	67
5	Heat Transfer Analysis of Inclined Magnetic Field Induced by a Stretching Surface	68
5.1	Mathematical Formulation	69
5.1.1	Continuity and Momentum Analysis	69
5.1.2	Heat Transfer Analysis	72
5.2	Results and Discussion	75
5.3	Conclusion	86
6	Heat Transfer Analysis of Shaped Nanoparticles.	88
6.1	Mathematical Formulation	88
6.1.1	Continuity and Momentum Analysis	89
6.1.2	Heat Transfer Analysis	92
6.2	Results and Discussion	96
6.3	Conclusion	107
7	Conclusion and Future Work	109
7.0.1	Conclusion	109
7.0.1.1	Shrinking Case:	109
7.0.1.2	Stretching Case:	110
7.0.1.3	Exponentially Stretching Case:	111
7.0.2	Future work	111
	Bibliography	113

List of Figures

2.1	Fluid mechanics flow chart	12
2.2	Viscosity	13
2.3	Uniform and non-uniform flows	15
2.4	Types of fluid	16
2.5	Boundary layer flow	17
2.6	Heat transfer	20
2.7	Entropy	21
3.1	Geometrical view of the physical model	26
3.2	Impact of variation in ϕ on $f'(\eta)$	35
3.3	Impact of variation in S on $f'(\eta)$	35
3.4	Impact of variation in ϕ on $\theta(\eta)$	36
3.5	Impact of variation in N on $f'(\eta)$	36
3.6	Impact of variation in M_2 on local skin friction	36
3.7	Impact of variation in ϕ on local skin friction	37
3.8	Impact of variation in Pr on Nusselt number	37
3.9	Impact of variation in N on Nusselt number	37
3.10	Impact of variation in n on Nusselt number	38
3.11	Impact of variation in Br on the entropy generation profile	38
3.12	Impact of variation in Ω on the entropy generation profile	38
3.13	Impact of variation in Re on the entropy generation profile	39
3.14	Impact of variation in M_2 on the entropy generation profile	39
3.15	Impact of variation in Br on the irreversibility ratio parameter	39
3.16	Impact of variation in Re on the irreversibility ratio parameter	40
3.17	Impact of variation in Ω on the irreversibility ratio parameter	40
3.18	Contour plot for $\phi = 0.0$	40
3.19	Contour plot for $\phi = 0.1$	41
3.20	Contour plot for $\phi = 0.2$	41
3.21	Contour plot for $M_2 = 0.5$	41
3.22	Contour plot for $M_2 = 1.0$	42
3.23	Variation of Pr on Nusselt number	42
3.24	Impact of variation in Pr on Nusselt number	42
4.1	Geometrical view of the physical model	46
4.2	Impact of variation in ϕ on $f'(\eta)$	56
4.3	Impact of variation in ϕ on $f'(\eta)$	56

4.4	Impact of variation in S on $f'(\eta)$	56
4.5	Impact of variation in S on $f'(\eta)$	57
4.6	Impact of variation in A on $f'(\eta)$	57
4.7	Impact of variation in S on $\theta(\eta)$	57
4.8	Impact of variation in Ec on $\theta(\eta)$	58
4.9	Impact of variation in K on $\theta(\eta)$	58
4.10	Impact of variation in Pr on $\theta(\eta)$	58
4.11	Impact of variation in M_2 on $\theta(\eta)$	59
4.12	Impact of variation in ϕ on $\theta(\eta)$	59
4.13	Impact of variation in A on $\theta(\eta)$	59
4.14	Impact of variation in Ec on $-\theta'(0)$	60
4.15	Impact of variation in M_2 on $-\theta'(0)$	60
4.16	Impact of variation in K on $-\theta'(0)$	60
4.17	Impact of variation in S on $-\theta'(0)$	61
4.18	Impact of variation in S on $-f''(0)$	61
4.19	Impact of variation in ϕ on $-f''(0)$	61
4.20	Impact of variation in M_2 on $-f''(0)$	62
4.21	Contour plot for $M_2 = 0.5$	62
4.22	Contour plot for $M_2 = 1.0$	62
4.23	Contour plot for $M_2 = 1.5$	63
4.24	Impact of variation in m on $-\theta'(0)$	63
4.25	Impact of variation in ϕ on $-\theta'(0)$	63
5.1	Geometrical view of the physical model	69
5.2	Impact of variation in ϕ on $f'(\eta)$	77
5.3	Impact of variation in ϕ on $f'(\eta)$	77
5.4	Impact of variation in β and M_2 on $f'(\eta)$	77
5.5	Impact of variation in β and M_2 on $f'(\eta)$	78
5.6	Impact of variation in L on $f'(\eta)$	78
5.7	Impact of variation in L on $f'(\eta)$	78
5.8	Impact of variation in ϕ on $\theta(\eta)$	79
5.9	Impact of variation in ϕ on $\theta(\eta)$	79
5.10	Impact of variation in β on $f'(\eta)$	79
5.11	Impact of variation in β on $f'(\eta)$	80
5.12	Impact of variation in L on $\theta(\eta)$	80
5.13	Impact of variation in L on $\theta(\eta)$	80
5.14	Impact of variation in β on $\theta(\eta)$	81
5.15	Impact of variation in β on $\theta(\eta)$	81
5.16	Impact of variation in N on $\theta(\eta)$	81
5.17	Impact of variation in N on $f'(\eta)$	82
5.18	Impact of variation in β on $-f''(0)$	82
5.19	Impact of variation in M_2 on $-f''(0)$	82
5.20	Impact of variation in M_2 on $-\theta'(0)$	83
5.21	Impact of variation in L on $-\theta'(0)$	83

5.22	Impact of variation in β on $-\theta'(0)$	83
5.23	Impact of variation in N on $-\theta'(0)$	84
5.24	Contour plot for $\phi = 0.0$	84
5.25	Contour plot for $\phi = 0.1$	84
5.26	Contour plot for $\phi = 0.2$	85
5.27	Contour plot for $L = 0.0$	85
5.28	Contour plot for $L = 0.5$	85
5.29	Contour plot for $L = 1.0$	86
6.1	Geometrical view of the physical model	89
6.2	Impact of variation in ϕ on $f'(\eta)$	98
6.3	Impact of variation in L on $f'(\eta)$	98
6.4	Impact of variation in M_2 on $f'(\eta)$	99
6.5	Impact of variation in ϕ on $\theta(\eta)$	99
6.6	Impact of variation in M_2 on $\theta(\eta)$	99
6.7	Impact of variation in L on $\theta(\eta)$	100
6.8	Impact of variation in Pr on $\theta(\eta)$	100
6.9	Impact of variation in N on $\theta(\eta)$	100
6.10	Impact of variation in Ec on $-\theta'(0)$	101
6.11	Impact of variation in M_2 on $-\theta'(0)$	101
6.12	Impact of variation in Pr on $-\theta'(0)$	101
6.13	Impact of variation in N on $-\theta'(0)$	102
6.14	Impact of variation in M_2 on $-f''(0)$	102
6.15	Impact of variation in L on $-f''(0)$	102
6.16	Impact of variation in ϕ on $-f''(0)$	103
6.17	Impact of variation in K on $-f''(0)$	103
6.18	Contour plot for $L = 0.5$	103
6.19	Contour plot for $L = 1.0$	104
6.20	Contour plot for $L = 1.5$	104
6.21	Contour plot for $\phi = 0.0$	104
6.22	Contour plot for $\phi = 0.1$	105
6.23	Contour plot for $\phi = 0.2$	105
6.24	Impact of variation in ϕ on $-\theta'(0)$, bricks	105
6.25	Impact of variation in ϕ on $-\theta'(0)$, cylinders	106
6.26	Impact of variation in ϕ on $-\theta'(0)$, platelets	106
6.27	Impact of variation in thermal conductivity for different shapes	106

List of Tables

3.1	Thermal characteristics of conventional fluid and nanoparticles. . .	43
3.2	Numerical values of $-f''(0)$	43
3.3	Numerical computation of $-\theta''(0)$	43
4.1	Thermal characteristics of conventional fluid and nanoparticles. . .	64
4.2	Numerical values of m (shape factor).	64
4.3	Comparison table.	64
4.4	Numerical values of $f''(0)$	65
4.5	Numerical values of $-\theta'(0)$ for $Ec = 0.3$, $m = 3.7$, $Pr = 6.2$ and $N = 0.5$	65
4.6	Numerical values of $-\theta'(0)$ for $Ec = 0.3$, $m = 4.9$, $Pr = 6.2$ and $N = 0.5$	66
4.7	Numerical values of $-\theta'(0)$ for $Ec = 0.3$, $m = 5.7$, $Pr = 6.2$ and $N = 0.5$	66
5.1	Thermal characteristics of conventional fluid and solid nanoparticles.	75
6.1	Thermal characteristics of conventional fluid and solid nanoparticles.	107
6.2	Numerical values of m (shape factor).	107

Abbreviations

MHD	Magnetohydrodynamics
PST	Prescribed Surface Temperature
SAE	Society of Automotive Engineering
SLM	Successive Linearization Method

Symbols

Al_2O_3	Aluminum oxide
A	Velocity ratio parameter
$\alpha (k/\rho C_p)[m^2/s]$	Thermal diffusivity
$Br \left(\frac{\eta w^2}{\lambda \Delta T} \right)$	Brinkmann number
Be	Bejan number
β	Angle of inclination
$B_0 [kg/m^2 \cdot sec^2]$	Applied magnetic field
cP	Centipoise
CuO	Copper oxide
Cu	Copper
$C_f \left(\frac{\tau_w}{\rho u_w^2} \right)$	Skin friction coefficient
$c_p [J/kgK]$	Specific heat
∇	Differential operator
D/Dt	Material derivative
du/dy	Rate of shear deformation
$Ek [J/K]$	Entropy due to heat transfer
$Em [J/K]$	Entropy due to magnetic field
$Ec \left(\frac{u^2}{(T_w - T_\infty) C_p} \right)$	Eckert number
E_G	Entropy number
Fe_3O_4	Magnetite
f'	Dimensionless velocity
ϕ	Solid volume fraction

$K \left(\frac{u_0 k}{l \nu_f} \right)$	Permeability parameter
k_{nf}	Effective thermal conductivity
k_f [S/m]	Thermal conductivity of base fluid
k^*	Rosseland mean absorption coefficient
$L (l(a/\nu)^{0.5})$	Velocity slip parameter
l [L]	Characteristic length
μ [kg/m.sec]	Dynamic viscosity
$M_2 \left(\frac{2l\sigma B_0^2}{u_0 \rho_f} \right)$	Hartmann number
μ_{nf}	Effective dynamic viscosity
M	Kummer function of the 1st kind
m	Nanoparticles shape factor
μ_f [kg/m.sec]	Dynamic viscosity of base fluid
ν [kg/m.sec]	Kinematics viscosity
n	Power-law index
Nu	Local Nusselt number
$N \left(\frac{4\sigma^* T_\infty^3}{K^* K_f} \right)$	Radiation parameter
$\Omega \left(\frac{T_\infty}{\Delta T} \right)$	Dimensionless temperature difference
P [N/m ²]	Pressure
$Pr \left(\frac{\nu_f}{\alpha_f} \right)$	The Prandtl number
$q_r \left(-\frac{4\sigma^*}{3k^*} \frac{\partial T^4}{\partial y} \right)$ [W/m ²]	Radiative heat flux
ρ [kg/m ³]	Density
ρc_p [kg/m ³]	Heat capacity of the material
$Re_x \left(\frac{x u_w}{\nu} \right)$	Reynolds number
ρ_{nf} [kg/m ³]	Effective density
$(\rho c_p)_{nf}$ [kg/m ³]	Heat capacitance
ρ_f [kg/m ³]	Density of base fluid
$\rho c_p)_f$ [kg/m ³]	Heat capacitance of base fluid
$S \left(-\left(\frac{2l}{u_0 \nu_f} \right)^{1/2} e^{-x/2l} v_w \right)$	Wall mass transfer parameter
S_G [J/K]	Volumetric entropy generation

S_g [J/K]	Characteristic entropy generation
σ [S/m]	Electric conductivity
σ^* [W/m ² K ⁴]	Stefan-Boltzmann constant
$\tau_w \left(\mu_n f \left(\frac{\partial u}{\partial y} \right)_{y=0} \right)$ [N/m ²]	Shear stress at wall
θ	Dimensionless temperature
τ [N/m ²]	Shear stress
T [K]	Temperature
T_0 [K]	Constant reference temperature
T_w [K]	Temperature of the sheet
T_∞ [K]	Free stream temperature
u [m/s]	Velocity component along x -axis
u_0 [m/s]	Reference Velocity
u_e [m/s]	Stagnation point flow Velocity
v_w [m/s]	Wall mass transfer velocity
v [m/s]	Velocity component along y -axis

Chapter 1

Introduction

This chapter provides literature review of the enclosed flow model based on heat transfer characteristics.

1.1 Background

The science of fluid dynamics encompasses the movement of gases and liquids, interaction of fluid with solid and the study of forces related to these phenomena. Fluid dynamics plays an important role in every aspect of our daily life for example from morning bath to evening coffee. It has potential applications in the fields of science, engineering, manufacturing, transportation, environment, medicine, energy etc. Flows are essential for the existence of natural and technical world. Properties of the fluid, forces acting on the fluid particles and boundaries of the flow domain determine the resultant flow pattern. Deformation of fluids occurs continuously under application of shear stress which makes them isotropic substances. There will be no deformation in fluids in the absence of shear stress. Whenever linear relationship takes place between shear stress and shear strain the fluid is called Newtonian fluid, otherwise it is categorized as non-Newtonian fluid. Navier-Stokes equations are the fundamental equations of the fluid that portray

the stream of Newtonian/non-Newtonian fluids [1]. This system of nonlinear differential equations describing the balance of momentum in the fluid flow has no general solution yet.

There is a broad scope of heat transfer applications in numerous industrial processes involving mechanical, electrical and chemical industry. Indeed it is a significant assignment, where heat must be added, subtracted, or transferred from one place to another. Consequently this process requires a bulk amount of vitality to manage the method of fluid heating/cooling and transport of heat. The increment in thermal conductivity plays a significant role in the improvement of heat exchange behavior of fluids. In this regard, many researchers represented several articles on heat transfer analysis. Das et al. [2] analyzed convective heat transfer for metallic nanoparticle based fluid induced by vertical stretching surface with the impact of MHD. Stability analysis for heat transport provoked due to a stretching/shrinking sheet for metallic nanoparticle based fluid along with regression is presented by Jahan et al. [3]. Bilal et al. [4] introduced the fluid flow past a bidirectional nonlinear stretching surface with MHD and thermal conductivity which depends on temperature. Hafeez et al. [5] analyzed the Carreau fluid flow with heat transport analysis. Prasannakumara et al. [6] studied the heat exchange of Sisko nanofluid with MHD and nonlinear radiative flow past a nonlinear stretching surface. Numerical results are obtained for heat transport of water based nanofluid induced by a nonlinearly stretching sheet using thermal and velocity wall slip effect by Ramya et al. [7].

Nowadays, the crisis of energy has become a crucial point of concern for scientists. To meet an expanding need for energy, another rush of creative models is required that can supplant the customary ones. The resources for renewable power source, sunlight oriented, geothermal heat, tides and wind control are contributing in a well manner to meet the energy requirements in both developing and creating economies. Thermal radiation increases an incredible impact for such procedures, where the system is working involving high temperature for example, thermal energy storage, nuclear power plants, solar power technology and heat/cooling chamber at industrial level [8]. Because of the tremendous applications, numerous

researchers have analyzed many radiative fluid flows for different physical aspect [9–13]. Singh and Kumar [14] investigated the impact of micropolar fluid past a stretching sheet with the effect of viscous dissipation and thermal radiation on mixed convection flow. Dzulkipli et al. [15] examined nanofluid with the impact of wall mass transfer, thermal radiation, velocity slip and stagnation impact. Maxwell fluid with thermal radiation past a stretching/shrinking surface along with the effect of stagnation point flow was examined by Ishak et al. [16]. Nasir et al. [17] discussed the influence of velocity slip condition on a stagnation point flow over a stretching/shrinking rigid plate.

Low thermal conductivity is an essential impediment in the improvement of energy proficient heat transfer fluids which are in huge demand in numerous industrial applications, in spite of the fact that a variety of methods is enforced to improve heat exchange. Thermal characteristic of energy transporting fluids is responsible for increasing the heat exchange in a system. Therefore, low thermal conductivity is a limitation of customary fluids, for example, oil, ethylene, water, glycol in enhancement the production and the compactness of several engineering electronic gadgets. Incorporating the percentage of solid nanoparticles into the conventional fluids is an inventive method to increase the thermal conductivity of the conventional fluids. Such types of fluids are known as nanofluids. A nanofluid is a suspension of nanometer sized particles incorporating host fluid which massively improves the heat exchange attributes of the fluid. Many sorts of nanoparticles, for example, metallic, polymeric and non-metallic are incorporated into base fluids to make nanofluids. Choi [18] was the first, who introduced the word nanofluids to mention to the fluids with incorporated small solid particles in 1995. Eastman et al. [19] reported that an increment in thermal conductivity of roughly 60 percent can be acquired for the nanofluid comprising of water and 5 vol percent CuO nanoparticles by few preliminary outcomes. Nanofluids are foremost for the making of nano organized materials for the engineering of complex fluids and also to clean oil from surfaces, because of their outstanding spreading and wetting compartment [20]. Pertinent experimental information [21] has demonstrated that the nanofluids have better heat exchange properties as compared to those of normal

fluids. Such reviews also show that these suspensions are generally stable on account of the nanoparticle size. There are many researchers, whom are working on the heat transfer abilities of nanofluids. Hamad [22] discussed the impact of natural convection flow of MHD nanofluid due to linearly stretching surface. The analysis of flow and heat transport of nanofluid past a time dependent shrinking wall in the presence of suction effect was examined by Azizah et al. [23]. The influence of partial slip condition on the velocity and energy transport of nanofluid due to a stretching surface for PST was studied by Noghrehabadi et al. [24]. Oztop et al. [25] presented the numerical solution of natural convection flow of nanofluid filled in partially heated rectangular compound. The study of nanofluid flow provoked by a stretching/shrinking surface under an external uniform shear flow in the presence of a convective sheet case was investigated by Yacob et al. [26]. The problem of laminar fluid flow past a stretching surface is investigated by Khan and Pop [27]. The impact of magnetohydrodynamics nanofluid induced due to vertical stretching surface in the presence of viscoelastic effect and entropy generation was studied by Ullah et al. [28]. The viscous dissipation influence on Jeffrey nanofluid flow provoked by a stretching surface was discussed by Zokri et al. [29]. Chandrasekar and Kasiviswanathan [30] presented the energy and mass transport impact on nanofluid flow provoked by a stretching sheet. The effect of nanofluid having variable characteristics for unsteady MHD flow in the existence of thermal radiation and chemical reaction was examined by Mjankwi et al. [31]. Vasanthakumari and Pondy [32] have used two types of nanoparticles with water to study the effect of magnetohydrodynamic, suction and energy generation on nanofluid past an inclined stretching surface. The impact of MHD and chemical reaction for time dependent nanofluid provoked because of a stretching surface was investigated by Tarakaramu and Narayan [33]. Suriyakumar and Devi [34] inspected Buongiorno model to analyzed the MHD convective flow in the presence of variable flow effect. Saif et al. [35] discussed the 2nd grade fluid in the existence of stagnation point and variable thickness for nanofluid.

The investigation of fluid flows over a stretching/shrinking surface have excellent consideration, because of its broad usage in engineering applications, for example,

in the drawing of plastic films and to make polymer sheet from a dye by extrusion process, hot rolling, manufacturing of paper, wire rolling, helpful in packing process of bulk products such as shrinking wrapping, extrusion of sheet material and glass fiber [36]. To relate the such type of a stretching/shrinking surface with fluid [37], first time, Sakiadis [38, 39] introduced the idea of continuously stretching sheet. Crane [40] presented the encouraging work to continue the concept of Sakiadis. He investigated the fluid flow for stretching and exponentially surface and derived the closed form analytical solutions. Meanwhile, numerous researcher extended the concept of stretching surface for both linear and exponentially stretching surface for several fluids model [41–45]. Many authors made endeavors to investigate the heat transport induced because of a stretching sheet. Raza [46] discussed the effects of thermal radiation, MHD and wall slip effects past a stretching surface. MHD, thermophoresis and Brownian motion effect for Casson fluid induced by a stretching sheet by Rabbi et al. [47]. Akinobola and Okoya [48] studied the heat source/sink and variable viscosity impact on the non-Newtonian fluid flow with the influence of thermal conductivity over a stretching surface. Lakshmi et al. [49] computed the numerical results for two-phase boundary layer flow with fluid particle suspension with diffusion-thermo and thermo-diffusion effects past a stretching sheet.

Melting heat transport phenomena is illustrated for MHD Casson fluid with the effect of thermal radiation embedded in the porous media was examined by Mabood and Das [50]. Ali et al. computed the exact solution for viscous flow induced by a stretching/shrinking surface soaked in a permeable media [51]. The closed form results was obtained by Rashid et al. [52] for nanofluid using alumina and copper nanoparticles over a shrinking sheet. Haq et al. [53] obtained the closed form solution of nanofluid with aligned magnetic field past a stretching sheet. Impermeable shrinking surface is used to analyze the viscous fluid flow in [54]. Mishra et al. [55] studied the micropolar fluid and heat transfer with heat source past a shrinking surface. Numerical study using successive linearization technique is introduced by Bhatti et al. [56] for fluid flow over a stretching sheet soaked into a permeable media. Bearing a variable temperature of exponential design and Boundary layer

flow are examined by Magyari and Keller [57]. Damseh [58] discussed the magnetohydrodynamics fluid flow over an exponentially stretching sheet. Casson fluid past a nonlinearly stretching surface with the influence of MHD and velocity slip condition are analyzed by Ullah et al. [59]. Srinivasacharya and Jagadeeshwar analyzed a doubly stratified Newtonian fluid with the impact of cross-diffusion [60]. Analytical solution for the Eyring-Powell fluid induced over a nonlinear stretching surface was given by Jafarimoghaddam [61]. Bilal et al. [62] studied the impact of MHD on viscoelastic fluid induced by an exponentially stretching surface and solved numerically. Elbashbeshy et al. [63] discussed unsteady convection flow with magnetohydrodynamics, suction, radiation and internal energy generation/absorption past an exponentially stretching sheet. The energy transport mechanism through the impact of suction provoked by an exponentially stretching sheet was given by Elbashbeshy [64].

The study of magnetohydrodynamic flow has gained the attention of modern era scientist on account of its extensive industrial and engineering application. Such applications incorporate the design of cooling frameworks by including liquid metals, MHD generators, petroleum industries, accelerators, nuclear reactors, energy stockpiling, pumps, gas turbines and flow meters. Having such idea as a top priority the scientists and mathematician investigated the behavior of MHD flows in different physical angles. Sheikholeslami et al. [65] scrutinized the properties of magnetohydrodynamic nanofluid. The MHD flow of nanofluid provoked by a stretching surface was examined by Rashidi et al. [66]. Zeeshan et al. [67] inspected the results of magnetic dipole on ferrofluid. Hayat et al. [68] inspected the consequences of Jeffrey fluid model with convective boundaries. Jat et al. [69] scrutinized magnetohydrodynamic viscous fluid past a nonlinearly stretching surface implanted into a permeable media. The author witnessed that the velocity diminishes effectively while expanding the porosity parameter, which consequently expanding the local skin friction. The stagnation point and energy transport of magnetohydrodynamic nanofluid was discussed by Ibrahim and Makinde [70]. Das et al. [71] analyzed the effect of energy exchange into magneto-nanofluid embedded in a porous media in a revolving system. The numerical results of MHD

viscoelastic fluid flow together with chemical reaction due to a stretching surface was analyzed by Ramesh et al. [72]. Mahanthesh et al. [73] illustrated the exponential space dependent energy and thermal source for MHD flow of nanofluid using carbon nano tubes over a stretchable rotating sheet. Alarifi et al. [74] explored the heat transport over a vertical stretching sheet with energy sink/source impact for MHD flow. Kunnegowda et al. [75] discussed the homotopy perturbation technique to calculate the results of Casson fluid model in a micro channel with induced magnetic field. Oudina and Bessah [76] discussed the stability for MHD in cylindrical configuration.

Under the umbrella of thermodynamics, entropy defines, the measure of disorder of a system and its surroundings or a measure of achievement towards the thermodynamics equilibrium. As, we are dealing with the thermodynamics system, therefore the entropy generation analysis is very pertinent in this regard. Because entropy computes the efficiency of any engendered system containing thermofluids. The entropy of any system is determined from the second law of thermodynamics. From recent studies, it is analyzed that the 2nd law of thermodynamic is a fruitful way for evaluating entropy.

The entropy generation is related to a large number of important applications, for example, cooling of present day electronic system, geothermal power system and solar based power system. In the beginning, Bejan [77] recommended the idea of entropy generation in fluid flow and energy transport systems. Afridi et al. [78] described the chaos analysis in stagnation point flow with MHD, ohmic heating and fluid friction effect. Entropy analysis in MHD nanofluid due to a heated stretching surface with viscous dissipation and radiation are analyzed by Sithole [79]. Bhatti et al. [80] investigated the entropy generation in nanofluid over a porous stretching sheet for practical tool of optimization by SLM. Noghrehabadi et al. [81] analyzed the entropy generation in nanofluid with the impact of partial slip and energy generation or absorption past a stretching surface. Numerical results for entropy formation in Carreau nanofluid embedded in a shrinking surface with the impact of radiation and MHD are presented by Bhatti et al. [56]. Aziz et al. [82] examined

the entropy generation into Casson fluid along with the hall impact and MHD over a stretchable surface.

The analysis of incompressible fluid and energy transport because of a porous stretching/shrinking surface is of great influence as it locates several practical application in numerous field. More particularly, in mechanical and chemical industries such as geophysical systems, metallurgy, food storage and processing, fibrous insulation, electrochemistry and microelectronics cooling [83].

In the literature, several researchers have analyzed the porous medium in their articles. Barik et al. [84] analyzed the impact of MHD flow induced by a stretching surface soaked in permeable media. Etwire et al. [85] analyzed an impact of thermal conductivity and variable suction over a stretching surface soaked in porous medium for oil based nanofluid. Boundary layer flow analysis over a nonlinearly stretching sheet with the effects of partial slip is examined by Mukhopadhyay [86]. Singh et al. [87] examined the MHD flow with porosity and radiation parameters with porous medium. Nadeem et al. [42] discussed the Casson fluid provoked by a stretching surface with the impact of MHD on three dimensional flow. Effects of Newtonian heating on Casson nanofluid using sodium alginate particles using MHD effect was examined by Khan et al. [88].

1.2 Novelty in Thesis

The primary focus of this thesis is to enhance the thermal abilities of the conventional base fluid by adding small volume of nanoparticles, namely copper, alumina, and magnetite. Chapter 3 highlights the importance of $Cu - H_2O$ nanofluid under the combine effect of magnetic field and linear thermal radiation. Next chapter portrays the importance of shaped nanoparticles under the impact of Ohmic heating in a porous medium. Chapter 5 comprehensively gives the comparison of Cu and Al_2O_3 nanoparticles along with the impact of inclined magnetic field. Chapter 6 analyzes the heat transfer analysis of magnetic nanoparticles over a porous medium.

1.3 Thesis Outcomes

Highlights of the considered analysis are following:

- It is found that the velocity profile of nanofluid decreases with increasing values of ϕ in *Cu*-water and shows opposite behavior for *Al₂O₃*-water, *Fe₃O₄*-engine oil and in shrinking case.
- It is observed that the velocity profile is a decreasing function of L and M_2 in *Cu*-water, *Al₂O₃*-water and *Fe₃O₄*-engine oil.
- It is figured out that the temperature profile increases for accelerating values of ϕ , M_2 , β and L in case of *Cu*-water, *Al₂O₃*-water and *Fe₃O₄*-engine oil.
- The platelets nanoparticles have highest thermal conductivity and cylinders have least in case of *Fe₃O₄*-engine oil.
- It is found that the local skin friction coefficient is increased by enhancing the value of M_2 .
- It is noticed that the local Nusselt number is decreased by an increment in N in case of stretching sheet.

1.4 Thesis Layout

Chapter 1:

This chapter provides literature review related to the fluid models used in this PhD research work.

Chapter 2:

Chapter 2 comprehensively explains the basic preliminaries and dimensionless parameters used in this thesis.

Chapter 3:

In chapter 3, the closed form solution of *Cu*-water based nanofluid with magnetic and radiation effects are examined.

Chapter 4:

In Chapter 4, the impact of Joule heating on a stagnation point flow over an exponentially stretching surface in the presence of porous wall are discussed.

Chapter 5:

This chapter analyzes the simultaneous effects of inclined magnetic field and prescribed surface temperature (PST) on nanofluid flow provoked by a stretching surface

Chapter 6:

Chapter 6 investigates the magnetohydrodynamics flow of magnetite-engine oil based nanofluid with impact of non-identical shaped nanoparticles subject to the porous medium, velocity slip, thermal radiation and Joule heating effects.

Chapter 7:

Chapter 7 summarizes the research work of Ph.D. and proposes possible directions for future research.

Chapter 2

Preliminaries

This chapter contains some basic definitions of fluid flow, fundamental concepts and ideas of fluid and dimensionless numbers regarding the presented work.

Definition 2.1. (Fluid) [89]

“A substance in the liquid or gas phase is referred to as a fluid. Distinction between a solid and a fluid is made on the basis of the substances ability to resist an applied shear (or tangential) stress that tends to change its shape. A solid can resist an applied shear stress by deforming, whereas a fluid deforms continuously under the influence of shear stress, no matter how small. In solids, stress is proportional to strain but in fluids stress is proportional to strain rate. When a constant shear force is applied, a solid eventually stops deforming at some fixed strain angle, whereas a fluid never stops deforming and approaches a certain rate of strain.”

Definition 2.2. (Stress)[89]

“Stress is defined as force per unit area and is determined by dividing the force by the area upon which it acts. The normal component of a force acting on a surface per unit area is called the normal stress, and the tangential component of the force acting on a surface per unit area is called shear stress. In a fluid at rest, the normal stress is called pressure.”

Definition 2.3. (Mechanics)[89]

“Mechanics is the oldest physical science that deals with both stationary and

moving bodies under the influence of forces. The branch of mechanics that deals with bodies at rest is called statics, while the branch that deals with bodies in motion is called dynamics. The subcategory fluid mechanics is defined as the science that deals with the behavior of fluids at rest (fluid statics) or in motion (fluid dynamics), and the interaction of fluids with solids or other fluids at the boundaries. Fluid mechanics is also referred to as fluid dynamics by considering fluids at rest as a special case of motion with zero velocity (see Figure 2.1).”

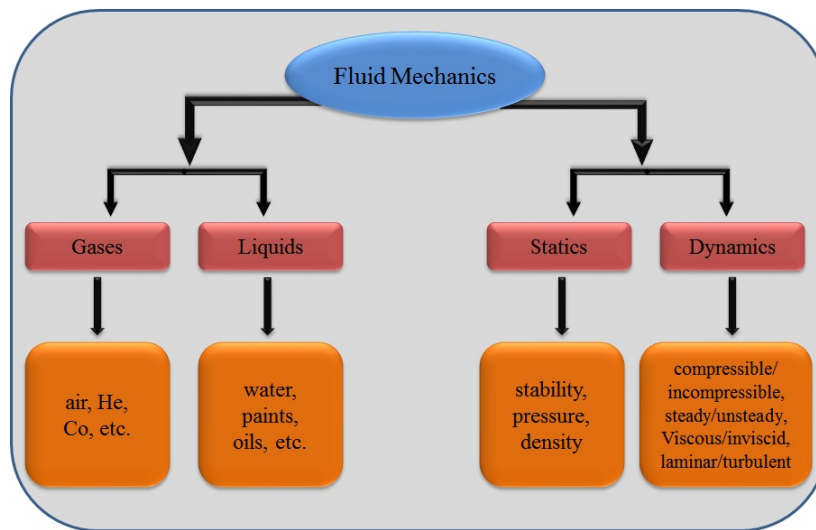


FIGURE 2.1: Fluid mechanics flow chart

Definition 2.4. (Viscosity) [89], [90], [91]

“Viscosity is a quantitative measure of a fluids resistance to flow. More specifically, it determines the fluid strain rate that is generated by a given applied shear stress. We can easily move through air, which has very low viscosity. Movement is more difficult in water, which has 50 times higher viscosity then air. Still more resistance is found in Society of Automotive Engineers (SAE) 30 oil, which is 300 times more viscous than water. Fluids may have a vast range of viscosities. The viscosity of liquids decreases with the increase of temperature and while the viscosity of gases increases with the increase of temperature. Viscosity is caused by cohesive forces between the molecules in liquids and by molecular collisions in gases. There is no fluid with zero viscosity, and thus all fluid flows involve viscous effects to some degree (see Figure 2.2). Flows in which the frictional effects are significant are called viscous flows.

Mathematically:

$$\mu = \frac{\tau}{\left(\frac{du}{dy}\right)}, \quad (2.1)$$

where μ is called the constant of proportionality, and is known as the coefficient of dynamic viscosity or only viscosity, τ is the shear stress and du/dy represents the velocity gradient or rate of shear deformation. Thus viscosity is also defined as shear stress required to produce unit area of strain. The unit of viscosity is centipoise (cP). The viscosity of water at 20°C is 1 centipoise.”

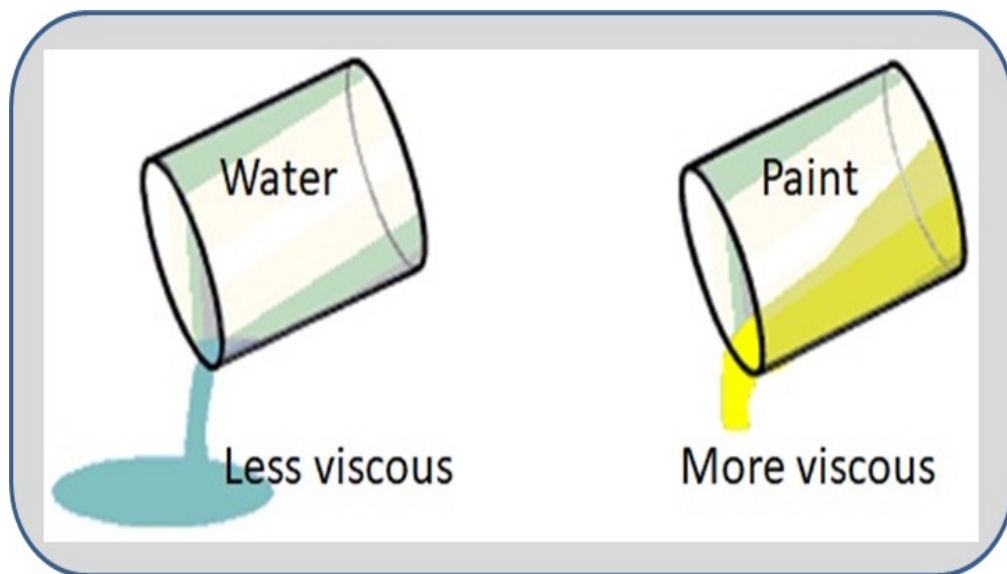


FIGURE 2.2: Viscosity

Definition 2.5. (Kinematics viscosity)[91]

“It is defined as the ratio between dynamic viscosity and density of fluid. It is denoted by Greek letter ν . Thus, mathematically,

$$\nu = \frac{\text{viscosity}}{\text{density}}, \quad (2.2)$$

$$= \frac{\mu}{\rho}, \quad (2.3)$$

the SI unit of kinematics viscosity is $m^2/sec.$ ”

Definition 2.6. (Newton’s law of viscosity)[91]

“It states that shear stresses (τ) on a fluid element layer is directly proportional to the rate shear strain. The constant of proportionality is called the coefficient

of viscosity. Mathematically, it is expressed as given by the equation:

$$\tau = \mu \frac{du}{dy}, \quad (2.4)$$

in the above equation, μ is the viscosity and $\frac{du}{dy}$ is the deformation rate. Fluids which obey the above relation are known as Newtonian fluids and the fluids which do not obey the above relations are called non-Newtonian fluids”.

Definition 2.7. (Thermodynamic properties of a fluid)[90]

“The three most common thermodynamic properties of a fluid are:

- Pressure

The pressure (P) is the most dynamic variable in fluid mechanics. Pressure is defined as a normal force exerted by a fluid per unit area. We speak of pressure only when we deal with a gas or a liquid. The counterpart of pressure in solids is normal stress. Differences or gradients in pressure often drive a fluid flow, especially in ducts.

- Temperature [92]

Temperature (T) is a measure of the kinetic energies of the particles such as the molecules or atoms of a substance. In a liquid or gas, the kinetic energy of the molecules is due to their random translational motion as well as their vibrational and rotational motions. The higher the temperature, the faster the molecules move and the higher the number of such collisions, and the better the heat transfer.

- Density

The density of a fluid, denoted by ρ , is its mass per unit volume. Density is highly variable in gases and increases nearly proportionally to the pressure level. The most liquid flows are treated analytically as nearly incompressible.”

Definition 2.8. (Uniform and non-uniform flows)[90]

“The flow is said to be uniform if the magnitude and direction of flow velocity are

the same at every point and flow is said to be non-uniform if the velocity is not the same at each point of the flow, at a given instant (see Figure 2.3).”

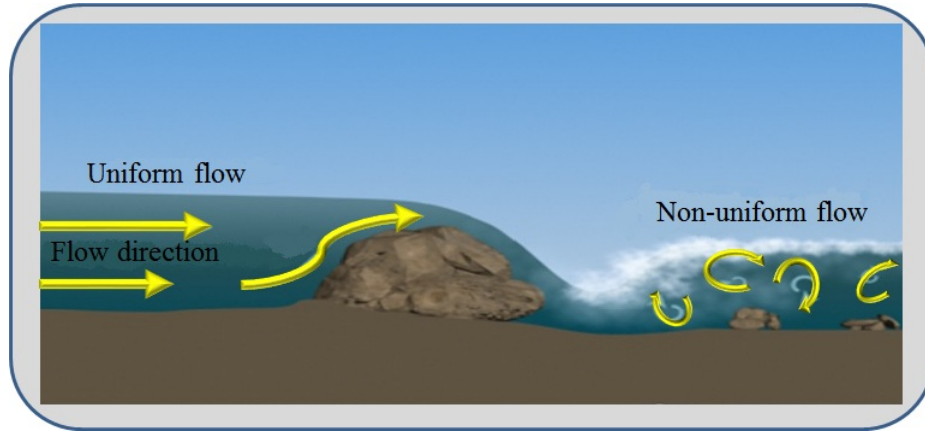


FIGURE 2.3: Uniform and non-uniform flows

Definition 2.9. (Steady and unsteady flows)[90]

“A flow whose flow state expressed by velocity, pressure, density, etc, at any position, does not change with time, is called a steady flow. A flow whose flow state does change with time is called an unsteady flow.”

Definition 2.10. (Compressible and incompressible flows)[90]

“Flow in which variations in density are negligible is termed as incompressible other wise it is called compressible. The most common example of compressible flow is the flow of gases, while the flow of liquids may frequently be treated as incompressible. Mathematically,

$$\frac{D\rho}{Dt} = 0, \quad (2.5)$$

where ρ denotes the fluid density and $\frac{D}{Dt}$ is the material derivative given by

$$\frac{D}{Dt} = \frac{\partial}{\partial t} + V \cdot \nabla, \quad (2.6)$$

in above equation, V denotes the velocity of the flow and ∇ is the differential operator. In Cartesian coordinate system, ∇ is given as:

$$\nabla = \frac{\partial}{\partial x} \hat{i} + \frac{\partial}{\partial y} \hat{j} + \frac{\partial}{\partial z} \hat{k}. \quad (2.7)$$

Definition 2.11. (Types of fluid)[91]

“The fluids may be classified into following five types (see Figure 2.4):

- Ideal Fluid

A fluid which is incompressible and having no viscosity, is known as ideal fluid. Ideal fluid is only an imaginary fluid as all the fluids, which exist, have some viscosity.

- Real fluid

A fluid, which possesses viscosity, is known as real fluid. All the fluids, in actual practice, are real fluid.

- Newtonian fluid

A real fluid, in which the shear stress is directly proportional to rate of shear strain (or velocity gradient), is known as Newtonian fluid.

- Non-Newtonian fluid

A real fluid, in which the shear stress is not directly proportional to rate of shear strain (or velocity gradient), known as non-Newtonian fluid.

- Ideal plastic fluid

A fluid, in which the shear stress is more than the yield value and shear stress is proportional to the rate of shear strain (velocity gradient), is known as ideal plastic fluid (also called Bingham plastic fluid).”

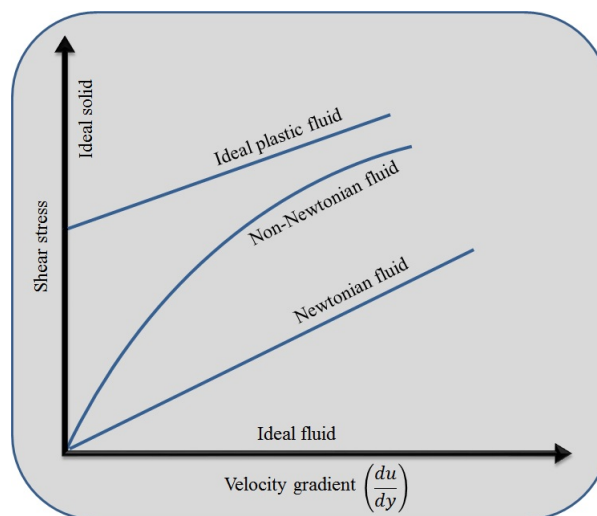


FIGURE 2.4: Types of fluid

Definition 2.12. (Boundary layer flow)[90]

“The concept of boundary layer was first introduced by Ludwig Prandtl, a German aerodynamicist, in 1904. Prandtl introduced the basic idea of the boundary layer in the motion of a fluid over a surface. Boundary layer is a flow layer of fluid close to the solid region of the wall in contact, where the viscosity effects are significant (see Figure 2.5). The flow in this layer is usually laminar. The boundary layer thickness is the measure of the distance apart from the surface. There are two types of boundary layers:

- Hydrodynamic (velocity) boundary layer

A region of a fluid flow, where the transition from zero velocity at the solid surface to the free stream velocity at some extent far from the surface in the direction normal to the flow takes place in a very thin layer, is known as the hydrodynamic boundary layer.

- Thermal boundary layer

The heat transfer exchange surface and the free stream a liquid or a gaseous agent for heat transfer. From wall to free stream we come across the change of temperature of heat transfer agent. It increases from wall to the main stream. The surface temperature is assumed to be equal to the temperature of the fluid layer closed to the wall inside the boundary and this temperature is equal to the temperature of the bulk at some point in the fluid.”

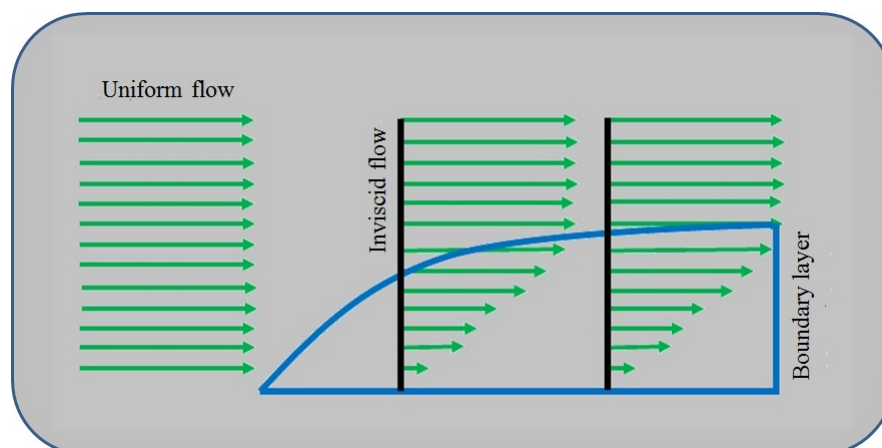


FIGURE 2.5: Boundary layer flow

Definition 2.13. (Nanofluid)[93]

“A nanofluid is the mixture of nanoparticles suspended in the base fluid. It is an advanced heat transfer fluid that possesses superior heat transfer properties. Recent developments in nanotechnology bring out fluids that possess better thermal properties than conventional fluids. The inherent properties like the larger relative surface area of nanoparticles and superior thermal conductivity makes them a choice for thermal engineers over conventional fluid. A suspended nanoparticle significantly improves heat transfer capabilities and stability of the suspension. Nanofluids possess wide range of possibilities as it can enhance heat transfer performance in comparison to that of pure liquids and hence can be considered as next generation heat transfer fluids. The most recent popular nanoparticles which are used to produce nanofluids are aluminum oxide (Al_2O_3), copper oxide (CuO), copper (Cu). While the most common base fluids which are being employed for producing nanofluids are water, oil, decene, acetone and ethylene glycol.”

2.0.1 Applications of Nanofluid

Nanofluids can be used as engineering applications because of their enhanced thermal transfer and energy ability in a mixture of thermal system.

The following segment gives a direction of several fields of nanofluid applications according to the existing literatures [94]:

- Solar devices
- Nanofluid in fuel
- Nanofluid as coolant
- Applications in automotive
- Industrial cooling applications
- Applications of nanofluid in domestic refrigerator

Definition 2.14. (Magnetohydrodynamics)[95]

“Magnetohydrodynamics describe the study of motion of electrically conducting fluid (e.g. liquid metals and Plasmas) in the presence of a magnetic field. The key hypothesis behind magnetohydrodynamic is that magnetic fields can generate current in a moving conductive fluid, which sequentially produce a force on the fluid and also alter the magnetic field itself. The basic equations of magnetohydrodynamics have been proposed by Hannes Alfvén, who realized the importance of the electric currents carried by a plasma and the magnetic field they generate. Alfvén combined the equations of fluid dynamics with Faradays and Amperes laws of electrodynamics, thus obtaining a novel mathematical theory, which helped understanding space plasmas in earth and planetary magnetospheres, as well as the physics of the sun, solar wind, and stellar atmospheres.”

Definition 2.15. (Joule heating)[90]

“The heat which is produced due to flow of current through conductor is called Joule heating, also known as Ohmic heating.”

Definition 2.16. (Heat transfer)[92]

“Heat is the form of energy that can be transferred from one system to another as a result of temperature difference. The basic requirement for heat transfer is the presence of a temperature difference (see Figure 2.7). There can be no net heat transfer between two mediums that are at the same temperature. The temperature difference is the driving force for heat transfer, just as the voltage difference is the driving force for electric current flow and pressure difference is the driving force for fluid flow. The rate of heat transfer in a certain direction depends on the magnitude of the temperature gradient (the temperature difference per unit length or the rate of change of temperature) in that direction. The larger the temperature gradient, the higher the rate of heat transfer.”

Definition 2.17. (The first law of thermodynamics)[92]

“The first law of thermodynamics, also known as the conservation of energy principle, states that energy can neither be created nor destroyed; it can only change forms. The conservation of energy principle (or the energy balance) for any system undergoing any process may be expressed as follows: The net change (increase or



FIGURE 2.6: Heat transfer

decrease) in the total energy of the system during a process is equal to the difference between the total energy entering and the total energy leaving the system during that process.”

Definition 2.18. (Thermal conductivity)[92]

“The rate of heat transfer through a unit thickness of the material per unit area per unit temperature difference. The thermal conductivity of a material is a measure of the ability of the material to conduct heat. A high value for thermal conductivity indicates that the material is a good heat conductor, and a low value indicates that the material is a poor heat conductor or insulator.”

Definition 2.19. (Specific heat)[92]

“The product ρc_p , which is frequently encountered in heat transfer analysis, is called the heat capacity of a material. Both the specific heat (c_p) and the heat capacity (ρc_p) represent the heat storage capability of a material. But c_p expresses it per unit mass, whereas ρc_p expresses it per unit volume.”

Definition 2.20. (Entropy)[96]

“Entropy is a Greek terms means change. It is a measure of disorder or randomness of molecular motion of the system (see Figure 2.7). It is a thermal property of a system, which remains constant as long as no heat enters or leaves the system. Entropy of a system increases if heat flows into the system at constant temperature and decreases, if leaves the system at constant temperature. Noted that such kind of energy loss can not be regained so system and surrounding cannot come to its

initial state without doing any extra work on it be. Therefore, entropy is called the measure of irreversibilities. In nature there is no reversible process due to friction and heat transfer. So every thermodynamic process is irreversible.”

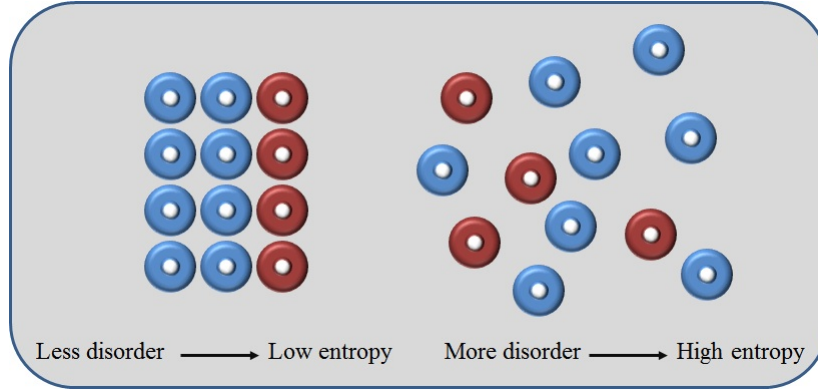


FIGURE 2.7: Entropy

Definition 2.21. (Dimensionless physical quantities)[97]

“In physics and mathematics, dimensionless physical quantities have been widely used. Some of these quantities, which are useful in this thesis are:

- Reynolds number

$$Re = \frac{wL\rho}{\eta}, \quad (2.8)$$

$$= \frac{wL^2}{\nu}, \quad (2.9)$$

$$Re_{rot} = \frac{\omega L^2}{\nu}, \quad (2.10)$$

$$= \frac{\rho n L^2}{\eta}, \quad (2.11)$$

$w (ms^{-1})$ - flow velocity; $L (m)$ - characteristic length; ρ - density; $\eta (Pas)$ - dynamic viscosity; $\nu (m^2s^{-1})$ - kinematic viscosity; $\omega (Hz)$ - angular frequency; $n (s^{-1})$ - rotational frequency.

This number expresses the ratio of the fluid inertia force to that of molecular friction (viscosity). It characterizes the hydrodynamic conditions for viscous fluid flow. It determines the character of the flow (laminar, turbulent and transient flows).

- Eckert number

$$Ec = \frac{w_\infty^2}{c_p \Delta T} = 2R_f, \quad (2.12)$$

$$Ec = (k - 1)M_\infty^2 \frac{T_\infty}{\Delta T} = 2 \frac{\Delta T_{ad}}{\Delta T} = 2 \frac{T_{ad,\infty} - T_\infty}{T_\infty - T}, \quad (2.13)$$

w_∞ (ms^{-1}) - fluid flow velocity far from body; c_p ($Jkg^{-1}K^{-1}$) - specific heat capacity of fluid; ΔT (K) - temperature difference; T , T_{ad} , T_∞ (K) - static, adiabatic and far from body temperatures; k - specific heat ratio; R_f - temperature recovery factor.

It expresses the ratio of kinetic energy to a thermal energy change.

- Bejan number

$$Be = \frac{S_1}{S_1 + S_2}, \quad (2.14)$$

S_1 (JK^{-1}) - entropy generation contribution by heat transfer; S_2 (JK^{-1}) - entropy generation contribution by fluid friction.

It expresses the ratio of heat transfer unreturnability to the total unreturnability caused by heat transfer and fluid friction.

- Entropy generation number

$$Ns = \frac{L^2 T_0 E_0}{\lambda (T_w - T_0)^2}, \quad (2.15)$$

$$E_G = \frac{\lambda}{T_0^2} [(\Delta_x T)^2 + (\Delta_y T)^2], \quad (2.16)$$

L (m) - characteristic length (wall thickness); T_0 (K) - input fluid temperature; E_G ($Wm^{-3}K^{-1}$) - entropy change (volume density of heat flux) by temperature change $1 K$; λ ($Wm^{-1}K^{-1}$) - wall thermal conductivity; T_w (K) -

wall temperature; η ($Pa\ s$) - dynamic viscosity of the fluid; $\Delta_x T, \Delta_y T$ (Km^{-1}) - temperature gradient in the direction of x and y axis; $\Delta_y u$ (s^{-1}) - velocity gradient in the direction of y axis.

It characterizes the fluid entropy change in laminar streaming of viscous incompressible fluid through an inclined canal with isothermic walls. It was determined from the analysis of the second law of thermodynamics.

- Hartmann number

$$Ha = \mu H L \sqrt{\frac{\gamma}{\eta}} = B L \sqrt{\frac{\gamma}{\eta}}, \quad (2.17)$$

$$= \sqrt{St Re} = \sqrt{Re Eu_m Re_m}, \quad (2.18)$$

μ (Hm^{-1}) - permeability; H (Am^{-1}) - magnetic field intensity; L (m) - characteristic length; γ (Sm^{-1}) - specific electrical conductance; η ($Pa\ s$) - dynamic viscosity; B (T) - magnetic induction; St - Stuart number; Re - Reynolds number; Eu_m - Euler magnetic number; Re_m - Reynolds magnetic number.

It is an important criterion of magneto-hydrodynamics. It expresses the ratio of the induced electrodynamic (magnetic) force to the hydrodynamic force of the viscosity or, alternatively, the ratio of the ponderomotive force (the electromagnetic volume force by means of which the magnetic field acts on a conductor through which electric current flows, which causes magnetic pressure) to the molecular friction force. It characterizes the magnetic field influence on the flow of viscous, electrically conducting fluid. With small Ha values, the motion proceeds as if no magnetic field were acting. With great Ha values, the viscosity forces act only on a thin layer of the electrically conducting fluid (ionized gas) which adheres closely to a by-passed wall surface. In other cases, the motion resistance does depend on the viscosity and is determined completely by electromagnetic volume forces which are acting on the fluid. With high velocities and turbulent flow, it is more suitable to use the Stuart number, expressing the mutual magnetohydrodynamic action, instead of the Ha number.

- Brinkmann number

$$Br = \frac{\eta w^2}{\lambda \Delta T} = \frac{\eta w^2}{\lambda (T_s - T_\infty)} \quad (2.19)$$

η ($Pa\ s$) - dynamic viscosity; w (ms^{-1}) - flow velocity; λ ($Wm^{-1}K^{-1}$) - thermal conductivity; ΔT (K) - temperature difference; T_s (K) - surface temperature; T_∞ (K) - temperature in the thermal undisturbed fluid area.

Brinkmann number (Br) expresses the ratio of the heat arising due to viscous friction of a fluid to the heat transferred by molecular conduction. It characterizes the heat conduction in viscous fluid flow. For high fluid viscosity values and low thermal conductivity values (e.g. molten polymers), the value is $Br \gg 1$."

Chapter 3

Impact of Radiation on *Cu*-Water Based MHD Nanofluid

This chapter investigates the closed form solution of *Cu*-water based nanofluid with magnetic effects. The radiation effect is also considered in the energy equation. Tiwari-Das model is used for the analysis of the effective thermal conductivity. Mathematical modeling is carried out. Exact solutions for the momentum and energy equations are computed and interpreted for the diverse physical interest. It is depicted that by enhancing the magnitude of solid volume fraction of nanoparticles and velocity slip parameter, the velocity profile is increased. The results indicate that enhancing the magnitude of the Hartmann number enhances the temperature profile. It is examined that the entropy generation is enhanced by increasing the value of Brinkmann number and Reynolds number. The irreversibility parameter is a decreasing function of the Brinkmann number.

3.1 Mathematical Formulation

In this chapter, we have considered the incompressible, two dimensional, steady nanofluid flow passed a shrinking sheet. Here the shrinking of the sheet is considered along the x - and y -axis is considered perpendicular to the flow. Magnetic

field of strength B_0 is enforced normal to the fluid flow.

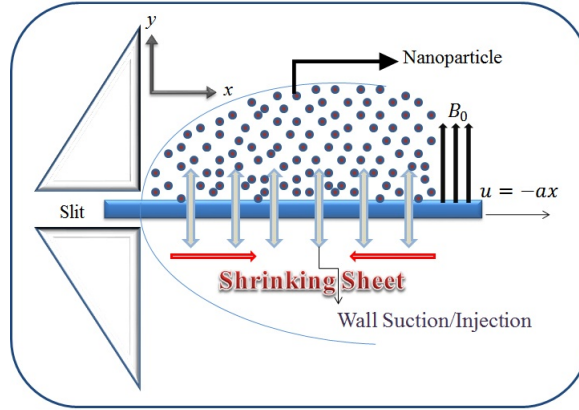


FIGURE 3.1: Geometrical view of the physical model

3.1.1 Continuity and Momentum Analysis

The elementary system of equations for the considered flow are [37]:

$$\frac{\partial u}{\partial x} + \frac{\partial v}{\partial y} = 0, \quad (3.1)$$

$$u \frac{\partial u}{\partial x} + v \frac{\partial u}{\partial y} = \frac{\mu_{nf}}{\rho_{nf}} \frac{\partial^2 u}{\partial y^2} - \frac{\sigma_{nf} B_0^2}{\rho_{nf}} u, \quad (3.2)$$

where u and v represent the velocity elements along x - and y -axis respectively. The subscript nf represents the nanofluid, μ_{nf} shows the effective dynamic viscosity and σ_{nf} electric conductivity of the nanofluid. The thermophysical correlation can be shown as follow [98, 99]:

$$\left. \begin{aligned} \mu_{nf} &= \frac{\mu_f}{(1-\phi)^{2.5}}, & \alpha_{nf} &= \frac{k_{nf}}{(\rho c_p)_{nf}}, \\ (\rho c_p)_{nf} &= (1-\phi)(\rho c_p)_f + \phi(\rho c_p)_s, \\ \nu_{nf} &= \frac{\mu_{nf}}{\rho_{nf}}, & \rho_{nf} &= (1-\phi)\rho_f + \phi(\rho_s), \\ \frac{k_{nf}}{k_f} &= \frac{(k_s + 2k_f) - 2\phi(k_f - k_s)}{(k_s + 2k_f) + \phi(k_f - k_s)}, \\ \frac{\sigma_{nf}}{\sigma_f} &= 1 + \frac{3\left(\frac{\sigma_{nf}}{\sigma_f} - 1\right)\phi}{\left(\frac{\sigma_{nf}}{\sigma_f} + 2\right) - \left(\frac{\sigma_{nf}}{\sigma_f} - 1\right)\phi}. \end{aligned} \right\} \quad (3.3)$$

In the above equations, ρ_f express the density, $(\rho c_p)_f$ the effective heat capacity, the solid volume fraction is denoted by ϕ , k_f represents the thermal conductivity and $k_{n,f}$ denotes the thermal conductivity of nanoparticles. The boundary conditions are:

$$\left. \begin{aligned} u &= -ax, & v &= -v_x & \text{at } & y = 0, \\ u &\rightarrow 0, & & & \text{as } & y \rightarrow \infty. \end{aligned} \right\} \quad (3.4)$$

In the above equation, the wall mass transfer velocity is represented by v_x with suction $v_x > 0$ and injection $v_x < 0$. To non-dimensionalize the flow system, following similarity variables have been introduced [100].

$$u = axf'(\eta), \quad v = -(\nu a)^{1/2}f(\eta), \quad \eta = y\left(\frac{a}{\nu}\right)^{1/2}. \quad (3.5)$$

After applying the similarity transformation, we have

$$f''' + A_1A_2ff'' - A_1A_2f'^2 - A_1M_2f' = 0, \quad (3.6)$$

the transformed boundary conditions are

$$\left. \begin{aligned} f(\eta) &= S, & f'(\eta) &= -1, & \text{at } & \eta = 0, \\ f'(\eta) &\rightarrow 0 & & & \text{as } & \eta \rightarrow \infty. \end{aligned} \right\} \quad (3.7)$$

In the above (3.6) and (3.7), $M_2 = \sqrt{\frac{\sigma B_0^2}{\rho_f a}}$ the Hartmann number and $S = \frac{v_x}{(\nu a)^{1/2}}$ the wall mass transfer parameter. Moreover, $A_2 = \left(1 - \phi \left(1 - \frac{\rho_s}{\rho_f}\right)\right)$ and $A_1 = (1 - \phi)^{2.5}$.

Chakrabarti and Gupta [101] acquired the analytical solution in 1979 for these type of 3rd order nonlinear differential equations. Recently, Bhattacharyya et al. [102] obtained the closed form solution of the momentum equation by taking the same trial solution as given in (3.8).

$$f(\eta) = a_{3.1} + b_{3.1}e^{-\alpha_{3.1}\eta}. \quad (3.8)$$

Putting (3.7) into (3.8), we get

$$f(\eta) = S - \left(\frac{1}{\alpha_{3.1}} - \frac{e^{-\alpha_{3.1}\eta}}{\alpha_{3.1}} \right). \quad (3.9)$$

Using (3.9) in (3.6), we have

$$\alpha_{3.1} = \frac{SA_1A_2 + \sqrt{(SA_1A_2)^2 - 4A_1A_2 + 4M_2A_1}}{2}. \quad (3.10)$$

Using in (3.9), one can have

$$a_{3.1} = S - \frac{2}{SA_1A_2 + \sqrt{(SA_1A_2)^2 - 4A_1A_2 + 4M_2A_1}}, \quad (3.11)$$

$$b_{3.1} = \frac{2}{SA_1A_2 + \sqrt{(SA_1A_2)^2 - 4A_1A_2 + 4M_2A_1}}, \quad (3.12)$$

where $a_{3.1}$, $b_{3.1}$ and $\alpha_{3.1}$ are constants.

Now, using the above constants in (3.9), we get the following velocity profile

$$f(\eta) = S - \frac{2 \left(1 - e^{-\frac{SA_1A_2 + \sqrt{(SA_1A_2)^2 - 4A_1A_2 + 4M_2A_1}}{2}\eta} \right)}{SA_1A_2 + \sqrt{(SA_1A_2)^2 - 4A_1A_2 + 4M_2A_1}}. \quad (3.13)$$

The local skin friction is written as

$$\left. \begin{aligned} C_f &= \frac{\tau_w}{\rho u_w^2} = -\frac{Re_x^{-1/2}}{A_1} f''(0), \\ A_1 C_f Re_x^{1/2} &= -f''(0), \end{aligned} \right\} \quad (3.14)$$

where $\frac{\tau_w}{\mu_n f} = \left(\frac{\partial u}{\partial y} \right)_{y=0}$ is the stress at surface wall and $Re_x = \frac{xu_w}{\nu}$ shows the Reynolds number.

3.1.2 Heat Transfer Analysis

In this segment, heat transport analysis is analyzed with the thermal radiation phenomenon. The governing equation is given as [103]

$$u \frac{\partial T}{\partial x} + v \frac{\partial T}{\partial y} = \alpha_{nf} \frac{\partial^2 T}{\partial y^2} - \frac{1}{(\rho c_p)_{nf}} \frac{\partial q_r}{\partial y}, \quad (3.15)$$

where

$$q_r = -\frac{4\sigma^*}{3k^*} \frac{\partial T^4}{\partial y}. \quad (3.16)$$

Here, σ^* the Stefan's constant, k^* denotes the mass absorption coefficient, α_{nf} is the thermal diffusivity, T expresses the temperature field and $(C_p)_{nf}$ the specific heat. Assuming that the temperature differences with in the flow field are sufficiently small, so that T^4 can be linearized using Taylor series. After expanding T^4 about free stream temperature and ignoring the higher order terms.

$$\begin{aligned} T^4 &= \frac{T_\infty^4 (T - T_\infty)^0}{0!} + \frac{4T_\infty^3 (T - T_\infty)^1}{1!} \dots, \\ &= T_\infty^4 + 4T_\infty^3 T - 3T_\infty^4, \\ T^4 &\approx 4T_\infty^3 T - 3T_\infty^4, \end{aligned} \quad (3.17)$$

using (3.16) into (3.15), we get

$$\begin{aligned} q_r &= -\frac{4\sigma^*}{3k^*} \frac{\partial (4T_\infty^3 T - 3T_\infty^4)}{\partial y}, \\ q_r &= -\frac{4\sigma^* 4T_\infty^3}{3k^*} \frac{\partial T}{\partial y}, \\ q_r &= -\frac{16\sigma^* T_\infty^3}{3k^*} \frac{\partial T}{\partial y}. \end{aligned} \quad (3.18)$$

Putting $q_r = -\frac{16\sigma^* T_\infty^3}{3k^*} \frac{\partial T}{\partial y}$ into (3.15)

$$u \frac{\partial T}{\partial x} + v \frac{\partial T}{\partial y} = \alpha_{nf} \frac{\partial^2 T}{\partial y^2} + \frac{1}{3(\rho c_p)_{nf}} \frac{16\sigma^* T_\infty^3}{k^*} \frac{\partial^2 T}{\partial y^2}. \quad (3.19)$$

The boundary conditions are

$$\left. \begin{aligned} T = T_w = T_\infty + T_0 \left(\frac{x}{l} \right)^n & \quad \text{at} \quad y = 0, \\ T \rightarrow T_\infty & \quad \text{as} \quad y \rightarrow \infty, \end{aligned} \right\} \quad (3.20)$$

where (3.19) expresses the boundary condition at the wall ($y = 0$) and at the free stream temperature ($y \rightarrow \infty$). T_0 expresses the constant reference temperature, T_w the temperature of the sheet, n shows the power-law index and T_∞ represents the free stream temperature. The similarity transformation for the temperature field is given as [104]:

$$\theta(\eta) = \frac{T - T_\infty}{T_w - T_\infty}. \quad (3.21)$$

The following non dimensional energy equation is obtained after utilizing the similarity variables defined in (3.5) and (3.20).

$$\Psi\theta'' + Prf\theta' - nPrf'\theta = 0, \quad (3.22)$$

where

$$\left. \begin{aligned} A_3 &= \frac{(k_s + 2k_f) + (-2\phi k_f + 2\phi k_s)}{(k_s + 2k_f) + (2\phi k_f - 2\phi k_s)}, & \Psi &= \left(A_3 + \frac{4N}{3} \right), \\ A_4 &= \left(1 - \phi + \phi \frac{(\rho Cp)_s}{(\rho Cp)_f} \right). \end{aligned} \right\} \quad (3.23)$$

Here $Pr = \frac{\nu_f}{\alpha_f}$ is the Prandtl number and $N = \frac{4\sigma^* T_\infty^3}{k^* k_f}$ the radiation parameter.

The reduced boundary condition get the form:

$$\left. \begin{aligned} \theta(\eta) = 1 & \quad \text{at} \quad \eta = 0, \\ \theta(\eta) \rightarrow 0 & \quad \text{as} \quad \eta \rightarrow \infty. \end{aligned} \right\} \quad (3.24)$$

Now, putting (3.9) in (3.21), it is easy to get

$$\Psi\theta_{\eta\eta} + Pr \left(S - \left(\frac{1 - e^{-\alpha_{3.1}\eta}}{\alpha_{3.1}} \right) \right) \theta_\eta - nPre^{-\alpha_{3.1}\eta}\theta = 0. \quad (3.25)$$

Above linear differential equation of second order can be reduced to Kummer's ordinary differential equation. For this purpose, a new variable

$$\xi_{3.1} = \frac{Pr e^{-\alpha_{3.1}\eta}}{\Psi\alpha_{3.1}^2} \quad (3.26)$$

is introduced.

As a result, (3.24) becomes Kummer's ordinary differential equation:

$$\xi_{3.1} \frac{\partial^2 \theta}{\partial \xi_{3.1}^2} + (Q - \xi_{3.1}) \frac{\partial \theta}{\partial \xi_{3.1}} - g\theta = 0, \quad (3.27)$$

where $g = -n$, $Q = (1 - q)$ and $q = \frac{Pr}{\Psi\alpha_{3.1}} \left(S - \frac{1}{\alpha_{3.1}} \right)$. The boundary conditions are

$$\theta(\xi_{3.1}) = 1, \quad \theta(0) = 0. \quad (3.28)$$

The closed form solution of (3.26) with (3.27) in terms of the Kummer's functions [105] is

$$\begin{aligned} \theta(\xi_{3.1}) = & \frac{M \left(\frac{Pr}{\Psi\alpha_{3.1}} \left(S - \frac{1}{\alpha_{3.1}} \right) - n, 1 + \frac{Pr}{\Psi\alpha_{3.1}} \left(S - \frac{2/2}{\alpha_{3.1}} \right), \xi_{3.1} \right)}{M \left(\frac{2Pr}{\Psi\alpha_{3.1}} \left(S - \frac{1}{\alpha_{3.1}} \right) - n, 1 + \frac{Pr}{\Psi\alpha_{3.1}} \left(S - \frac{1}{\alpha_{3.1}} \right), \frac{Pr}{\Psi\alpha_{3.1}^2} \right)} \\ & \times \left(\frac{\Psi\alpha_{3.1}^2 \xi_{3.1}}{Pr} \right)^{\frac{Pr}{\Psi\alpha_{3.1}} \left(S - \frac{1}{\alpha_{3.1}} \right)}, \end{aligned} \quad (3.29)$$

where M represents the 1st kind of the Kummer function. The solution of (??) is given as follows

$$\begin{aligned} \theta(\eta) = & \frac{M \left(\frac{2Pr/2}{\Psi\alpha_{3.1}} \left(S - \frac{1}{\alpha_{3.1}} \right) - n, 1 + \frac{Pr}{\Psi\alpha_{3.1}} \left(S - \frac{1}{\alpha_{3.1}} \right), \frac{Pr e^{-\alpha_{3.1}\eta}}{\Psi\alpha_{3.1}^2} \right)}{M \left(\frac{Pr}{\Psi\alpha_{3.1}} \left(S - \frac{1}{\alpha_{3.1}} \right) - n, 1 + \frac{Pr}{\Psi\alpha_{3.1}} \left(S - \frac{1}{\alpha_{3.1}} \right), \frac{Pr}{\Psi\alpha_{3.1}^2} \right)} \\ & \times e^{-\frac{Pr}{\Psi\alpha_{3.1}} \left(S - \frac{1}{\alpha_{3.1}} \right) \eta}, \end{aligned} \quad (3.30)$$

where

$$\alpha_{3.1} = \frac{SA_1A_2 + \sqrt{(SA_1A_2)^2 - 4A_1A_2 + 4M_2A_1}}{2}. \quad (3.31)$$

The non-dimensional wall temperature is

$$\theta_\eta(0) = \frac{M \left(1 + \frac{Pr}{\Psi\alpha_{3.1}} \left(S - \frac{1}{\alpha_{3.1}} \right) - n, 2 + \frac{Pr}{\Psi\alpha_{3.1}} \left(S - \frac{1}{\alpha_{3.1}} \right), \frac{Pr}{\Psi\alpha_{3.1}^2} \right)}{M \left(\frac{Pr}{\Psi\alpha_{3.1}} \left(S - \frac{1}{\alpha_{3.1}} \right) - n, 1 + \frac{Pr}{\Psi\alpha_{3.1}} \left(S - \frac{1}{\alpha_{3.1}} \right), \frac{Pr}{\Psi\alpha_{3.1}^2} \right)} \quad (3.32)$$

$$\times \frac{Pr}{\Psi\alpha_{3.1}} \left(\frac{\frac{Pr}{\Psi\alpha_{3.1}} \left(S - \frac{1}{\alpha_{3.1}} \right) - n}{\frac{Pr}{\Psi\alpha_{3.1}} \left(S - \frac{1}{\alpha_{3.1}} \right) + 1} \right) + \frac{Pr}{\Psi} \left(S - \frac{1}{\alpha_{3.1}} \right). \quad (3.33)$$

The local Nusselt number is defined as:

$$Nu_x = \frac{-k_{nf}x \left(\frac{\partial T}{\partial y} \right)_{y=0}}{k_f(T_w - T_\infty)} = -\frac{k_{nf}}{k_f} Re_x^{1/2} \theta_\eta(0). \quad (3.34)$$

The above equation is reduced to the following form

$$\frac{k_f}{k_{nf}} Nu_x Re_x^{-1/2} = -\theta_\eta(0). \quad (3.35)$$

3.1.3 Second law analysis

Whenever exchange of energy and momentum take place, non-equilibrium situation emerges, which leads to chaos effect inside the flow medium and at the boundaries. The volumetric entropy generation term S_G is given as:

$$S_G = \frac{K}{T_\infty^2} \left(\frac{\partial T}{\partial y} \right)^2 + \frac{\sigma B_0^2 u^2}{T_\infty}. \quad (3.36)$$

(3.35) displays the effect of two important factors generating irreversibility in a system. The rate of dimensionless entropy formation $E_G = \frac{S_G}{S_g}$ is given as

$$E_G = A_3 Re \theta'(\eta)^2 + Br \frac{M_2}{\Omega} f'(\eta)^2, \quad (3.37)$$

where

$$S_g = \frac{k_f}{T_\infty^2 \left(\frac{\Delta T}{x} \right)^2}, \quad \Omega = \frac{T_\infty}{\Delta T} \text{ and } M_2 = \frac{2L\sigma B_0^2}{\rho}. \quad (3.38)$$

Here Ω is the non dimensional temperature. To figure out the irreversibility in a system, Bejan parameter Be was introduced in 1979 [77], which gives the proportion of the energy transport irreversibility to the sum of all irreversibilities in the system and is given as:

$$Be = \frac{Eh}{Eh + Em}. \quad (3.39)$$

3.2 Results and Discussion

This segment reflects the behavior of several emerging pertinent parameters on the velocity and temperature profiles. Figure. 3.2 is developed to visualize the nature of the velocity profile for enhancing magnitude of ϕ . It is noted that the velocity profiles increases by enhancing the magnitude of ϕ . Impact of the suction parameter is illustrated in Figure 3.3. An increase in the velocity profile is observed with decrements in suction parameter over a shrinking surface depicted in Figure 3.3.

The impact of N and ϕ on the temperature profile is shown in Figures 3.4 and 3.5. Physically, the solid volume fraction strongly accelerates the temperature field by rising the magnitude of ϕ presented in Figure 3.4. This is due to the fact that the solid nanoparticles have pertinent effects on thermal properties. The augmented concentration of solid volume nanoparticles within the host fluid gives

higher thermal conductivity of the host fluid that correspondingly enhances the energy storage capacity of the host fluid. It is concluded that the boundary layer thickness is an increasing function of ϕ . In Figure 3.5, the influence of N on the temperature field is discussed. It is concluded that a gain into the thermal radiation parameter N shows a decrease in the temperature profile because of an enhancement in the radiative heat. It is examined that there is increase in the temperature because of an increment in the mean absorption parameter. Figures 3.6 and 3.7 portray impact of the Hartmann number M_2 and ϕ on the local skin friction coefficient. It is seen that due to increasing the Hartmann number M_2 with influence of suction and injection parameters, the local skin friction coefficient enhances in both cases. This is because of the Lorentz force that gives resistance to flow. The impact of Pr and the Hartmann number M_2 on the heat transfer rate is reported in Figures 3.8 and 3.9. It is observed that the non-dimensional temperature gradient $-\theta'(0)$ accelerates by enhancing the magnitude of Pr . The effect of N is displayed in Figure 3.9. It is perceived that the temperature profile enhances with an increment in the magnitude of N .

The effect of the power law index is illustrated in Figure 3.10. It is depicted that an enhancement in $-\theta'(0)$ is recorded by increasing the value of the power law index. Figure 3.11 expresses the impact of Br on the entropy generation profile E_G . It can be observed that the E_G rises by an increment in Br . Physically, Br is the product of Eckert and Prandtl number. Moreover, an increment in the E_G indicates that the heat dissipation decreases in the Eckert number. The purpose behind is clear, Brinkmann number produces heat within the layers of fluid particles during the flow because it is the heat source. The heat created together with the heat exchange from the heated wall empowers entropy generation inside the fluid flow. Therefore, the magnitude of the Brinkmann number should be controlled to minimize the entropy. Impact of Ω is plotted in Figure 3.12. It is seen that an increment in Ω reduces the chaos in the system. The impact of the Reynolds number Re on E_G is reflected in 3.13. It is seen that entropy enhances due to an increasing value of Re number which is provoked by fluid friction and energy transport. An increment in the Reynolds number interrupts the fluid, and

thus increases the entropy generation. Figure 3.14 illustrates an increase in E_G for M_2 . Moreover, enhancing magnitude of the Hartmann number increases E_G near to the sheet and distant from the wall, it is not influenced by the Hartmann number. The impact of Br on Be is illustrated in Figure 3.15. It is observed that an enhancement in Br effectively reduces the Be profile. The effect of Re and Ω is shown in Figures 3.16 and 3.17. It is visualized that an increment in magnitude of Re and Ω enhances Be .

The contour plots are shown in Figures 3.18, 3.19, 3.20, 3.21 and 3.22. Three dimensional bar graph of Pr against the Nusselt number is plotted in 3.23 and 3.24. Table 3.1 shows the thermophysical characteristics of host fluid and nano-meter sized particles are stated as [106] and [105]. Table 3.2 and Table 3.3, represent the numerical values of the local skin friction and local Nusselt number respectively.

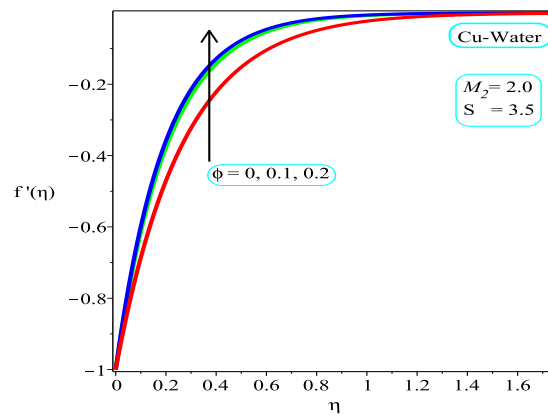


FIGURE 3.2: Impact of variation in ϕ on $f'(\eta)$

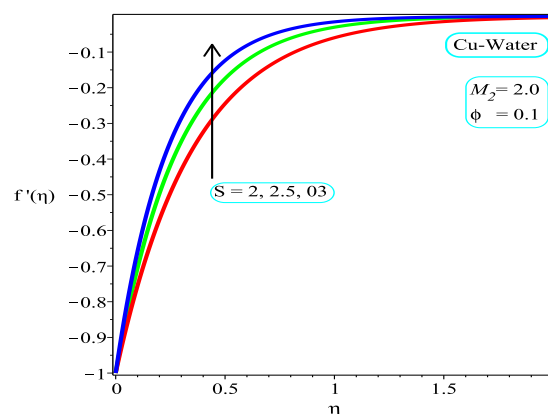


FIGURE 3.3: Impact of variation in S on $f'(\eta)$

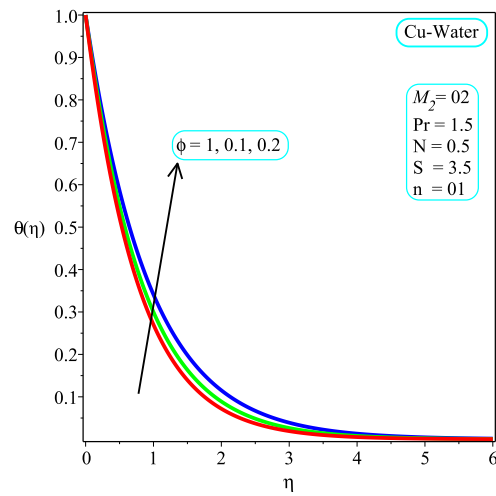


FIGURE 3.4: Impact of variation in ϕ on $\theta(\eta)$

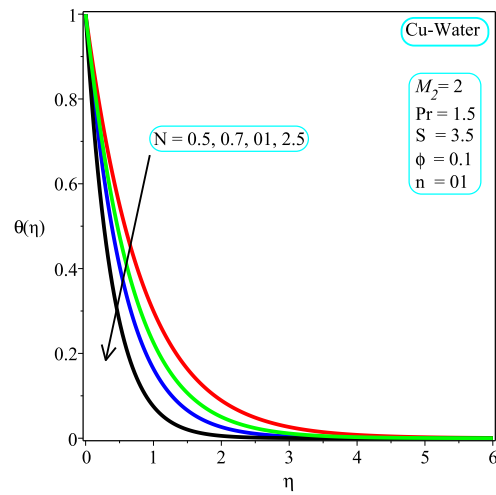


FIGURE 3.5: Impact of variation in N on $f'(\eta)$

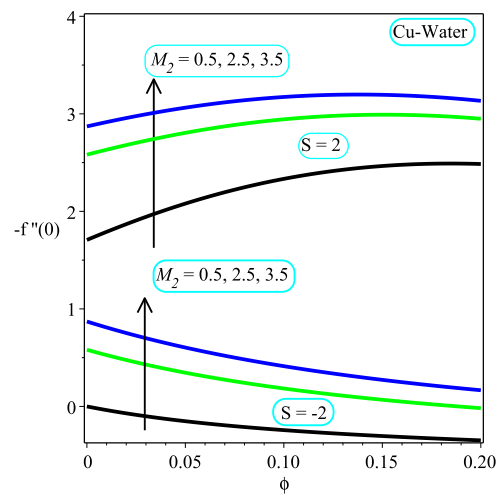


FIGURE 3.6: Impact of variation in M_2 on local skin friction

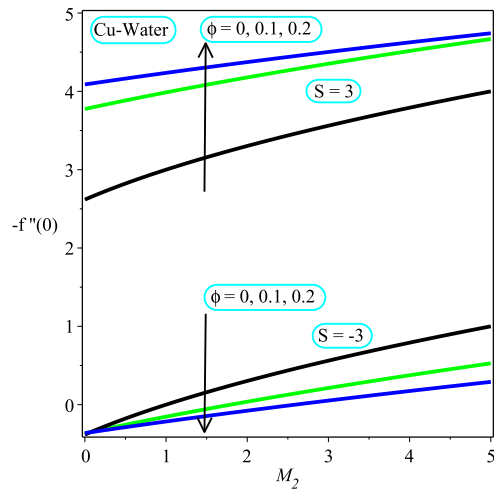


FIGURE 3.7: Impact of variation in ϕ on local skin friction

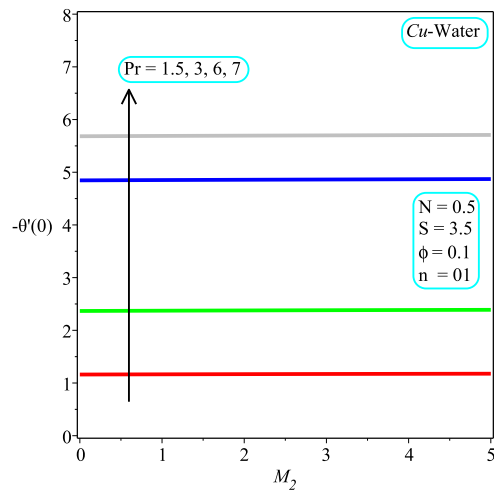


FIGURE 3.8: Impact of variation in Pr on Nusselt number

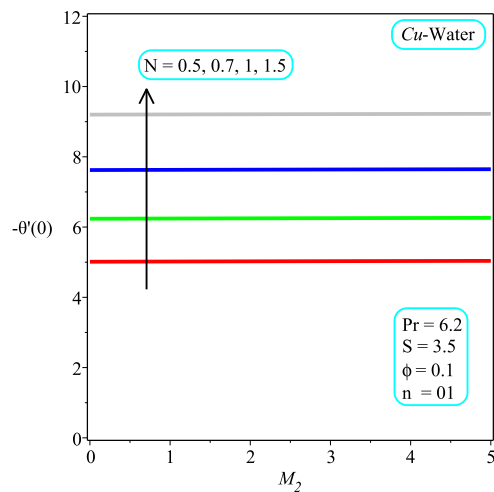


FIGURE 3.9: Impact of variation in N on Nusselt number

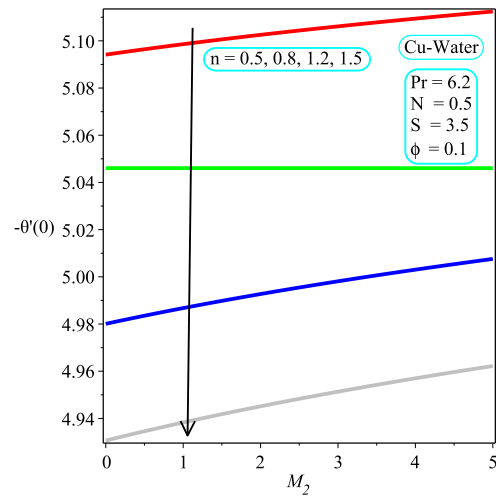


FIGURE 3.10: Impact of variation in n on Nusselt number

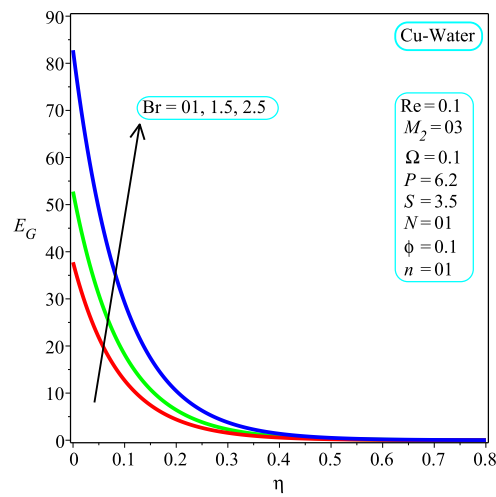


FIGURE 3.11: Impact of variation in Br on the entropy generation profile

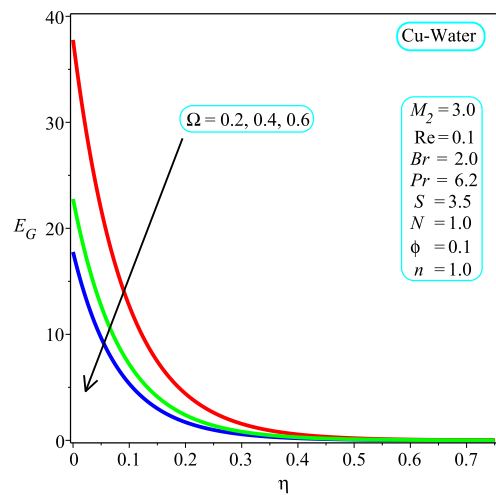


FIGURE 3.12: Impact of variation in Ω on the entropy generation profile

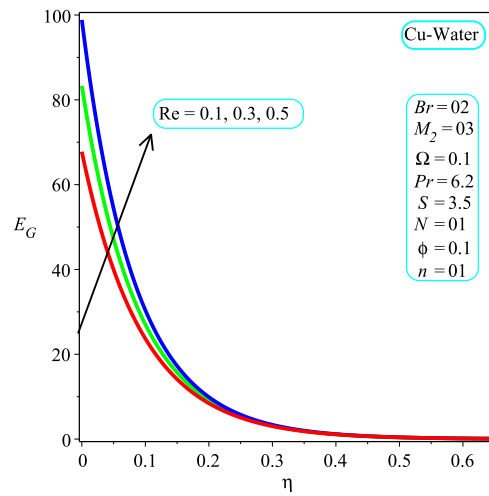


FIGURE 3.13: Impact of variation in Re on the entropy generation profile

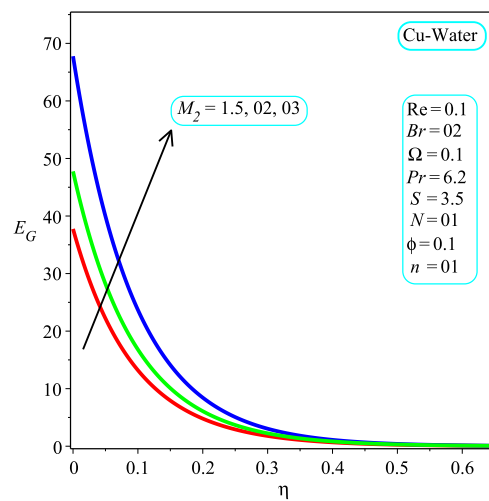


FIGURE 3.14: Impact of variation in M_2 on the entropy generation profile

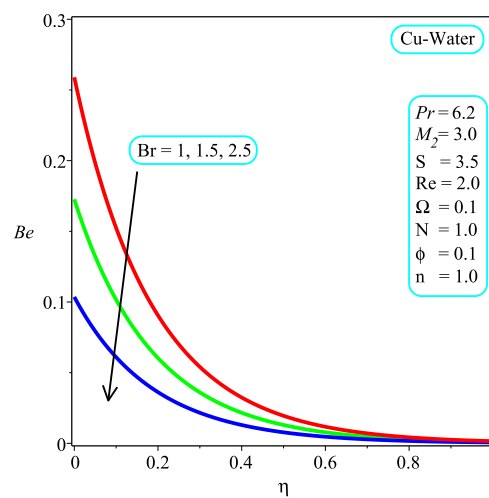


FIGURE 3.15: Impact of variation in Br on the irreversibility ratio parameter

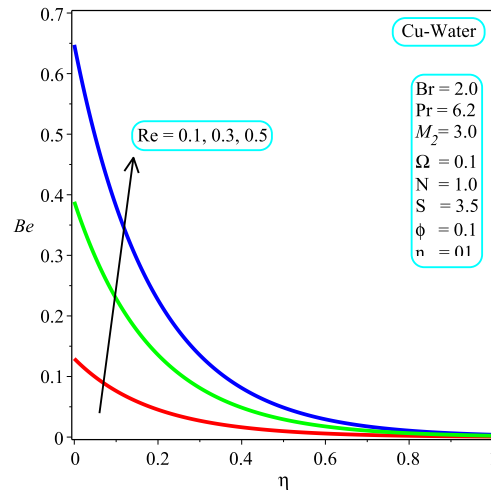


FIGURE 3.16: Impact of variation in Re on the irreversibility ratio parameter

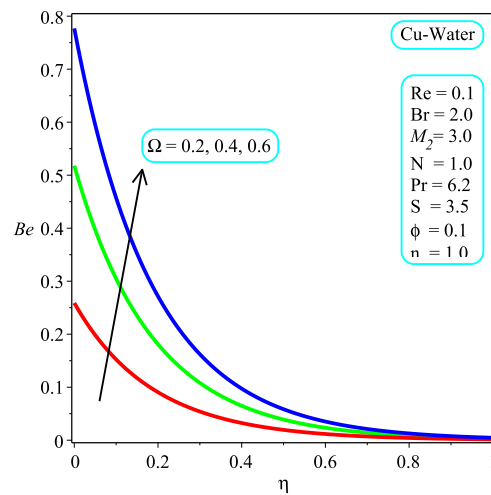


FIGURE 3.17: Impact of variation in Ω on the irreversibility ratio parameter

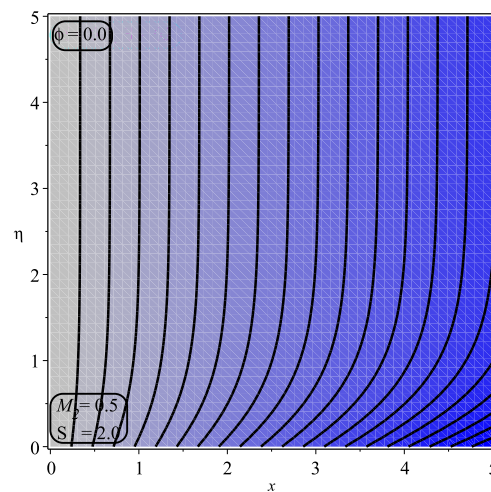
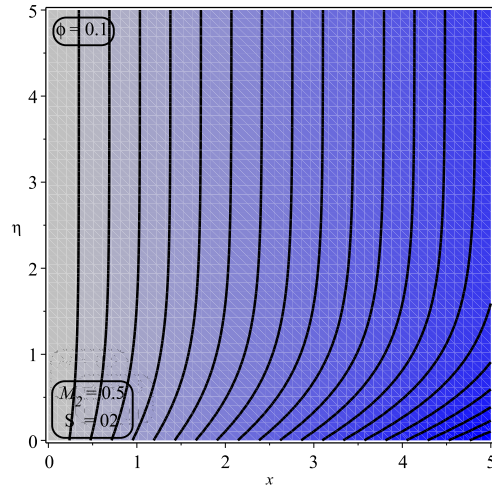
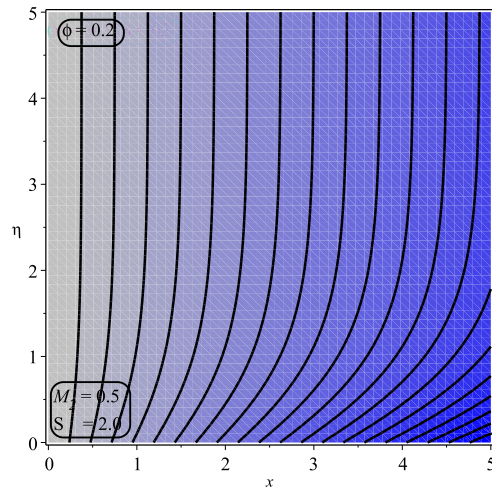
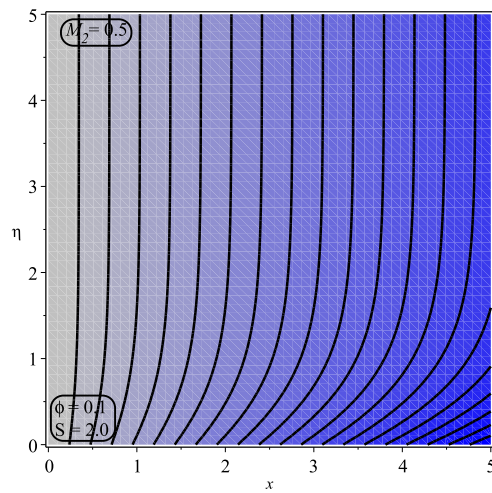


FIGURE 3.18: Contour plot for $\phi = 0.0$

FIGURE 3.19: Contour plot for $\phi = 0.1$ FIGURE 3.20: Contour plot for $\phi = 0.2$ FIGURE 3.21: Contour plot for $M_2 = 0.5$

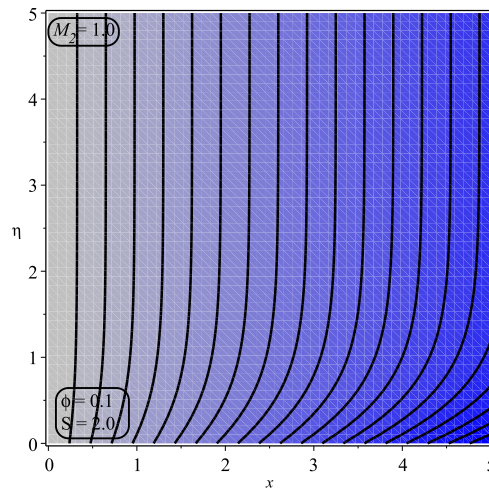


FIGURE 3.22: Contour plot for $M_2 = 1.0$

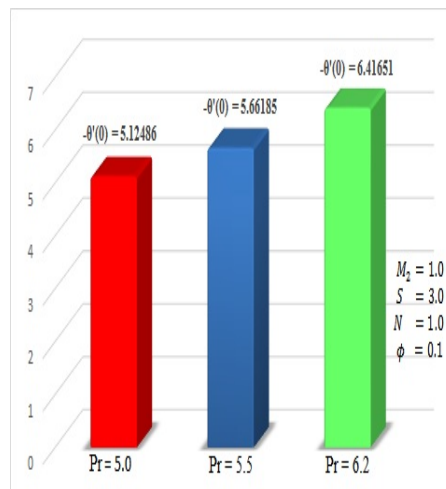


FIGURE 3.23: Variation of Pr on Nusselt number

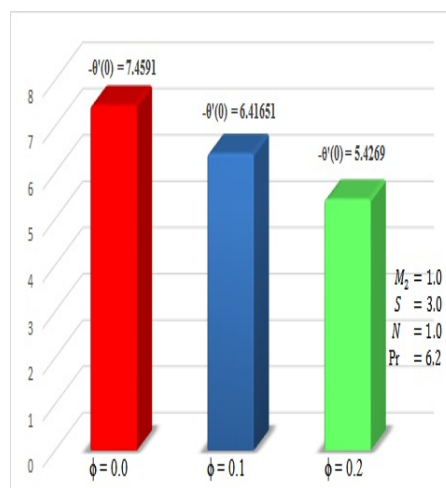


FIGURE 3.24: Impact of variation in Pr on Nusselt number

TABLE 3.1: Thermal characteristics of conventional fluid and nanoparticles.

Physical characteristics	$\rho(kg\ m^{-3})$	$c_p(J/kgK)$	$K(W/mk)$
Water	997.1	4179	0.613
Cu	8933	385	400

TABLE 3.2: Numerical values of $-f''(0)$.

ϕ	S	M_2	0	0.3	0.5	1
0.1	-2		-0.65583924	-0.51113253	-0.42678826	-0.2429780
		2	2.1042171	2.2489238	2.3332681	2.517078403
S	M_2	ϕ	0	0.1	0.15	0.2
-2	0.5		-0.29289321	-0.42678826	-0.4577315	-0.4817594
		2	1.7071067	2.3332681	2.4649646	2.4855020
ϕ	M_2	S	1.5	2.5	3.5	4
0.1	0.5		1.3097161	3.1321369	4.6142883	
		S	-1.5	-2.5	-3.5	-4
0.1	0.5		-0.76032619	-0.3179335	-0.2158104	-0.1867122
		S	1.5	2.5	3.5	4
			-0.76032619	-0.3179335	-0.2158104	-0.1867122

TABLE 3.3: Numerical computation of $-\theta''(0)$.

M_2	Pr	n	ϕ	S	R	0.5	0.7	1	1.5
1.5	6.2	1	0.1	3.5		5.021641	6.246060	7.631294	9.208324
R					M_2	0	1.5	2.5	3.5
0.5						5.012861	5.021641	5.026752	9.217130
	M_2				Pr	1.5	3	6	7
	0.5					1.162983	2.947318	7.372352	10.42720
			Pr	ϕ		0	0.1	0.15	0.2
			6.2			5.536168	6.240500	7.033973	7.585767

3.3 Conclusion

Final outcomes of the flow analysis are:

- The velocity profile is an increasing function of ϕ and S .
- The temperature profile accelerates by enhancing the value of ϕ whereas it found to be a decreasing function of the thermal radiation parameter N .
- It is found that the local skin friction is a growing function of the Hartmann number and increasing/decreasing function of ϕ .
- An increment in the Prandtl number and N is found responsible for a gain in the local Nusselt number.
- The entropy generation profile increases with an increase in Br , Re , Hartmann number and behaves oppositely for temperature difference parameter.
- The irreversibility parameter increases with an increment in Re , non dimensional temperature and the decreases with an increase in the Brickman number Br .

Chapter 4

Heat Transfer Analysis of Stagnation point flow past an Exponentially Stretching Surface

This chapter, examines the impact of Joule heating on a stagnation point flow over an exponentially stretching surface. Energy transport analysis is considered with the thermal radiation and Ohmic heating impact. Mathematical modeling is performed to transform the physical system into a set of mathematical equations which are further simplified by using suitable variables. Closed form solutions for the momentum and energy equations are obtained and depicted for the various physical parameters of concern. It is examined that enhancing the magnitude of ϕ , the velocity profile is accelerated. The results also indicate that the temperature profile is an enhancing function of the Eckert number. It is depicted that by enhancing the value of ϕ , the local skin friction coefficient is increased.

4.1 Mathematical Formulation

An incompressible, laminar, steady and two dimensional flow of the nanofluid passed a permeable exponentially stretching sheet has been considered. At x -axis

the exponentially stretching sheet is taken and y -axis is considered perpendicular to the flow that can be seen in Figure 4.1. The fluid occupies the space $y > 0$. Moreover, the magnetic field of strength B_0 is considered which is applied normally to the fluid flow.

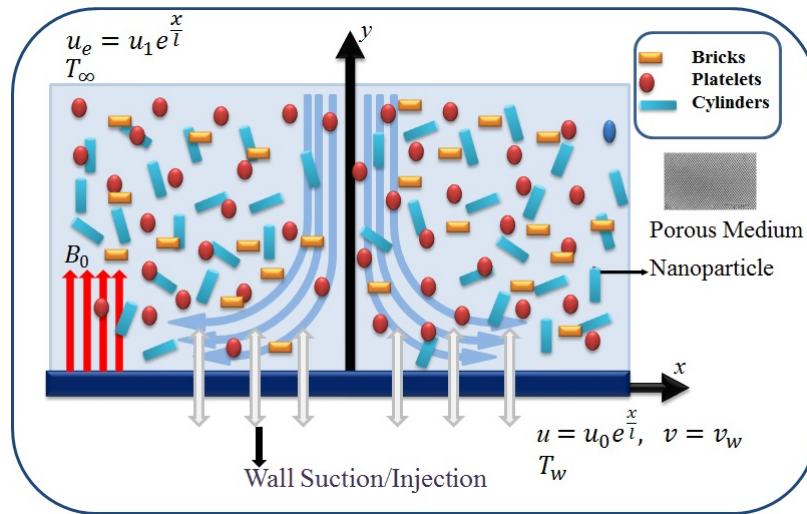


FIGURE 4.1: Geometrical view of the physical model

4.1.1 Continuity and Momentum Analysis

The elementary governing equations for the considered flow are [107]:

$$\frac{\partial u}{\partial x} + \frac{\partial v}{\partial y} = 0, \quad (4.1)$$

$$u \frac{\partial u}{\partial x} + v \frac{\partial v}{\partial y} = \frac{\mu_{nf}}{\rho_{nf}} \frac{\partial^2 u}{\partial y^2} + \frac{\mu_{nf}}{\rho_{nf} k} (u_e - u) + u_e \frac{\partial u_e}{\partial x} + \frac{\sigma_{nf} B_0^2}{\rho_{nf}} (u_e - u), \quad (4.2)$$

where u and v represent the velocity elements in the direction of x - and y - axis respectively. The density of nanofluid is denoted by ρ_{nf} , α_{nf} the thermal diffusivity, B_0 the magnetic parameter, μ_{nf} the dynamic viscosity, ν_{nf} the kinematic viscosity, $(\rho c_p)_{nf}$ the specific heat capacitance of the nanofluid.

Hamilton and Crosser model (1962) is considered for the shape factor of nanoparticles. The thermophysical correlation can be shown as follows [108, 109]:

$$\left. \begin{aligned} \mu_{nf} &= \frac{\mu_f}{(1-\phi)^{2.5}}, & \alpha_{nf} &= \frac{k_{nf}}{(\rho c_p)_{nf}}, \\ (\rho c_p)_{nf} &= ((\rho c_p)_f - \phi(\rho c_p)_f) + \phi(\rho c_p)_s, \\ \nu_{nf} &= \frac{\mu_{nf}}{\rho_{nf}}, & \rho_{nf} &= (\rho_f - \phi\rho_f) + \phi(\rho_s), \\ \frac{k_{nf}}{k_f} &= \frac{(k_s + (m+1)k_f) - (m+1)\phi(k_f - k_s)}{(k_s + (m+1)k_f) + \phi(k_f - k_s)}, \\ \frac{\sigma_{nf}}{\sigma_f} &= 1 + \frac{3\left(\frac{\sigma_{nf}}{\sigma_f} - 1\right)\phi}{\left(\frac{\sigma_{nf}}{\sigma_f} + 2\right) - \left(\frac{\sigma_{nf}}{\sigma_f} - 1\right)\phi}. \end{aligned} \right\} \quad (4.3)$$

In the above equations, $(\rho c_p)_f$ and ρ_f the heat capacity and density of the host fluid respectively, ϕ the solid volume fraction, σ_f and σ_{nf} express the electrical conductivity, k_f the thermal conductivity of the host fluid, the thermal conductivity of the nanofluid is expressed by k_{nf} . The suitable boundary conditions for the considered flow model is defined as:

$$\left. \begin{aligned} u &= u_0 e^{x/l}, & v &= v_w & \text{at } & y = 0, \\ u &\rightarrow u_e = u_1 e^{x/l} & & & \text{as } & y \rightarrow \infty. \end{aligned} \right\} \quad (4.4)$$

To non-dimensionalize the variables, following similarity variables have been used [110]:

$$u = u_0 e^{x/l} f', \quad v = -\left(\frac{u_0 \nu_f}{2l}\right)^{1/2} e^{x/2l} (f + \eta f'), \quad \eta = y \left(\frac{u_0}{2\nu l}\right)^{1/2} e^{x/2l}. \quad (4.5)$$

After using (4.5), we get

$$f''' + A_1 A_2 f f'' + 2A_1 A_2 (A^2 - f'^2) + (K + A_1 M_2)(A - f') = 0, \quad (4.6)$$

the considered boundary conditions are:

$$\left. \begin{aligned} f(\eta) &= S, & f'(\eta) &= 1, & \text{at } & \eta = 0, \\ f'(\eta) &\rightarrow \frac{u_e}{u_0} = A & & & \text{as } & \eta \rightarrow \infty. \end{aligned} \right\} \quad (4.7)$$

In above (4.6) and (4.7), u_0 represents the reference velocity, u_e the stagnation-point flow velocity, $M_2 = \frac{2l\sigma B_0^2}{u_0\rho_f}$ the Hartmann number and $K = \frac{u_0k}{l\nu_f}$ the permeability parameter. Furthrmore, $S = -\left(\frac{2l}{u_0\nu_f}\right)^{1/2} e^{-x/2l}v_w$, $A_2 = \left(1 - \phi + \phi\frac{\rho_s}{\rho_f}\right)$ and $A_1 = (1 - \phi)^{2.5}$. The closed form soltuion computed by Chakrabarti and Gupta [101], and [111]:

$$f(\eta) = a_{4.1} + b_{4.1}e^{-\alpha_{4.1}\eta}. \quad (4.8)$$

Using (4.7) in (4.8), we obtain

$$f(\eta) = S + \left(\frac{1 - e^{-\alpha_{4.1}\eta}}{\alpha_{4.1}}\right). \quad (4.9)$$

Now using (4.9) into (4.6), we have,

$$\alpha_{4.1} = \frac{1}{2}\sqrt{A_1^2A_2^2S^2 - 8A^2A_1A_2 - 4AA_1M - 4AK + 8A_1A_2 + 4MA_1 + 4K} \quad (4.10)$$

$$+ A_1A_2S. \quad (4.11)$$

$$a_{4.1} = S + \frac{1}{A_{4.1} + \frac{1}{2}\sqrt{A_1^2A_2^2S^2 - 8A^2A_1A_2 - 4AA_1M + A_{4.2}}}, \quad (4.12)$$

$$b_{4.1} = \frac{-1}{A_{4.1} + \frac{1}{2}\sqrt{A_1^2A_2^2S^2 - 8A^2A_1A_2 - 4AA_1M + A_{4.2}}}, \quad (4.13)$$

where $\alpha_{4.1} > 0$, $A_{4.2} = -4AK + 8A_1A_2 + 4MA_1 + 4K$ and $A_{4.1} = A_1A_2S$. Now, putting the above constant in (4.8), the solution of the velocity profile as follows

$$f(\eta) = S + \frac{1}{A_{4.1} + \frac{1}{2}\sqrt{A_1^2A_2^2S^2 - 8A^2A_1A_2 - 4AA_1M + A_{4.2}}} \times \left(1 - e^{-\left(A_{4.1} + \frac{1}{2}\sqrt{A_1^2A_2^2S^2 - 8A^2A_1A_2 - 4AA_1M + A_{4.2}}\right)\eta}\right). \quad (4.14)$$

The local skin friction is expressed as

$$C_f = \frac{\tau_w}{\rho u_w^2} = \frac{Re_x^{-1/2}}{A_1} f''(0), \quad A_1 C_f Re_x^{-1/2} = f''(0). \quad (4.15)$$

In (4.15), $\tau_w = \mu_{nf} \left(\frac{\partial u}{\partial y} \right)_{y=0}$ is the stress at wall and $Re_x = \frac{xu_w}{\nu}$ the Reynolds number.

4.1.2 Heat Transfer Analysis

In this segment, the heat tranapport investigation with the radioactive and Joule heating phenomenon is presented. The elementary equation is given below [112]:

$$u \frac{\partial T}{\partial x} + v \frac{\partial T}{\partial y} = \alpha_{nf} \frac{\partial^2 T}{\partial y^2} - \frac{1}{(\rho C_p)_{nf}} \frac{\partial q_r}{\partial y} + \frac{\sigma_{nf} B_0^2}{(\rho C_p)_{nf}} u^2, \quad (4.16)$$

where

$$q_r = -\frac{4\sigma^*}{3k^*} \frac{\partial T^4}{\partial y}. \quad (4.17)$$

Here α_{nf} is the thermal diffusivity, T shows the temperature field, $(C_p)_{nf}$ the specific heat, σ^* the Stefan's constant and k^* denotes the mass absorption coefficient.

Using (4.17) into (4.16), we have

$$u \frac{\partial T}{\partial x} + v \frac{\partial T}{\partial y} = \alpha_{nf} \frac{\partial^2 T}{\partial y^2} + \frac{1}{3(\rho c_p)_{nf}} \frac{16\sigma^* T_\infty^3}{k^*} \frac{\partial^2 T}{\partial y^2} + \frac{\sigma_{nf} B_0^2}{(\rho c_p)_{nf}} u^2. \quad (4.18)$$

The boundary conditions are

$$\left. \begin{aligned} T &= T_w = T_\infty + T_0 e^{x/l} & \text{at } & y = 0, \\ T &\rightarrow T_\infty & \text{as } & y \rightarrow \infty, \end{aligned} \right\} \quad (4.19)$$

where T_0 expresses the constant reference temperature, l the characteristic length, T_w the temperature of the sheet and T_∞ represents the free stream temperature.

The similarity transformation for temperature profile is introduced as [112]:

$$\theta(\eta) = \frac{T - T_\infty}{T_w - T_\infty}. \quad (4.20)$$

The following dimensionless energy equation is found after utilizing the similarity variables shown in (4.5) and (4.20).

$$\theta'' + Pr f \theta' - 2Pr f' \theta + \frac{Pr M_2}{A_4} Ec f'^2 = 0, \quad (4.21)$$

where

$$Ec = \frac{u^2}{(T_w - T_\infty) Cp}, \quad Pr = \frac{\nu_f}{\alpha_f}, \quad N = \frac{4\sigma^* T_\infty^3}{K^* K_f}, \quad \Psi = \left(A_3 + \frac{4N}{3} \right) \quad (4.22)$$

$$A_3 = \frac{(k_s + 2k_f) - 2\phi(k_f - k_s)}{(k_s + 2k_f) + 2\phi(k_f - k_s)}, \quad A_4 = \left(1 - \phi + \phi \frac{(\rho Cp)_s}{(\rho Cp)_f} \right). \quad (4.23)$$

Here Pr is the Prandtl number, the Eckert number is denoted by Ec and N the radiation parameter. The reduced boundary conditions are:

$$\left. \begin{aligned} \theta(\eta) &= 1 & \text{at} & \quad \eta = 0, \\ \theta(\eta) &\rightarrow 0 & \text{as} & \quad \eta \rightarrow \infty. \end{aligned} \right\} \quad (4.24)$$

Now, putting (4.9) into (4.21), it is easy to get

$$\Psi \theta_{\eta\eta} + Pr \left(S + \frac{1}{\alpha_{4.1}} \left(\frac{1 - e^{-\alpha_{4.1}\eta}}{\alpha_{4.1}} \right) \right) \theta_\eta - 2Pre^{-\alpha_{4.1}\eta} \theta + \frac{Pr M_2}{A_4} Ec (e^{-\alpha_{4.1}\eta})^2 = 0. \quad (4.25)$$

A linear differential equation of second order can be converted into Kummer's ordinary differential equation. For this purpose, a new variable

$$\xi_{4.1} = -\frac{Pre^{-\alpha_{4.1}\eta}}{\Psi \alpha_{4.1}^2} \quad (4.26)$$

is introduced.

As a result, (4.25) becomes Kummer's ordinary differential equation:

$$\xi_{4.1} \frac{\partial^2 \theta}{\partial \xi_{4.1}^2} + (E - \xi_{4.1}) \frac{\partial \theta}{\partial \xi_{4.1}} - g\theta = -\frac{Pr M_2}{A_4} Ec (e^{-\alpha_{4.1}\eta})^2, \quad (4.27)$$

where $E = (1 - F)$, $F = \frac{Pr}{\Psi\alpha_{4.1}} \left(S + \frac{1}{\alpha_{4.1}} \right)$ and $g = -2$. The boundary conditions are

$$\theta(\xi_{4.1}) = 1, \quad \theta(0) = 0. \quad (4.28)$$

The exact solution of (4.27) with (4.28) in forms of the Kummer's functions [105] is expressed as follows

$$\begin{aligned} \theta(\xi_{4.1}) = & \frac{M\left(-2 + \frac{Pr}{\Psi\alpha_{4.1}} \left(2S/(1S + S) + \frac{1}{\alpha_{4.1}} \right), 1 + \frac{Pr}{\Psi\alpha_{4.1}} \left(S + \frac{1}{\alpha_{4.1}} \right), \xi_{4.1}\right)}{M\left(\frac{Pr}{\Psi\alpha_{4.1}} \left(S + \frac{1}{\alpha_{4.1}} \right) - 2, 1 + \frac{Pr}{\Psi\alpha_{4.1}} \left(S + \frac{1}{\alpha_{4.1}} \right), \frac{-Pr}{\Psi\alpha_{4.1}^2}\right)} \\ & \times \frac{\xi_{4.1} \frac{Pr}{\Psi\alpha_{4.1}} \left(s + \frac{1}{\alpha_{4.1}} \right)}{\left(\frac{-2Pr}{\Psi\alpha_{4.1}^2} \right) \frac{Pr}{\Psi\alpha_{4.1}} \left(s + \frac{1}{\alpha_{4.1}} \right) \Psi\alpha_{4.1}^2 A_4 \left(-2 + \frac{Pr}{\Psi\alpha_{4.1}} \left(S + \frac{1}{\alpha_{4.1}} \right) \right)} \\ & + \left(\frac{Pr}{\Psi\alpha_{4.1}} \left(S + \frac{1}{\alpha_{4.1}} \right) \right)^2 - (\xi_{4.1} + 3) \frac{Pr}{\Psi\alpha_{4.1}} \left(S + \frac{1}{\alpha_{4.1}} \right) + \xi_{4.1}^2 - 2 \\ & \times \left(\frac{M_2 Ec \Psi\alpha_{4.1}^2}{\left(\frac{Pr}{\Psi\alpha_{4.1}} \left(S + \frac{1}{\alpha_{4.1}} \right) \right)} - \frac{2\xi_{4.1} - 1 + \frac{Pr}{\Psi\alpha_{4.1}} \left(S + \frac{1}{\alpha_{4.1}} \right)}{2A_4 Pr} \right), \quad (4.29) \end{aligned}$$

in (4.29), M represents the confluent hypergeometric function of the 1st kind. The closed form solution of 4.21 is defined as follows

$$\theta(\eta) = \frac{e^{\alpha_{4.1} \frac{-Pr}{\Psi \alpha_{4.1} a_{4.5} P \eta}} M \left(\frac{Pr}{\Psi \alpha_{4.1}} - 2a_{4.5}, 1 + \frac{Pr}{\Psi \alpha_{4.1}} a_{4.5}, \frac{-Pr}{\Psi \alpha_{4.1}^2} e^{-\alpha_{4.1} \eta} \right)}{2M \left(\frac{Pr}{\Psi \alpha_{4.1}} - 2a_{4.5}, 1 + \frac{Pr}{\Psi \alpha_{4.1}} a_{4.5}, \frac{-Pr}{\Psi \alpha_{4.1}^2} \right)}$$

$$\times \left(\frac{1}{(\Psi \alpha_{4.1}^2 A_4) \left(\frac{Pr}{\Psi \alpha_{4.1}} - 2a_{4.5} \right)} \right)$$

$$+ \left(\frac{Pr}{\Psi \alpha_{4.1}} a_{4.5}^2 + \left(\frac{-Pr}{\Psi \alpha_{4.1}^2} e^{-\alpha_{4.1} \eta} - 3 \right) \frac{Pr}{\Psi \alpha_{4.1}} a_{4.5} + \left(\frac{Pr}{\Psi \alpha_{4.1}^2} e^{-\alpha_{4.1} \eta} \right)^2 \right)$$

$$\times \left(\frac{M_2 Ec \Psi \alpha_{4.1}^2}{2A_4 Pr \left(-2 + \frac{Pr}{\Psi \alpha_{4.1}} a_{4.5} \right)} - M_2 Ec \Psi \alpha_{4.1}^2 \frac{2\xi_{4.1} - 1 + \frac{Pr}{\Psi \alpha_{4.1}} a_{4.5}}{2A_4 Pr} \right). \quad (4.30)$$

$$\theta_\eta(0) = \frac{Pr^2 \left(S + \frac{1}{\alpha_{4.1}^2} \right)^2 a_{4.2} (2A_4 Pr \alpha_{4.1} a_{4.5} - 4A_4 \alpha_{4.1}^2 \Psi - M_2 Ec Pr)}{2\Psi^2 a_{4.2} A_4 \alpha_{4.1}^2 (-2 + P)}$$

$$+ \left(\frac{Pr a_{4.5} (a_{4.3} - a_{4.2}) (2A_4 Pr \alpha_{4.1} a_{4.5} - 4A_4 \alpha_{4.1}^2 \Psi - M_2 Ec Pr)}{\Psi^2 a_{4.2} A_4 \alpha_{4.1}} \right)$$

$$- \left(\frac{a_{4.3} - a_{4.4}}{2a_{4.2} A_4 \alpha_{4.1} \Psi} a_{4.6} + \frac{a_{4.3} - a_{4.2}}{2a_{4.2} A_4 \alpha_{4.1} \Psi} \right) \left(\frac{Pr S}{\Psi \alpha_{4.1}} - 2\xi_{4.1} + \frac{Pr}{\Psi \alpha_{4.1}^2} \right) \alpha_{4.1}$$

$$\times (2A_4 Pr \alpha_{4.1} a_{4.5} - 4A_4 \alpha_{4.1}^2 \Psi - M_2 Pr Ec)$$

$$+ \left(\frac{\left(\frac{-2Pr}{\Psi^2 \alpha_{4.1}} a_{4.5} + \frac{4Pr}{\Psi} \right) Ec M_2 \alpha_{4.1}^2 \Psi}{A_4 Pr \left(-2 + \frac{Pr}{\Psi \alpha_{4.1}} a_{4.5} \right)} + \frac{Ec M_2 \alpha_{4.1}^2}{A_4} \right), \quad (4.31)$$

where

$$a_{4.2} = M \left(\frac{2/2Pr}{\Psi \alpha_{4.1}} \left(S + \frac{1}{\alpha_{4.1}} \right) - 2, 1 + \frac{2/2Pr}{\Psi \alpha_{4.1}} \left(S + \frac{1}{\alpha_{4.1}} \right), -\frac{Pr}{\alpha_{4.1}^2 \Psi} \right),$$

$$a_{4.3} = M \left(-1 + \frac{Pr}{\Psi \alpha_{4.1}} \left(S + \frac{1}{\alpha_{4.1}} \right), 1 + \frac{Pr}{\Psi \alpha_{4.1}} \left(S + \frac{1}{\alpha_{4.1}} \right), -\frac{Pr}{\alpha_{4.1}^2 \Psi} \right),$$

$$a_{4.4} = M \left(\frac{Pr}{\Psi \alpha_{4.1}} \left(S + \frac{1}{\alpha_{4.1}} \right), 1 + \frac{Pr}{\Psi \alpha_{4.1}} \left(S + \frac{1}{\alpha_{4.1}} \right), -\frac{Pr}{\alpha_{4.1}^2 \Psi} \right),$$

$$a_{4.5} = S + \frac{1}{\alpha_{4.1}},$$

$$a_{4.6} = \left(\frac{PrS}{\Psi \alpha_{4.1}} + \frac{Pr}{\Psi \alpha_{4.1}^2} - 1 \right) \alpha_{4.1},$$

$$\alpha_{4.1} = A_{4.1} + \frac{1}{2} \sqrt{A_1^2 A_2^2 S^2 - 8A^2 A_1 A_2 - 4AA_1 M + A_{4.2}}.$$

Accordingly, the above equation initiated the non-dimensional wall temperature can be written as:

$$Nu_x = \frac{-k_{nf} x \left(\frac{\partial T}{\partial y} \right)_{y=0}}{k_f (T_w - T_\infty)} = -\frac{k_{nf}}{k_f} Re_x^{1/2} \theta_\eta(0). \quad (4.32)$$

In the current study, it is acquired as:

$$\frac{k_f}{k_{nf}} Nu_x Re_x^{-1/2} = -\theta_\eta(0). \quad (4.33)$$

4.2 Results and Discussion

The effect of several emerging parameters on the velocity and temperature profile are discussed in this segment. In this regard, Figures 4.2 - 4.25 are prepared. The graphs shown in Figures 4.2 and 4.3 are plotted to visualize the trend of velocity

field of the nanofluid for ϕ with the suction/injection phenomena separately, while keeping the other parameters constant.

It is examined in these figures that the velocity field reduces efficiently by an increment in ϕ . Influence of the suction/injection parameter is depicted in Figures 4.4 and 4.5. The velocity profile increases for increasing the value of the mass blowing ($S < 0$) is seen in Figure 4.4 and a quite opposite behavior of the same profile is recorded for the mass suction ($S > 0$) in Figure 4.5. An increment in the velocity ratio parameter $A = \frac{u_e}{u_o}$ strongly accelerates the velocity profile see Figure 4.6. Moreover, it is also perceived that velocity field rises because of an increment within the magnitude of A , while the velocity of stretching wall is higher than the velocity at $y \rightarrow \infty$. The stagnation point flow is found zero, when velocity ratio parameter is taken zero.

Physical insight of the temperature profile with respect to the mass suction/injection, Ec , permeability parameter K , Pr , M_2 , ϕ and the velocity ratio parameter A is plotted in Figures 4.7 - 4.14 respectively. Figure 4.7 displays the influence of S on the temperature field. Temperature profile decreases for increasing the value of S . Physically, impact of $S > 0$ makes distribution of the temperature distribution more consistent inside the boundary layer. Suction of fluid at the sheet has a ability to diminish the thermal boundary layer thickness, which consequently reduces the temperature field. Further, increasing value of $S (< 0)$ enhances the thermal boundary layer thickness which causes the heat transport rate decrease. Figure 4.8 portrays the impact of Ec on the temperature field. It is noticed that there is a gradual decrease in the fluid energy by an increment in Ec . Here, it is observed that the temperature increases for gaining the values of Ec , since frictional heating is provoked the heat energy within the fluid. Such increment in heat energy enhances the temperature profile. Figure 4.9 expresses the behavior of K on the temperature field. As the permeability of fluid increases there is a rise in the fluid temperature. Physically, the impact of permeable media originated more friction to flow, for which retards the velocity of considered fluid, and due to which there is an increase in the temperature. Figure 4.11 is prepared to study the effect of Pr on the temperature field. It is seen that the temperature profile decreases

effectively with an increment in the Prandtl number. Physically, it signifies that an enhancement in Pr means that the viscosity of fluid is increased, for which the temperature distribution is decreased. The effect of M_2 on the temperature field is portrayed in Figure 4.12. It is observed that an increase into M_2 increases the fluid energy significantly. Actually, the M_2 is dependent on Lorentz force. Increasing the values of M_2 has the more grounded Lorentz force and opposite for the lower magnitude of M_2 . The higher Lorentz force generates high heat energy in fluid motion which presents an increment in the temperature. The variation of ϕ with combine effects of S on the temperature field is plotted in Figure 4.13. It is examined that the fluid temperature increases for the suction and decreasing trend is noticed for the injection parameter with an increase ϕ . The trend of the velocity ratio parameter on the temperature field is plotted in Figure 4.14. The temperature of fluid reduces effectively by enhancing the velocity ratio parameter.

To capture the heat transport rate, the local Nusselt number is plotted against the variation in Ec , M_2 , permeability parameter and S see Figures 4.15 - 4.18. It is seen that heat transport rate is increasing function of the Eckert number, Hartmann parameter and K . Figure 4.18 shows that heat transfer rate is high for ($S < 0$) as compared to the suction parameter. The value of $-f''(0)$ is decreased for increasing the value of $S < 0$ and increases efficiently for $S > 0$ is shown Figure 4.19. In Figure 4.20, value of $-f''(0)$ is observed to decrease gradually by an increment in ϕ . An increment in the local skin friction is observed due to enhancing the values of M_2 in Figure 4.21. Figures 4.23 - 4.25 represent the contour plots. The value of $-\theta'(0)$ for various shaped nanoparticles is depicted in Figures 4.26 and 4.27.

Table 4.1, represents the thermal characteristics of conventional fluid (water) and solid nanoparticles (copper) are given as [113] and [114]. Table 4.2 displays the numerical values of nanoparticle shape factor m is given by Timofeeva et al. [115]. Results for code verification are shown in Table 4.3. Table 4.4 displays the magnitude of $-f''(0)$. The values of $-\theta'(0)$ owing the different emerging parameters for different shape factors of nanoparticles shown in Table 4.5 - 4.7.

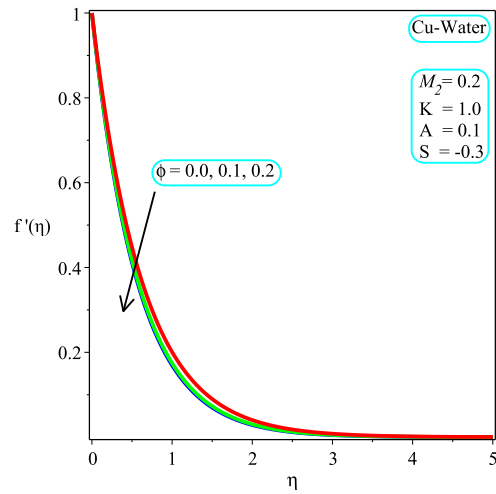


FIGURE 4.2: Impact of variation in ϕ on $f'(\eta)$

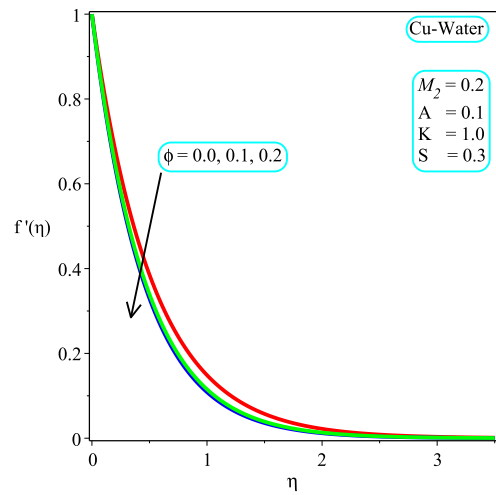


FIGURE 4.3: Impact of variation in ϕ on $f'(\eta)$

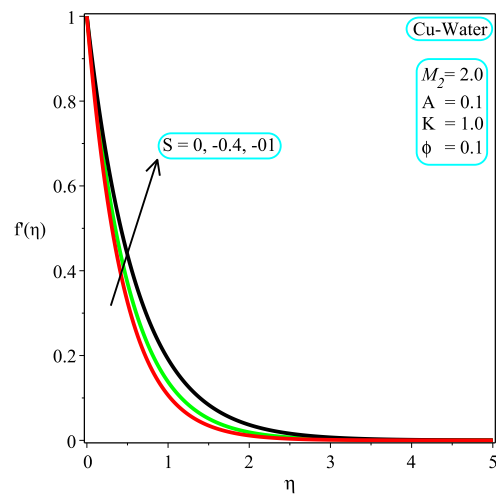


FIGURE 4.4: Impact of variation in S on $f'(\eta)$

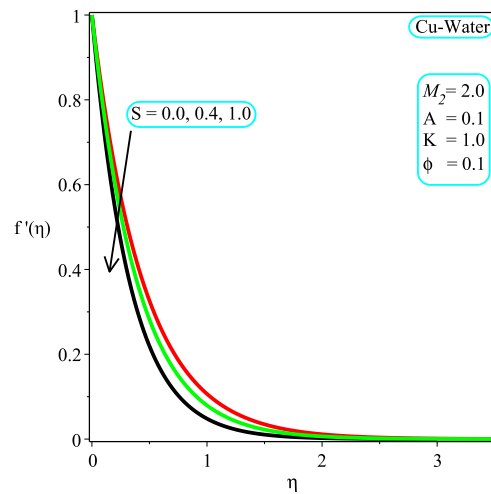


FIGURE 4.5: Impact of variation in S on $f'(\eta)$

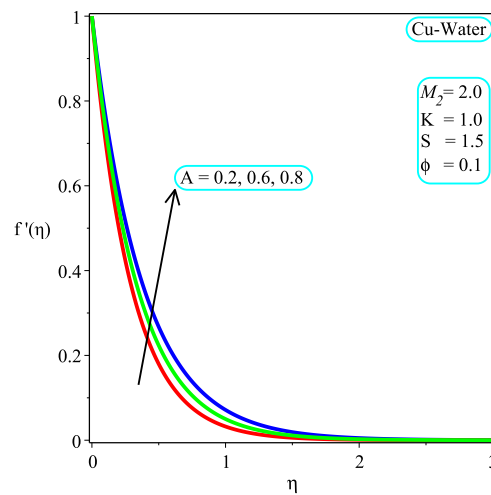


FIGURE 4.6: Impact of variation in A on $f'(\eta)$

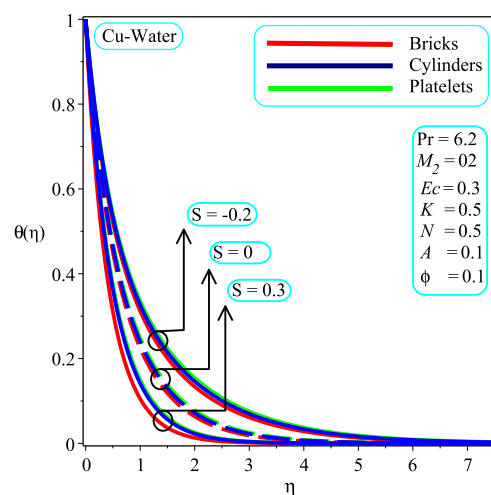


FIGURE 4.7: Impact of variation in S on $\theta(\eta)$

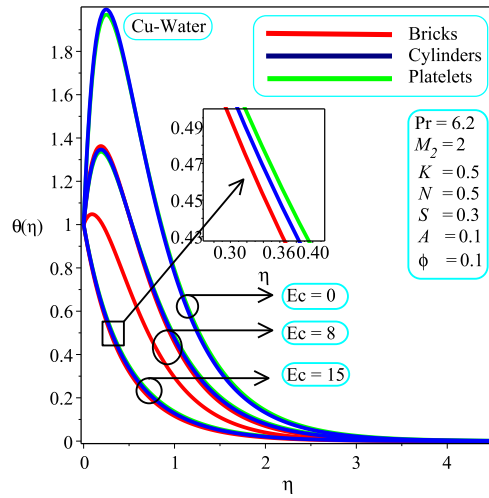


FIGURE 4.8: Impact of variation in Ec on $\theta(\eta)$

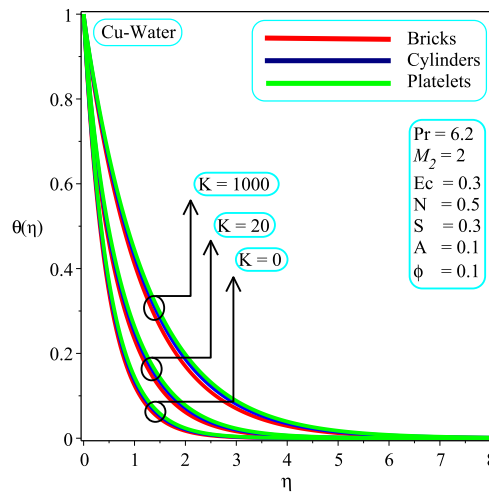


FIGURE 4.9: Impact of variation in K on $\theta(\eta)$

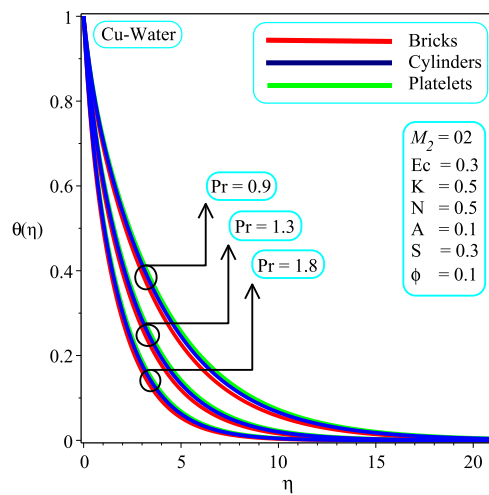


FIGURE 4.10: Impact of variation in Pr on $\theta(\eta)$

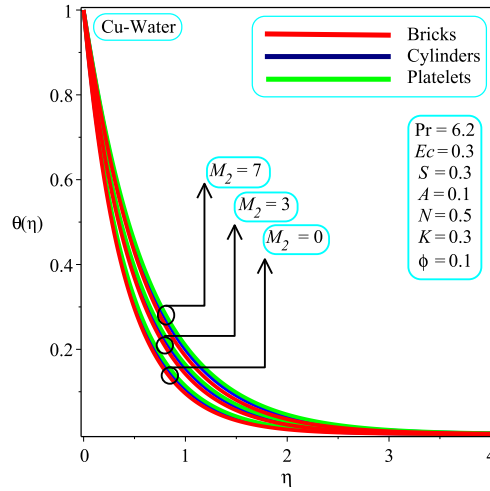


FIGURE 4.11: Impact of variation in M_2 on $\theta(\eta)$

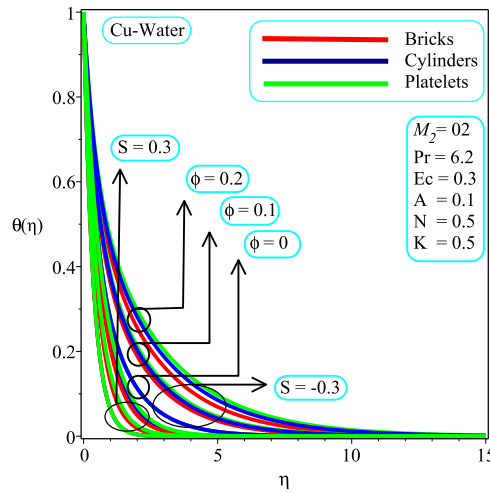


FIGURE 4.12: Impact of variation in ϕ on $\theta(\eta)$

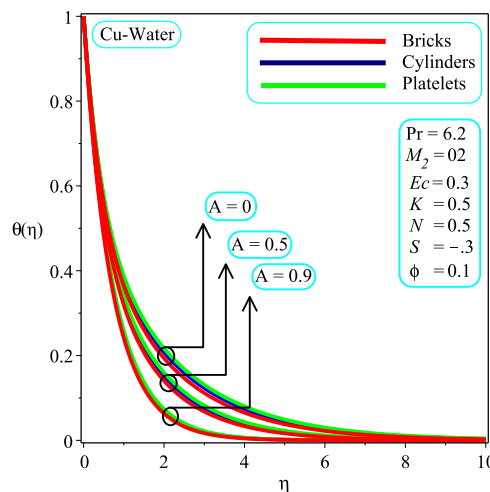


FIGURE 4.13: Impact of variation in A on $\theta(\eta)$

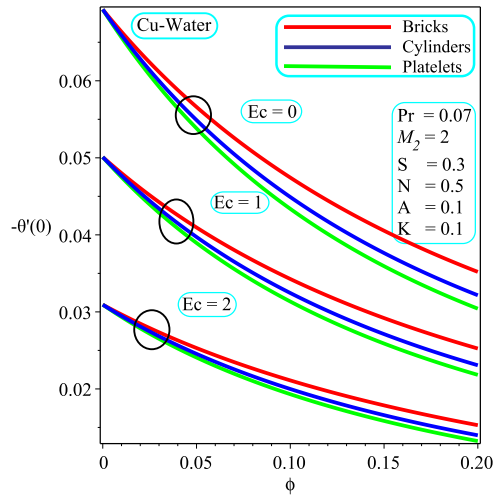


FIGURE 4.14: Impact of variation in Ec on $-\theta'(0)$

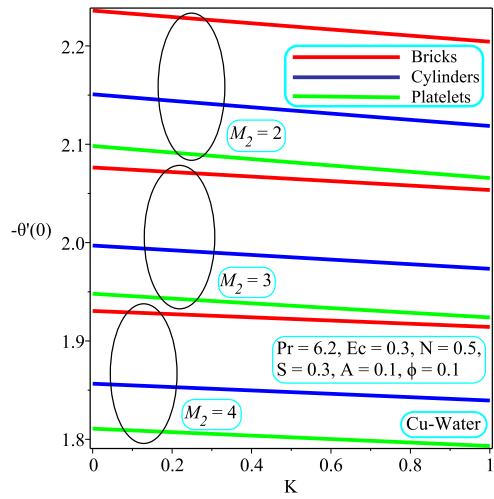


FIGURE 4.15: Impact of variation in M_2 on $-\theta'(0)$

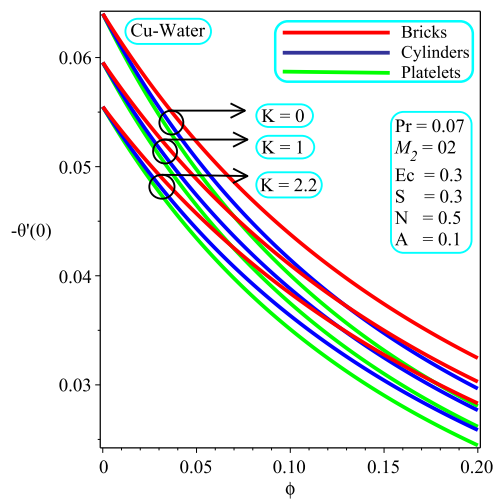


FIGURE 4.16: Impact of variation in K on $-\theta'(0)$

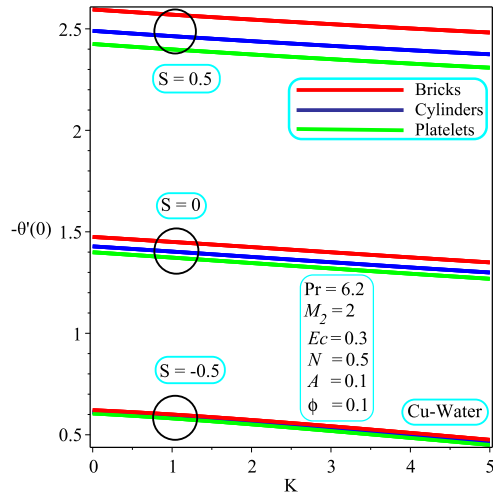


FIGURE 4.17: Impact of variation in S on $-\theta'(0)$

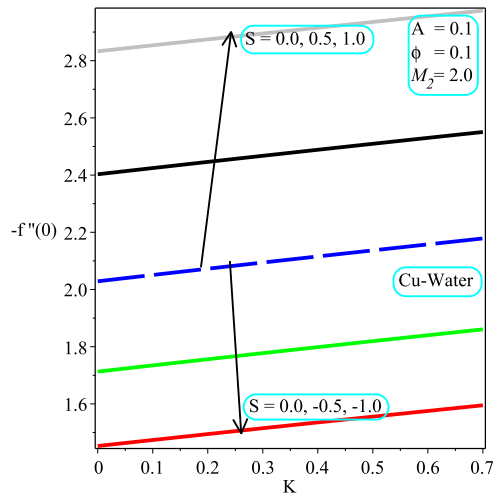


FIGURE 4.18: Impact of variation in S on $-f''(0)$

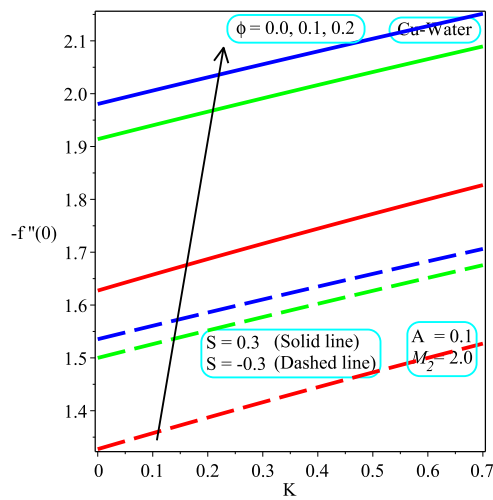


FIGURE 4.19: Impact of variation in ϕ on $-f''(0)$

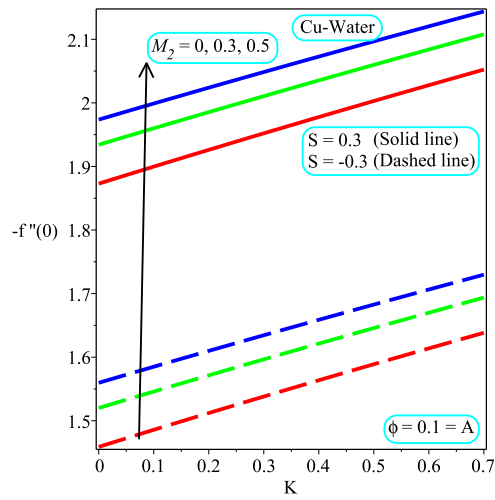


FIGURE 4.20: Impact of variation in M_2 on $-f''(0)$

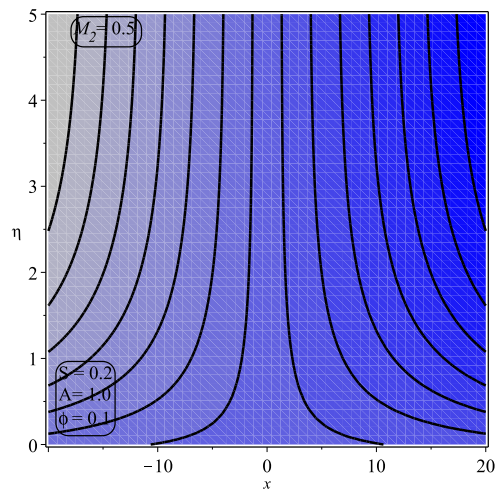


FIGURE 4.21: Contour plot for $M_2 = 0.5$

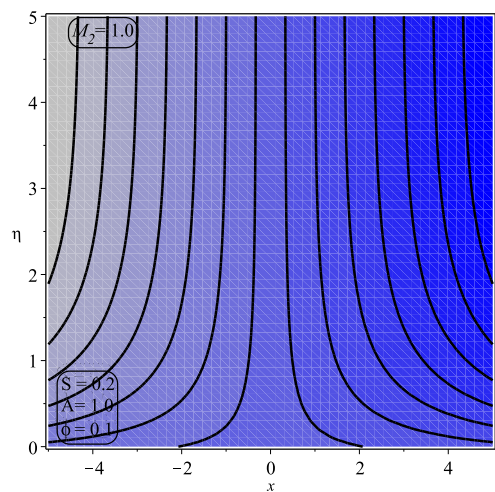


FIGURE 4.22: Contour plot for $M_2 = 1.0$

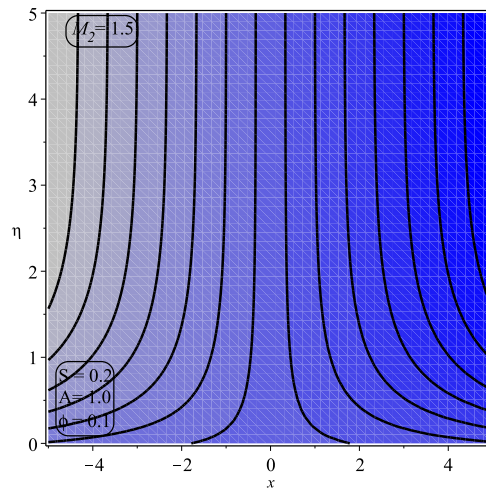


FIGURE 4.23: Contour plot for $M_2 = 1.5$

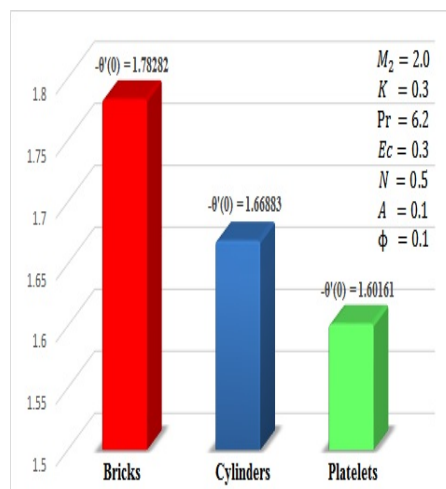


FIGURE 4.24: Impact of variation in m on $-\theta'(0)$

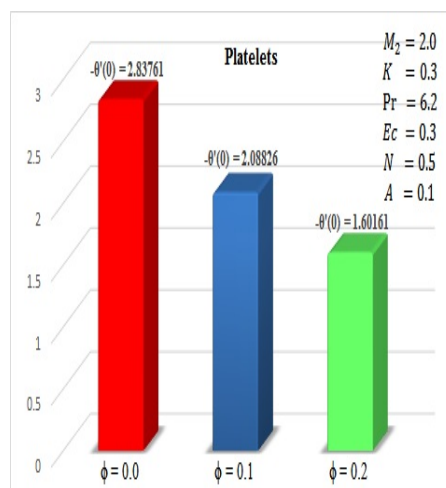


FIGURE 4.25: Impact of variation in ϕ on $-\theta'(0)$

TABLE 4.1: Thermal characteristics of conventional fluid and nanoparticles.

Physical characteristics	$\rho(kg\ m^{-3})$	$c_p(J/kgK)$	$K(W/mk)$
Water	997.1	4179	0.613
Cu	8933	385	400

TABLE 4.2: Numerical values of m (shape factor).




Nanoparticles	Shape	m
Bricks		$\frac{370}{100}$
Cylinders		$\frac{490}{100}$
Platelets		$\frac{570}{100}$

TABLE 4.3: Comparison table.

$S > 0$	3.5	4	4.5	5
Bhattacharyya et al. [102]	0.66667	1.00000	1.22871	1.43426
Present study	0.66667	1.00000	1.22871	1.43426

TABLE 4.4: Numerical values of $f''(0)$.

ϕ	A	M_2	S	$K = 0$	0.3	0.5	0.6	0.7
0	0.1	2	0.3	-2.15062	-2.21700	-2.26009	-2.28131	-2.30232
0.1				-1.81798	-1.89506	-1.94465	-1.96895	-1.99294
0.2				-1.51348	-1.60419	-1.66180	-1.68983	-1.71739
0.1	0			-1.82206	-1.90731	-1.96196	-1.98870	-2.01525
	0.2			-1.80567	-1.87483	-1.91947	-1.94138	-1.96303
	0.3			-1.78496	-1.84634	-1.88609	-1.90563	-1.92497
	0.1	0		-1.28712	-1.39628	-1.46420	-1.49691	-1.52887
		0.3		-1.38091	-1.48266	-1.54651	-1.57740	-1.60765
		0.5		-1.43978	-1.53735	-1.59887	-1.62869	-1.65795
		2	-1	-1.39512	-1.47083	-1.51961	-1.54352	-1.56714
			-0.5	-1.54363	-1.62046	-1.66990	-1.69413	-1.71806
			0	-1.70973	-1.78695	-1.83662	-1.86096	-1.88499
			0.5	-1.89371	-1.97054	-2.01999	-2.04422	-2.06814
			1	-2.09529	-2.17100	-2.21977	-2.24369	-2.26731

TABLE 4.5: Numerical values of $-\theta'(0)$ for $Ec = 0.3$, $m = 3.7$, $Pr = 6.2$ and $N = 0.5$.

ϕ	A	M_2	S	K	0	0.3	0.5	0.6	0.7	
0	0.1	2	0.3		2.8456	2.8376	2.8322	2.8296	2.8269	
0.1					2.2359	2.2262	2.2198	2.2167	2.2135	
0.2					1.7935	1.7828	1.7758	1.7723	1.7689	
0.2			-1		0.7939	0.7802	0.7709	0.7662	0.7614	
			-0.5		1.0302	1.0130	1.0015	0.9958	0.9901	
			0		1.4525	1.4389	1.4299	1.4255	1.4211	
			0.5		2.0508	2.0419	2.0360	2.0332	2.0303	
			1		2.7743	2.7688	2.7652	2.7634	2.7617	
A	M_2	K	S	ϕ	0	0.4	0.6	0.8	0.9	
0.1	2	0	0.3		2.8456	1.2072	0.8378	0.5503	0.3853	
		0.6			2.8296	1.1808	0.7993	0.4832	0.2955	
		1.2			2.8137	1.1566	0.7667	0.4366	0.2487	
		1.6			2.8032	1.1416	0.7476	0.4130	0.2285	
ϕ	K	M_2	Ec	S	A	0	0.4	0.6	0.8	1
0.1	0.3	0	0.5	0.3		2.5908	2.6314	2.6814	2.7650	2.9672
		1				2.3002	2.3238	2.3507	2.3889	2.4359
		2				2.0422	2.0548	2.0677	2.0828	2.0907
		3				1.8086	1.81346	1.8171	1.8182	1.8069

TABLE 4.6: Numerical values of $-\theta'(0)$ for $Ec = 0.3$, $m = 4.9$, $Pr = 6.2$ and $N = 0.5$.

ϕ	A	M_2	S	K	0	0.3	0.5	0.6	0.7	
0	0.1	2	0.3		2.8456	2.8376	2.8322	2.8296	2.8269	
0.1					2.1508	2.1409	2.1344	2.1312	2.1280	
0.2					1.6797	1.6688	1.6617	1.6582	1.6547	
0.2			-1		0.7634	0.7485	0.73844	0.7333	0.7281	
			-0.5		0.9820	0.9643	0.9526	0.9468	0.9410	
			0		1.3692	1.3554	1.3463	1.3419	1.3374	
			0.5		1.9135	1.9043	1.8984	1.8954	1.8925	
			1		2.5700	2.5643	2.5606	2.5588	2.5569	
A	M_2	K	S	ϕ	0	0.4	0.6	0.8	0.9	
0.1	2	0	0.3		2.8456	1.0940	0.7487	0.4946	0.3512	
		0.6			2.8296	1.0675	0.7102	0.4259	0.2587	
		1.2			2.8137	1.0435	0.6782	0.3809	0.2151	
		1.6			2.8032	1.0288	0.6597	0.3586	0.1967	
ϕ	K	M_2	Ec	S	A	0	0.4	0.6	0.8	1
0.1	0.3	0	0.5	0.3		2.4926	2.5333	2.5835	2.6674	2.8703
		1				2.2133	2.2374	2.2649	2.3045	2.3542
		2				1.9655	1.9788	1.9927	2.0096	2.0207
		3				1.7413	1.7470	1.7519	1.7550	1.7471

TABLE 4.7: Numerical values of $-\theta'(0)$ for $Ec = 0.3$, $m = 5.7$, $Pr = 6.2$ and $N = 0.5$.

ϕ	A	M_2	S	K	0	0.3	0.5	0.6	0.7	
0	0.1	2	0.3		2.8456	2.8376	2.8322	2.8296	2.8269	
0.1					2.0982	2.0882	2.0817	2.0784	2.0752	
0.2					1.6126	1.6016	1.5944	1.5909	1.5874	
0.2			-1		0.7443	0.7287	0.7181	0.7127	0.7073	
			-0.5		0.9525	0.9347	0.9228	0.9169	0.9111	
			0		1.3196	1.3056	1.2965	1.2920	1.2876	
			0.5		1.8329	1.8237	1.8176	1.8147	1.8118	
			1		2.4513	2.4455	2.4417	2.4398	2.4380	
A	M_2	K	S	ϕ	0	0.4	0.6	0.8	0.9	
0.1	2	0	0.3		2.8456	1.0307	0.7003	0.4647	0.3330	
		0.6			2.8296	1.0043	0.6620	0.3954	0.2396	
		1.2			2.8137	0.9806	0.6305	0.3516	0.1978	
		1.6			2.8032	0.9660	0.6124	0.3302	0.1805	
ϕ	K	M_2	Ec	S	A	0	0.4	0.6	0.8	1
0.1	0.3	0	0.5	0.3		2.4320	2.4727	2.5231	2.6072	2.8106
		1				2.1596	2.1840	2.2120	2.2523	2.3038
		2				1.9181	1.9318	1.9464	1.9643	1.9775
		3				1.6997	1.7059	1.7115	1.7158	1.7101

4.3 Conclusion

Final outcomes of the flow analysis are:

- The velocity profile is a decreasing function of ϕ and mass suction parameter $S > 0$ whereas it has an opposite behavior for the mass injection parameter $S < 0$ and velocity ratio parameter A .
- The temperature profile accelerates with an increment in the mass injection parameter, permeability parameter K , M_2 and ϕ .
- It is seen that the temperature field decreases by increasing $S > 0$, the Eckert number Ec , Pr and velocity ratio parameter A .
- An increment in $S > 0$ is found responsible for an augmentation in the rate of heat transfer.
- The impact of Platelets shaped nanoparticles are greater than that of cylinders and bricks in the temperature variation.
- The local Nusselt number is a decreasing function of Ec , Hartmann number and K .
- The local skin friction coefficient increases with an increase in ϕ and M_2 .

Chapter 5

Heat Transfer Analysis of Inclined Magnetic Field Induced by a Stretching Surface

This chapter, analyzes the simultaneous effect of inclined magnetic field and prescribed surface temperature (PST) on nanofluid flow provoked by a stretching surface. In order to make this mechanism more feasible, we have further considered the velocity slip and thermal radiation effects. Moreover, this perusal is made to consider the two kinds of nanofluid namely: *Cu*-water and *Al₂O₂*-water. Inclined magnetic field is utilized to accompanying an aligned angle that varies from 0 to $\pi/2$. The exact solutions are acquired from the transformed non-dimensional differential equations in the formation of confluent hypergeometric function. Lorentz forces and aligned magnetic field depict the significant effects on nanofluid. We found that due to an increase in the aligned angle provides an enhancement in the value of $-f''(0)$ and a reduction in the magnitude of $-\theta'(0)$. The combine impacts of an inclined magnetic field with other emerging parameters such as velocity slip, radiation parameter and nanoparticles ratio on velocity field, temperature field, $-f''(0)$ and $-\theta'(0)$ are examined. Flow behavior of nanofluid is also shown via stream lines pattern.

5.1 Mathematical Formulation

Consider two dimensional, steady, incompressible flow of nanofluid over a stretching sheet with slip effects at the surface. In this study, we consider the two kinds of nanofluid namely: Cu -water and Al_2O_2 -water. Inclined magnetic field is applied along y -axis of strength B_0 with an acute angle β and stretchable surface is taken along the x -axis. That is to suppose influenced magnetic field which is negated in correspondence with enforced magnetic range. The applied magnetic field occurs normal to the surface with transverse magnetic field at $\beta = \pi/2$ i.e. $\sin(\pi/2) = 1$.

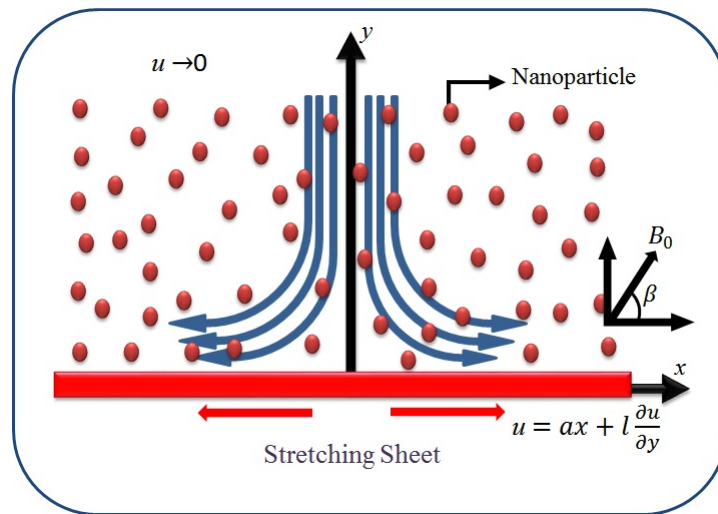


FIGURE 5.1: Geometrical view of the physical model

5.1.1 Continuity and Momentum Analysis

The elementary equations for considered flow are [116]:

$$\frac{\partial u}{\partial x} + \frac{\partial v}{\partial y} = 0, \quad (5.1)$$

$$u \frac{\partial u}{\partial x} + v \frac{\partial v}{\partial y} = \left(\frac{\mu_{nf}}{\rho_{nf}} \right) \frac{\partial^2 v}{\partial y^2} - \left(\frac{\sigma_{nf} B_0}{\rho_{nf}} \right) u \sin^2(\beta), \quad (5.2)$$

where u and v represent the velocity elements along x - and y - axis respectively. The subscript nf represents the nanofluid. μ_{nf} and ρ_{nf} the dynamic viscosity and

density regarding nanofluid respectively. The thermal diffusivity is expressed as α_{nf} , ν_{nf} the kinematic viscosity. The thermophysical correlation can be shown as follows [117]:

$$\left. \begin{aligned} \mu_{nf} &= \frac{\mu_f}{(1-\phi)^{2.5}}, & \alpha_{nf} &= \frac{k_{nf}}{(\rho c_p)_{nf}}, \\ (\rho c_p)_{nf} &= (1-\phi)(\rho c_p)_f + \phi(\rho c_p)_s, \\ \nu_{nf} &= \frac{\mu_{nf}}{\rho_{nf}}, & \rho_{nf} &= (1-\phi)\rho_f + \phi(\rho_s), \\ \frac{k_{nf}}{k_f} &= \frac{(k_s + 2k_f) - 2\phi(k_f - k_s)}{(k_s + 2k_f) + \phi(k_f - k_s)}, \\ \frac{\sigma_{nf}}{\sigma_f} &= 1 + \frac{3\left(\frac{\sigma_{nf}}{\sigma_f} - 1\right)\phi}{\left(\frac{\sigma_{nf}}{\sigma_f} + 2\right) - \left(\frac{\sigma_{nf}}{\sigma_f} - 1\right)\phi}. \end{aligned} \right\} \quad (5.3)$$

The nanoparticle volume fraction parameter is denoted by ϕ . The appropriate boundary conditions for the presented fluid model are

$$\left. \begin{aligned} u &= ax + l \frac{\partial u}{\partial y}, & v &= 0 & \text{at} & y = 0, \\ u &\rightarrow 0 & & & \text{as} & y \rightarrow \infty. \end{aligned} \right\} \quad (5.4)$$

Here l represents the characteristics length, for the sake of simplifying the analysis, the following similarity transformation is used [118].

$$u = axf'(\eta), \quad v = -(a\nu_f)^{0.5}f(\eta), \quad \eta = y \left(\frac{a}{\nu}\right)^{0.5}. \quad (5.5)$$

Using (5.5), we have

$$\frac{1}{A_1 A_2} f''' + f f'' - \left(f' + \frac{M_2}{A_2} \sin^2(\beta) \right) f' = 0, \quad (5.6)$$

the transformed boundary conditions are

$$\left. \begin{aligned} f(\eta) &= 0, & f'(\eta) &= 1 + L f''(\eta) & \text{at} & \eta = 0, \\ f'(\eta) &\rightarrow 0 & & & \text{as} & \eta \rightarrow \infty. \end{aligned} \right\} \quad (5.7)$$

In (5.7), $L = l(a/\nu)^{0.5}$, $A_2 = \left(1 - \phi + \phi \frac{\rho_s}{\rho_f}\right)$ and $A_1 = (1 - \phi)^{2.5}$. $M_2 = \sqrt{\frac{\sigma B_0^2}{\rho_f a}}$ the Hartmann number. L shows the velocity slip parameter. The closed form solution of (5.6) using (5.7) can be found as follows [119]:

$$f(\eta) = \frac{\chi - \chi e^{-\alpha_{5.1}\eta}}{\alpha_{5.1}}, \quad (5.8)$$

where

$$\chi = \frac{1}{L\alpha_{5.1} + 1}, \quad (5.9)$$

$$\alpha_{5.1} = \frac{\sqrt[3]{a_{5.1} + 12\sqrt{3}\sqrt{A_1}a_{5.6}L}}{6L} - \frac{2a_{5.5}}{3L\sqrt[3]{a_{5.1} + 12\sqrt{3}\sqrt{A_1}a_{5.6}L}} - 1/3 L^{-1}, \quad (5.10)$$

$$a_{5.1} = -72 M_2 A_1 L^2 \cos^2(\beta) + 72 M_2 A_1 L^2 + 108 A_1 L^2 A_2 - 8, \quad (5.11)$$

$$\begin{aligned} a_{5.2} = & 4 M_2^3 A_1^2 L^4 \cos^6(\beta) - 12 M_2^3 A_1^2 L^4 \cos^4(\beta) + 8 M_2^2 A_1 L^2 \cos^2(\beta) \\ & + 12 M_2^3 A_1^2 L^4 \cos^2(\beta), \end{aligned} \quad (5.12)$$

$$\begin{aligned} a_{5.3} = & -16 M_2^2 A_1 L^2 \cos^2(\beta) + 4 (\cos(\beta))^2 M_2 - 4 M_2^3 A_1^2 L^4 + 8 M_2^2 A_1 L^2 \\ & - 4 M_2, \end{aligned} \quad (5.13)$$

$$a_{5.4} = -36 M_2 A_1 L^2 \cos^2(\beta) A_2 + 36 M_2 A_1 L^2 A_2 + 27 A_1 L^2 A_2^2 - 4 A_2, \quad (5.14)$$

$$a_{5.5} = 3 M_2 A_1 L^2 \cos^2(\beta) - 3 M_2 A_1 L^2 - 1, \quad (5.15)$$

$$a_{5.6} = A_1 (a_{5.2} + a_{5.3} + a_{5.4}). \quad (5.16)$$

The Local skin friction is defined as

$$C_f = \frac{\tau_w}{\rho u_w^2} = \frac{Re_x^{-0.5}}{A_1} f''(0), \quad (5.17)$$

where $\tau_w = \mu_{nf} \left(\frac{\partial u}{\partial y} \right)_{y=0}$ represents the stress at wall and $Re_x = \frac{x u_w}{\nu}$ is the Reynolds number.

5.1.2 Heat Transfer Analysis

In this part, we analyzed the basic thermal boundary layer partial differential equation for incompressible nanofluid [120]:

$$u \frac{\partial T}{\partial x} + v \frac{\partial T}{\partial y} = \alpha_{nf} \frac{\partial^2 T}{\partial y^2} - \frac{1}{(\rho C_p)_{nf}} \frac{\partial q_r}{\partial y}, \quad (5.18)$$

where k_{nf} is thermal conductivity and ρ_{nf} the density of nanofluid, T the temperature and nanofluid specific heat is shown by $(C_p)_{nf}$. Utilizing the Roseland diffusion approximation [119] as radiation is defined as

$$q_r = -\frac{4\sigma^*}{3k^*} \frac{\partial T^4}{\partial y}. \quad (5.19)$$

Here σ^* represents the Stefan's constant and k^* stands for the mass absorption coefficient. Additionally, suppose that change of temperature inside of nanofluid flow is abundantly small-scale in such a way T^4 can be written in a Taylor series expanding about T_∞ . Further, ignore the terms which have higher power. As follows

$$T^4 \cong 4T_\infty^3 \left(T - \frac{3}{4} T_\infty \right). \quad (5.20)$$

Putting (5.19) into (5.18), we obtain

$$u \frac{\partial T}{\partial x} + v \frac{\partial T}{\partial y} = \alpha_{nf} \frac{\partial^2 T}{\partial y^2} - \frac{16\sigma^* T_\infty^3}{3(\rho C_p)_{nf} k^*} \frac{\partial^2 T}{\partial y^2}. \quad (5.21)$$

The boundary conditions are

$$T = T_w = T_\infty + T_0 \left(\frac{x}{l}\right)^2 \quad \text{at } y = 0 \text{ and } T \rightarrow \infty \quad \text{as } y \rightarrow \infty, \quad (5.22)$$

where T_w is the sheet temperature, T_0 expresses the constant reference temperature, T_∞ the free stream temperature and l the characteristics length. The dimensionless temperature profile $\theta(\eta)$ is given by [119]

$$\theta(\eta) = \frac{T - T_\infty}{T_w - T_\infty}. \quad (5.23)$$

Now, we transform (5.21) by using (5.5) and (5.23). We get the dimensionless ODE for energy equation is

$$\Psi\theta'' + Prf\theta' - 2Prf'\theta = 0, \quad (5.24)$$

where $\Psi = \left(A_3 + \frac{4N}{3}\right)$, $A_3 = \frac{(k_s + 2k_f) - 2\phi(k_f - k_s)}{(k_s + 2k_f) + \phi(k_f - k_s)}$, $N = \frac{4\sigma^*T_\infty^3}{K^*K_f}$. Prandtl number is represented by Pr . Accordingly, the boundary condition (5.22) get the form

$$\theta(\eta) = 1 \quad \text{at } \eta = 0, \quad \theta(\eta) \rightarrow 0 \quad \text{as } \eta \rightarrow \infty. \quad (5.25)$$

Using the values of f and f' from (5.8) in (5.24), we obtain

$$\Psi\theta'' + Pr\chi \left(\frac{1 - e^{-\alpha_{5.1}\eta}}{\alpha_{5.1}}\right)\theta' - 2Pr\chi \left(\frac{\alpha_{5.1}e^{-\alpha_{5.1}\eta}}{\alpha_{5.1}}\right)\theta = 0. \quad (5.26)$$

Here, we introduced a new variable $\xi_{5.1} = -\left(\frac{Pr\chi e^{-\alpha_{5.1}\eta}}{\Psi\alpha_{5.1}^2}\right)$ and the (5.26) reduces to

$$\xi_{5.1} \frac{\partial^2\theta}{\partial\xi_{5.1}^2} + (h - \xi_{5.1}) \frac{\partial\theta}{\partial\xi_{5.1}} - g\theta = 0, \quad (5.27)$$

where $h = 1 - \frac{Pr\chi}{\Psi\alpha_{5.1}^2}$ and $g = -2$. Subject to the boundary conditions

$$\theta \left(-\frac{Pr\chi e^{-\alpha_{5.1}\eta}}{\Psi\alpha_{5.1}^2} \right) = 1, \quad \text{and} \quad \theta(0) = 0. \quad (5.28)$$

The solution of (5.27) is given by

$$\theta(\xi_{5.1}) = \xi_{5.1}^{\left(\frac{b_{5.1} + b_{5.2}}{2}\right)} \frac{M \left(\frac{b_{5.1} + b_{5.2} - 4}{2}, 1 + b_{5.2}, \xi_{5.1} \right)}{M \left(\frac{b_{5.1} + b_{5.2} - 4}{2}, 1 + b_{5.2}, -b_{5.2} \right)}, \quad (5.29)$$

where $b_{5.1} = b_{5.2} = \frac{Pr\xi_{5.1}}{\Psi\alpha_{5.1}^2}$, M is the confluent hypergeometric function of the Kummer function [105] and the temperature solution takes the form

$$\theta(\eta) = e^{-\alpha_{5.1} \left(\frac{b_{5.1} + b_{5.2}}{2}\right)\eta} \frac{M \left(\frac{b_{5.1} + b_{5.2} - 4}{2}, 1 + b_{5.2}, -\frac{Pr\chi e^{-\alpha_{5.1}\eta}}{\Psi\alpha_{5.1}^2} \right)}{M \left(\frac{b_{5.1} + b_{5.2} - 4}{2}, 1 + b_{5.2}, -\frac{Pr\chi}{\Psi\alpha_{5.1}^2} \right)}. \quad (5.30)$$

Hence the non-dimensional wall temperature is

$$\theta'(0) = \left(\frac{M \left(\frac{b_{5.1} + b_{5.2} - 2}{2}, 1 + b_{5.2}, \frac{Pr\chi}{\Psi\alpha_{5.1}^2} \right) - M \left(\frac{b_{5.1} + b_{5.2} - 4}{2}, 1 + b_{5.2}, -\frac{Pr\chi}{\Psi\alpha_{5.1}^2} \right)}{M \left(\frac{b_{5.1} + b_{5.2} - 4}{2}, 1 + b_{5.2}, -\frac{Pr\chi}{\Psi\alpha_{5.1}^2} \right)} \right) \times \left(\frac{b_{5.1} + b_{5.2} - 4}{2} \right) \alpha_{5.1} - \alpha_{5.1} \left(\frac{b_{5.1} + b_{5.2}}{2} \right). \quad (5.31)$$

The local Nusselt number is defined as

$$k_f Nu_x = \frac{xq_w}{(T_w - T_\infty)}, \quad (5.32)$$

where $q_w = - \left(k_{nf} + \frac{16\sigma^* T_\infty^3}{3k_*} \right) \left(\frac{\partial T}{\partial y} \right)_{y=0}$. In the current case, it is determined as

$$Nu_x Re_x^{-0.5} = - \left(A_3 + \frac{4}{3N} \right) \theta'(0). \quad (5.33)$$

TABLE 5.1: Thermal characteristics of conventional fluid and solid nanoparticles.

Physical characteristics	$\rho(kg\ m^{-3})$	$c_p(J/kgK)$	$K(W/mk)$
Water	997.1	4179	0.613
<i>Cu</i>	8933	385	400
<i>Al₂O₃</i>	3970	765	40

5.2 Results and Discussion

In this section, we analyzed the effect of inclined magnetic field along with several physical parameters on nanofluid past a stretching surface. The geometry of the problem shown in Figure 5.1. In Table 5.1, thermal characteristics of water and used nanoparticles are presented in the form of density, specific heat and thermal conductivity are given as [121] and [122]. We have examined the two important types of nanoparticles, namely: alumina *Al₂O₃* and copper *Cu*, within the base fluid (water). Influence of ϕ with the base fluid are described through the velocity and temperature profile are depicted in Figures 5.2, 5.3, 5.8 and 5.9. It can be examined in Figure 5.2, an increase of the value of ϕ decreases the velocity behavior of nanofluid for *Cu*-water. In case of *Al₂O₃*-water, it is observed that an increment in the magnitude of ϕ enhances the velocity trend is shown in Figure 5.3. In Figures 5.8 and 5.9, the temperature profile described the behavior of *Cu*-water and *Al₂O₃*-water for an increasing value of the ϕ . Figures 5.4, 5.5, 5.10, 5.11, 5.14 and 5.15 show the simultaneous effect of angle β and M_2 on the velocity and temperature field for each *Cu* and *Al₂O₃* nanoparticles. It is found that an increase in M_2 and β decreasing the velocity profile; however it enhances the temperature distribution. There is no effect of M_2 on the velocity field for $\beta = 0^\circ$ and the magnetic field applied transversely in case of $\beta = \frac{\pi}{2}$ along the flow section. The magnetic induction increases with an enhancement in the magnitude of β along the flow region. Due to the improvement of magnetic induction, there is a resistant force that produces a resistance within the boundary layer flow with an aligned magnetic field effect.

The importance of L on the nanofluid velocity profile and temperature profile with prescribed surface temperature are plotted in Figures 5.6, 5.7, 5.12 and 5.13. In Figures 5.6 and 5.7, it can be determined that velocity profile switch its behavior at $\eta = 2.2$ due to the slip effects in the vicinity of sheet surface. The temperature profile increases in same manners with an increasing magnitude of L for each considered nanofluid are examined in Figures 5.12 and 5.13. The nanofluid velocity and temperature profile behave oppositely an increasing value of L . This behavior of stretching sheet can comprises just partially carried to the fluid. Figures 5.16 and 5.17 describe the impact of N on the temperature profile for each Cu -water and Al_2O_3 -water respectively. It is determine that temperature is reduces by an increment in the value of N .

Figures 5.18 and 5.19 depict M_2 influences herewith ϕ and aligned angle on $-f''(0)$. In Figure 5.18, the coefficient of local skin friction enhances by a gain in β and M_2 . Since there is no effect of M_2 with $\beta = 0$ on local skin friction, it shows the less Hartmann number effects on the fluid flow. In Figure 5.19, one can see the increasing behavior of $-f''(0)$ due to escalating the magnitude of ϕ and M_2 . Further, it is observed that copper based nanofluid has more friction with surface than the Al_2O_3 -water.

Figures 5.20 and 5.21 illustrate the effect of M_2 , L and ϕ on $-\theta'(0)$. It is examined that the value of $-\theta'(0)$ increases due to an increase in the value of ϕ . In Figure 5.20, it can be noticed that Cu -water represents the heat transfer rate is faster than Al_2O_3 -water. In Figure 5.21 the magnitude of $-\theta'(0)$ decreases by L in Cu -water and Al_2O_3 -water. Furthermore, it is observed that Al_2O_3 based nanofluid has low heat transport ratio as compare to the Cu based nanofluid. The combined results for β and M_2 are shown in Fig. Figure 5.22 which shows that these parameters reducing the trend of $-\theta'(0)$. The heat transfer rate is decreasing function of N and M_2 for Cu -Water and Al_2O_3 -water are expressed in Figures 5.23. In case of Al_2O_3 -water, heat transfer rate decreases faster than Cu -water as plotted in Figures 5.23 and Figures 5.23. To analyze the flow behavior, stream lines are also plotted in Figures 5.24-5.29.

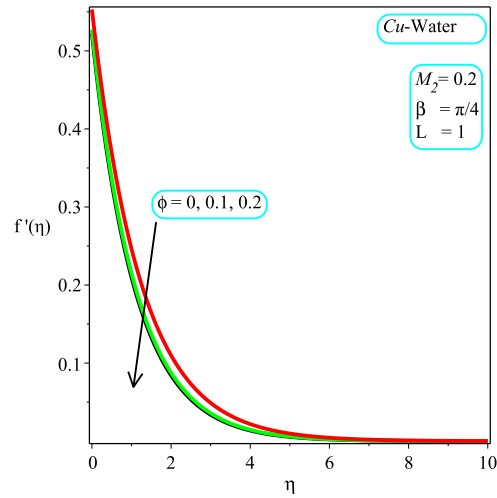


FIGURE 5.2: Impact of variation in ϕ on $f'(\eta)$

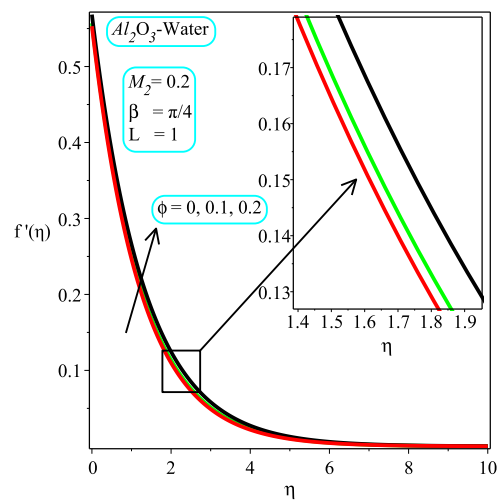


FIGURE 5.3: Impact of variation in ϕ on $f'(\eta)$

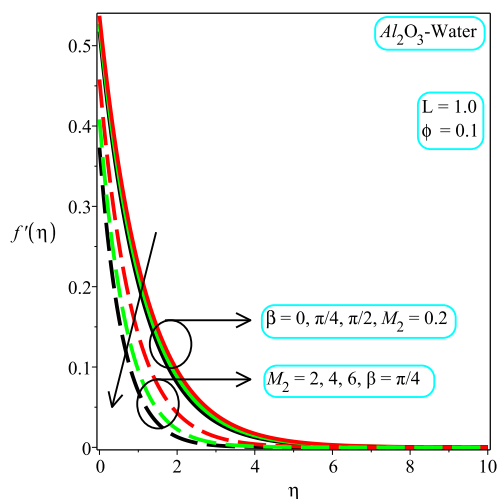


FIGURE 5.4: Impact of variation in β and M_2 on $f'(\eta)$

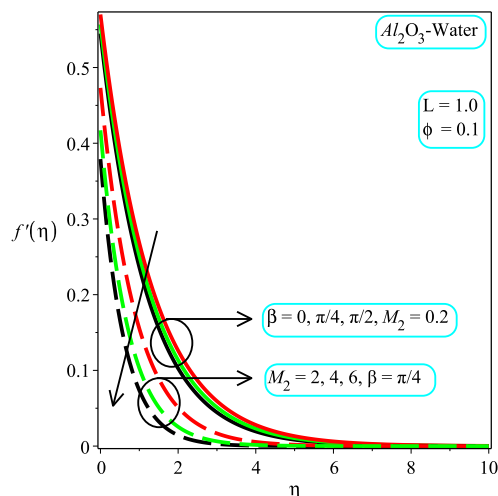


FIGURE 5.5: Impact of variation in β and M_2 on $f'(\eta)$

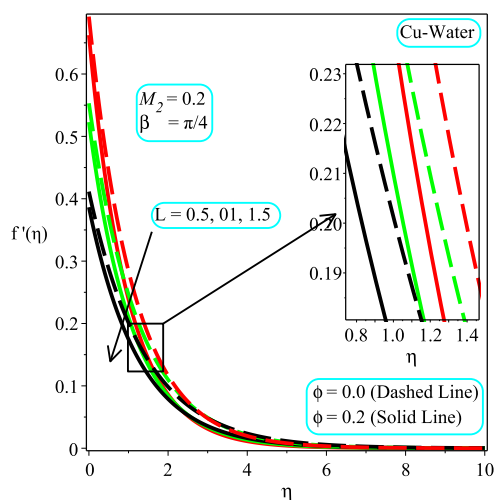


FIGURE 5.6: Impact of variation in L on $f'(\eta)$

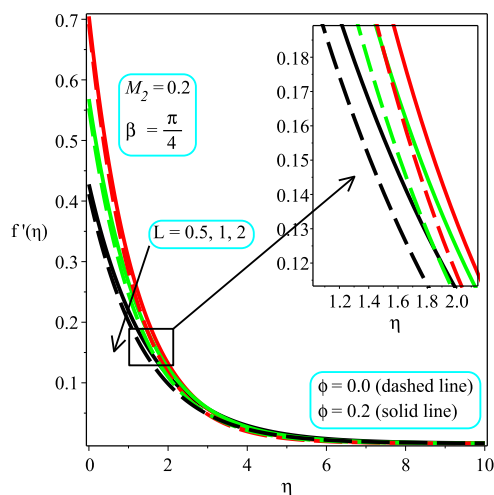


FIGURE 5.7: Impact of variation in L on $f'(\eta)$

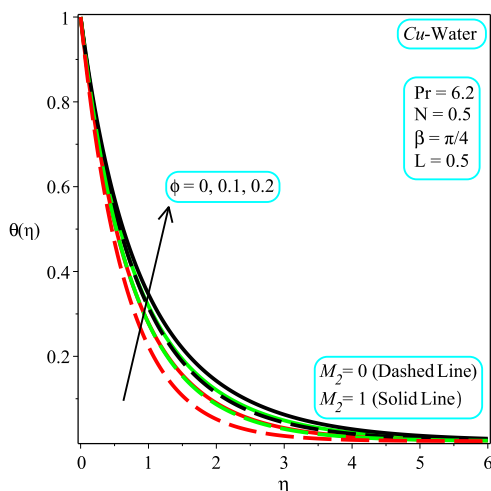


FIGURE 5.8: Impact of variation in ϕ on $\theta(\eta)$

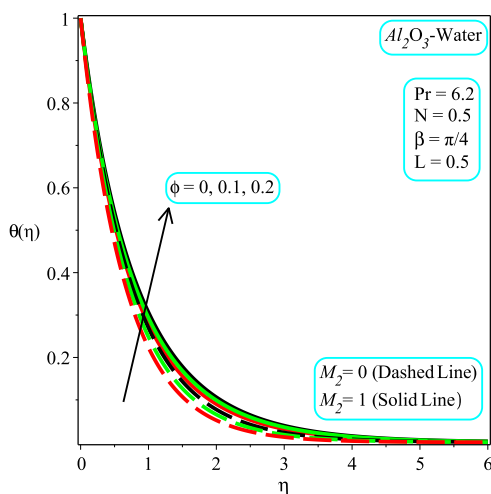


FIGURE 5.9: Impact of variation in ϕ on $\theta(\eta)$

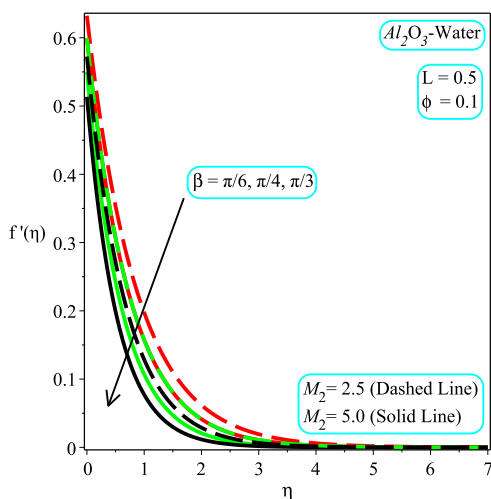


FIGURE 5.10: Impact of variation in β on $f'(\eta)$

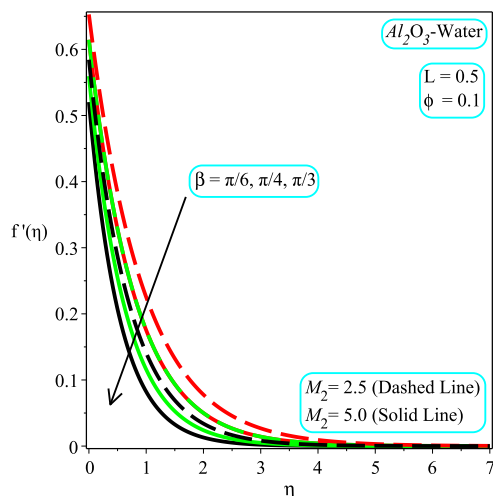


FIGURE 5.11: Impact of variation in β on $f'(\eta)$

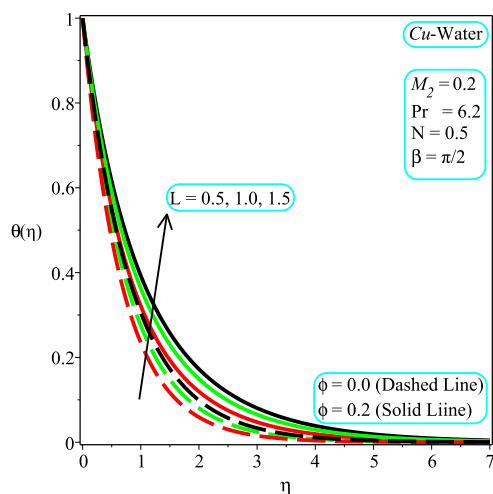


FIGURE 5.12: Impact of variation in L on $\theta(\eta)$

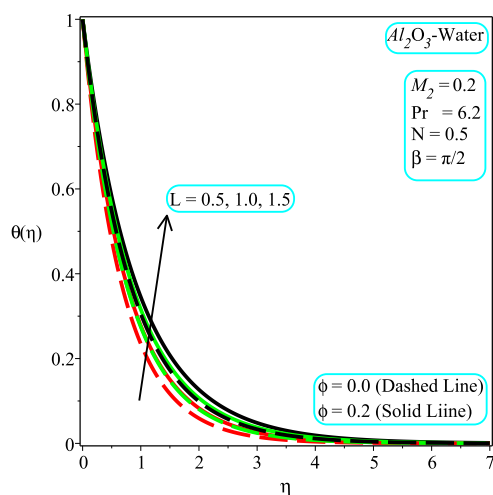


FIGURE 5.13: Impact of variation in L on $\theta(\eta)$

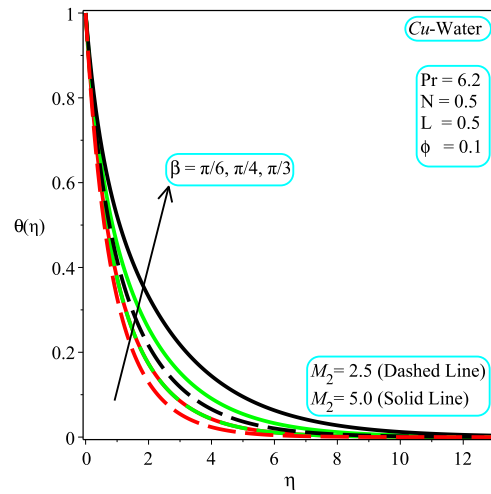


FIGURE 5.14: Impact of variation in β on $\theta(\eta)$

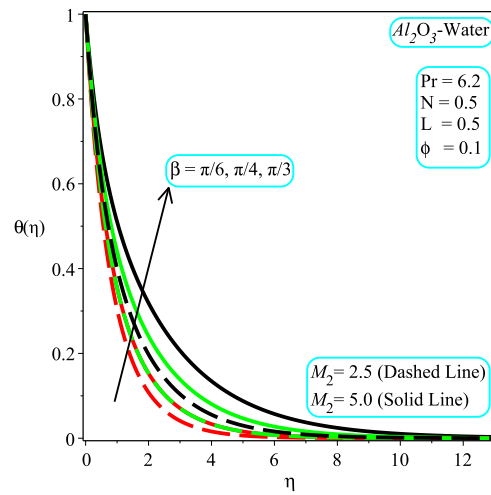


FIGURE 5.15: Impact of variation in β on $\theta(\eta)$

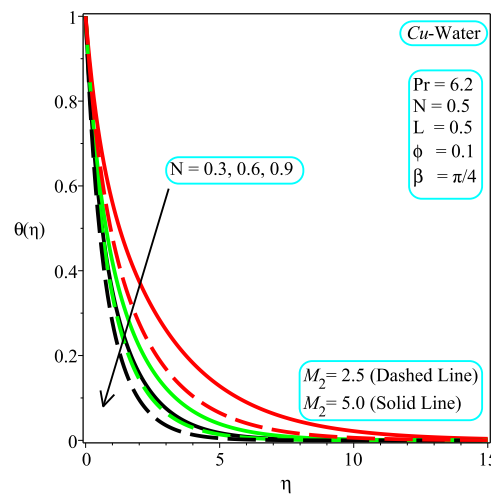


FIGURE 5.16: Impact of variation in N on $\theta(\eta)$

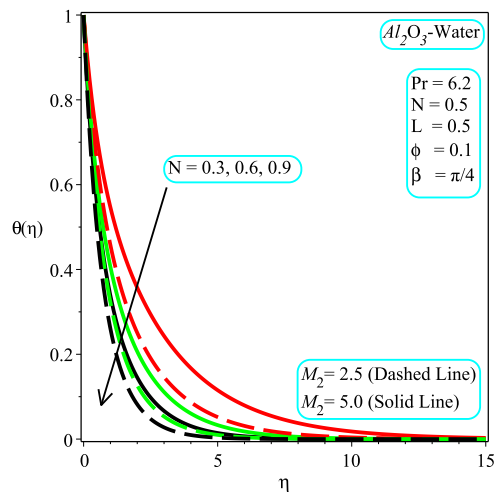


FIGURE 5.17: Impact of variation in N on $f'(\eta)$

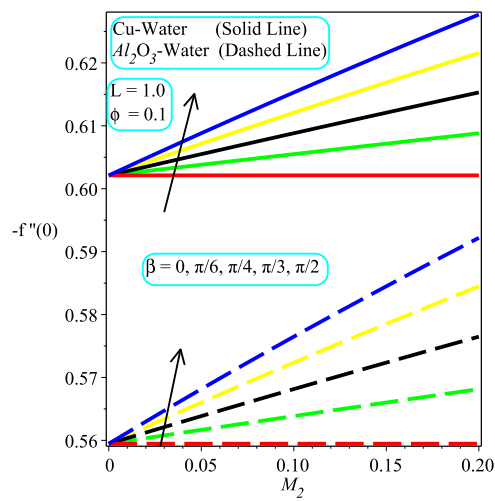


FIGURE 5.18: Impact of variation in β on $-f''(0)$

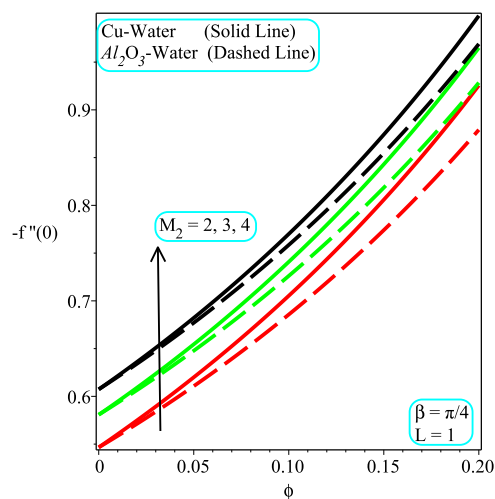


FIGURE 5.19: Impact of variation in M_2 on $-f''(0)$

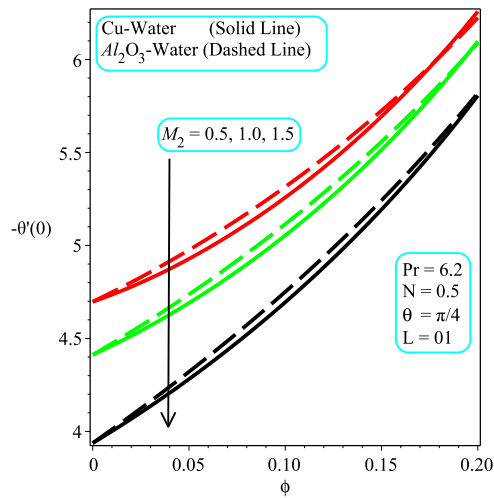


FIGURE 5.20: Impact of variation in M_2 on $-\theta'(0)$

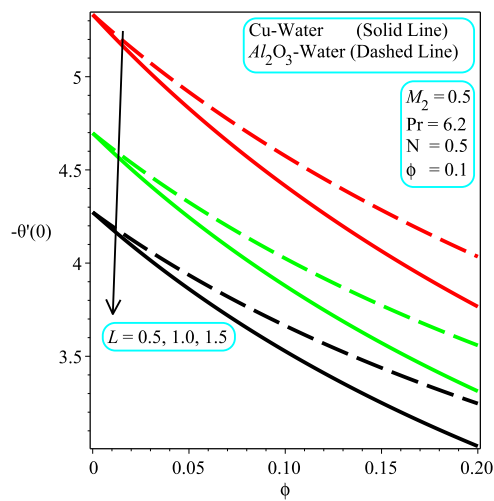


FIGURE 5.21: Impact of variation in L on $-\theta'(0)$

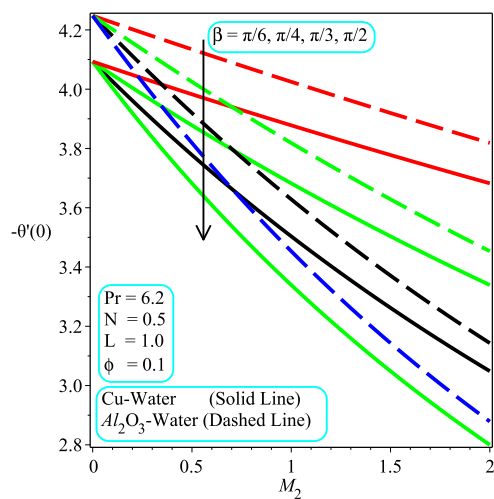


FIGURE 5.22: Impact of variation in β on $-\theta'(0)$

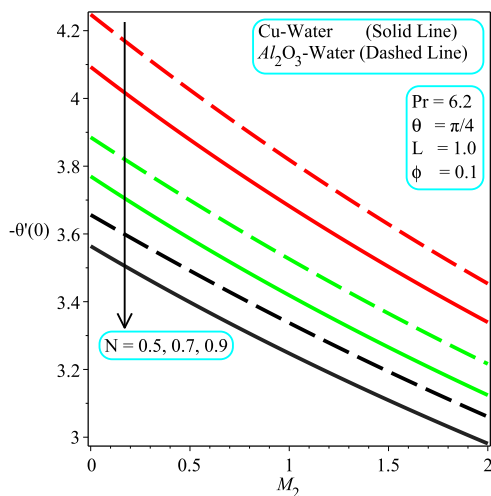


FIGURE 5.23: Impact of variation in N on $-\theta'(0)$

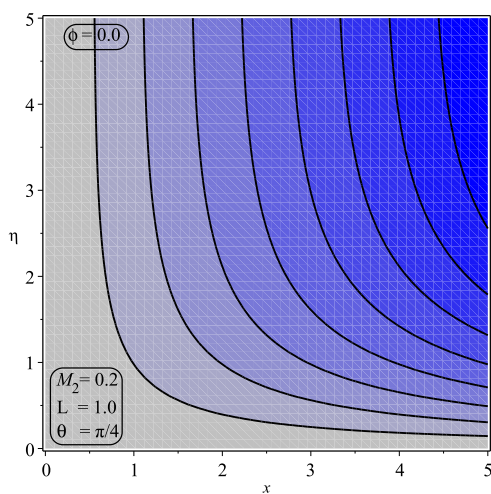


FIGURE 5.24: Contour plot for $\phi = 0.0$

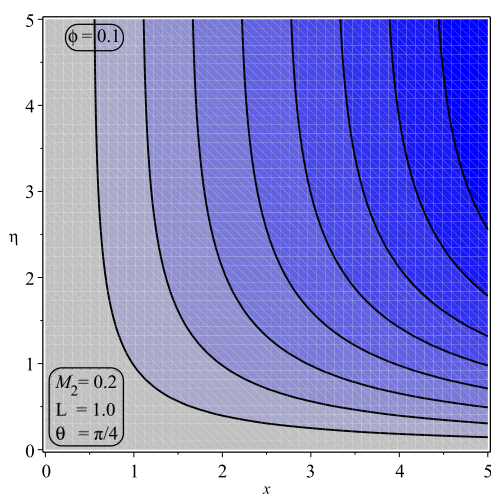


FIGURE 5.25: Contour plot for $\phi = 0.1$

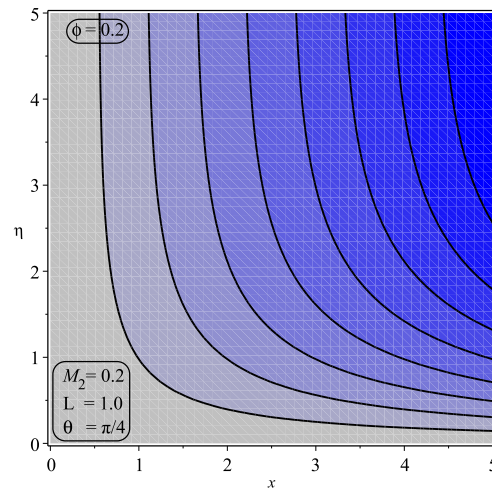


FIGURE 5.26: Contour plot for $\phi = 0.2$

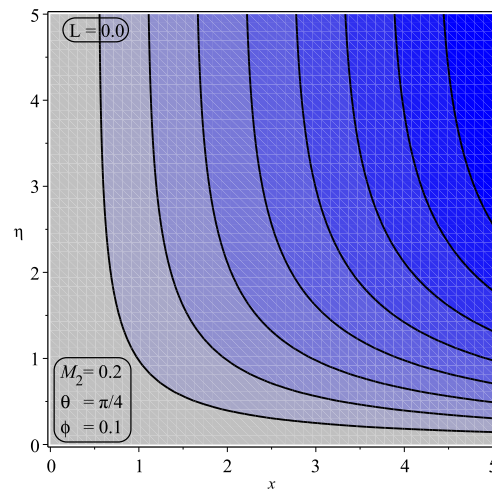


FIGURE 5.27: Contour plot for $L = 0.0$

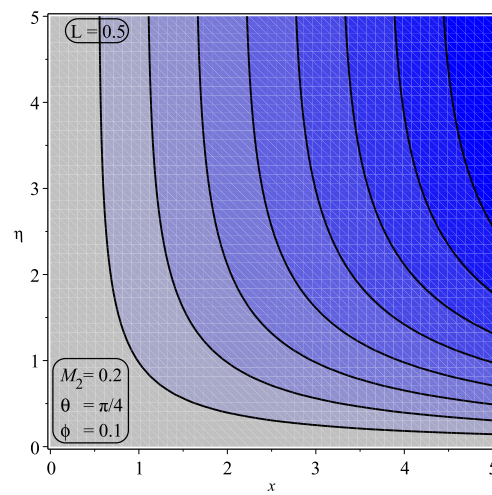
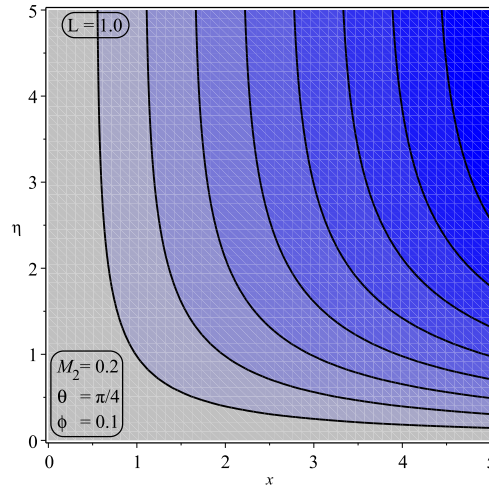


FIGURE 5.28: Contour plot for $L = 0.5$

FIGURE 5.29: Contour plot for $L = 1.0$

5.3 Conclusion

In this chapter, we have analyzed the effect of each β , velocity slip parameter and N on the flow of nanofluid past over a stretching sheet. This study has been carried out to examine the prescribed surface temperature and two types of nanofluid namely: Cu -water and Al_2O_3 -water. The following outcomes of the analysis are:

- The velocity profile of the nanofluid decreases by increasing the values of ϕ , Hartmann number, L , β and L for Cu -water/ Al_2O_3 -water.
- The velocity profile behavior is opposite for each Cu -water and Al_2O_3 -Water by gaining the rates of ϕ .
- The temperature profile increases by enhancing the value of ϕ , M_2 , β and L in case of both Cu water and Al_2O_3 water.
- The local skin friction coefficient gains by enhancing the values of M_2 and β in both Cu water and Al_2O_3 water. Moreover, it is observed that the local skin friction coefficient does not affected by $\beta = 0$ and Cu -water nanofluid but it is enhancing rapidly as compared to Al_2O_3 -water.

- The local Nusselt number decreases with an increment in the values of the Hartmann number, velocity ratio parameter, β and thermal radiation parameter for both *Cu*-Water and *Al₂O₃*-Water. The heat transfer rate is higher in *Al₂O₃*-Water as compared to the *Cu*-Water.

Chapter 6

Heat Transfer Analysis of Shaped Nanoparticles.

In this chapter, we analyze the magnetohydrodynamics flow of magnetite-engine oil based nanofluid with the impact of non-identical shaped nanoparticles subject to the porous medium, velocity slip, thermal radiation and Joule heating effects. The physical system is changed into the system of partial differential equations by mathematical modeling. To solve the dynamical system of equations, we converted the dynamical system of equations into the set of ordinary differential equation by suitable transformation. The closed form results are found for the momentum and energy equations. The effects of shaped nanoparticles with other physical parameters which are radiation parameter, velocity slip, and nanoparticles ratio on velocity field, temperature field, $-f''(0)$ and $-\theta'(0)$ are analyzed. Stream lines pattern is also plotted to study the flow behavior of nanofluid.

6.1 Mathematical Formulation

In this segment, we examine the two dimensional, steady, incompressible flow of magnetite-engine oil based fluid provoked by a stretching sheet. The fluid occupies the space $y > 0$. Magnetic field is applied along y -axis of strength B_0 which is

perpendicular to the surface and stretchable surface is taken parallel to the x -axis. That is to suppose influenced magnetic field which is negated in correspondence with enforced magnetic range. The applied magnetic field occurs normally to the surface. The sheet is stretchable along x -axis with a velocity $u = ax + l \frac{\partial u}{\partial y}$.

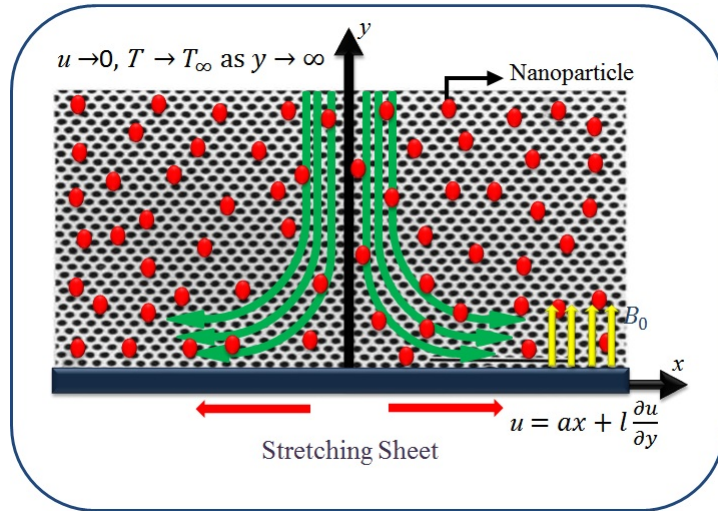


FIGURE 6.1: Geometrical view of the physical model

6.1.1 Continuity and Momentum Analysis

The elementary equations for the represented flow are [37]:

$$\frac{\partial u}{\partial x} + \frac{\partial v}{\partial y} = 0, \quad (6.1)$$

$$u \frac{\partial u}{\partial x} + v \frac{\partial v}{\partial y} = \frac{\mu_{nf}}{\rho_{nf}} \frac{\partial^2 u}{\partial y^2} - \frac{\sigma_{nf} B_0^2}{\rho_{nf}} u - \frac{\mu_{nf}}{\rho_{nf} k} u, \quad (6.2)$$

where u and v represent the velocity elements along x - and y -axis respectively, B_0 the magnetic parameter. The subscript nf expresses as the nanofluid. Hamilton and Crosser model (1962) is consider for different shaped particle to presenting a shape factor. The thermal correlations are expressed as [98, 99, 123]:

$$\left. \begin{aligned} \mu_{nf} &= \frac{\mu_f}{(1-\phi)^{2.5}}, & \alpha_{nf} &= \frac{k_{nf}}{(\rho c_p)_{nf}}, \\ (\rho c_p)_{nf} &= (1-\phi)(\rho c_p)_f + \phi(\rho c_p)_s, \\ \nu_{nf} &= \frac{\mu_{nf}}{\rho_{nf}}, & \rho_{nf} &= (1-\phi)\rho_f + \phi(\rho_s), \\ \frac{k_{nf}}{k_f} &= \frac{(k_s + (m+1)k_f) - (m+1)\phi(k_f - k_s)}{(k_s + (m+1)k_f) + \phi(k_f - k_s)}, \\ \frac{\sigma_{nf}}{\sigma_f} &= 1 + \frac{3\left(\frac{\sigma_{nf}}{\sigma_f} - 1\right)\phi}{\left(\frac{\sigma_{nf}}{\sigma_f} + 2\right) - \left(\frac{\sigma_{nf}}{\sigma_f} - 1\right)\phi}. \end{aligned} \right\} \quad (6.3)$$

In the above equations, $(\rho c_p)_f$ the heat capacity of the host fluid, ρ_f the density of the host fluid, ϕ the nanoparticle ratio, the thermal conductivity of host fluid shows by k_f , m the shape of nanopartilce, k_{nf} the thermal conductivity of nanoparticles. The suitable boundary conditions for considered flow are:

$$\left. \begin{aligned} u &= ax + l\frac{\partial u}{\partial y}, & v &= 0 & \text{at } y &= 0, \\ u &\rightarrow 0 & & & \text{as } y &\rightarrow \infty. \end{aligned} \right\} \quad (6.4)$$

To non-dimensionalize the variables, following similarity variables have been introduced [100]:

$$u = axf'(\eta), \quad v = -(\nu a)^{1/2}f(\eta), \quad \eta = y\left(\frac{a}{\nu}\right)^{1/2}. \quad (6.5)$$

After using the similarity transformation, the equation (??) is reduced to the form

$$f''' + A_1A_2ff'' - A_1A_2f'^2 - \left(A_1M_2 + \frac{1}{K}\right)f' = 0, \quad (6.6)$$

the boundary conditions are given as

$$\left. \begin{aligned} f(\eta) &= 0, & f'(\eta) &= 1 + Lf''(0), & \text{at } \eta &= 0, \\ f'(\eta) &\rightarrow 0 & & & \text{as } \eta &\rightarrow \infty. \end{aligned} \right\} \quad (6.7)$$

In (6.6) and (6.7), $M_2 = \sqrt{\frac{\sigma B_0^2}{\rho_f a}}$ is the Hartmann number, $A_1 = (1 - \phi)^{2.5}$ and $K = \frac{ak}{\nu_f}$ the permeability parameter. Furthermore, $A_2 = \left(1 - \phi + \phi \frac{\rho_s}{\rho_f}\right)$ and $L = l(a/\nu)^{1/2}$ the slip parameter. The analytical solution is obtained by Chakrabarti and Gupta [101] and [124].

$$f(\eta) = a_{6.1} + b_{6.1}e^{-\alpha_{6.1}\eta}. \quad (6.8)$$

By using (6.7) in (6.8), we obtain

$$f(\eta) = \frac{1}{L\alpha_{6.1} + 1} \left(\frac{1 - e^{-\alpha_{6.1}\eta}}{\alpha_{6.1}} \right). \quad (6.9)$$

Using (6.9) in (6.6), we get

$$\alpha_{6.1} = \frac{\sqrt[3]{a_{6.2}}}{6KL} + \frac{a_{6.3}}{3L\sqrt[3]{a_{6.2}}} - \frac{1}{3L}, \quad (6.10)$$

where

$$\begin{aligned} a_{6.2} &= \left(a_{6.4} + 12 \sqrt{-3 \frac{a_{6.5}}{K} L - 8K} \right) K^2, \\ a_{6.3} &= 2 \left(3A_1 KL^2 M_2 + 3L^2 + K \right), \\ a_{6.4} &= 108 A_1 A_2 KL^2 + 72 A_1 KL^2 M_2 + 72 L^2, \\ a_{6.5} &= 4 A_1^3 K^3 L^4 M_2^3 + 12 A_1^2 K^2 L^4 M_2^2 - 27 A_1^2 A_2^2 K^3 L^2 - 36 A_1^2 A_2 K^3 L^2 M_2 \\ &\quad - 8 A_1^2 K^3 L^2 M_2^2 + 12 A_1 KL^4 M_2 - 36 A_1 A_2 K^2 L^2 - 16 A_1 K^2 L^2 M_2 + 4, \\ &\quad A_1 A_2 K^3 + 4 A_1 K^3 M_2 + 4 L^4 - 8 KL^2 + 4 K^2. \end{aligned}$$

Using in (6.9), we obtain

$$a_{6.1} = \frac{1}{\left(L \left(\frac{\sqrt[3]{a_{6.2}}}{6KL} + \frac{a_{6.3}}{3L\sqrt[3]{a_{6.2}}} - \frac{1}{3L} \right)^2 + \frac{\sqrt[3]{a_{6.2}}}{6KL} + \frac{a_{6.3}}{3L\sqrt[3]{a_{6.2}}} - \frac{1}{3L} \right)}, \quad (6.11)$$

$$b_{6.1} = -\frac{1}{\left(L \left(\frac{\sqrt[3]{a_{6.2}}}{6KL} + \frac{a_{6.3}}{3L\sqrt[3]{a_{6.2}}} - \frac{1}{3L} \right)^2 + \frac{\sqrt[3]{a_{6.2}}}{6KL} + \frac{a_{6.3}}{3L\sqrt[3]{a_{6.2}}} - \frac{1}{3L} \right)}, \quad (6.12)$$

where $a_{6,1}$, $b_{6,1}$ and $\alpha_{6,1}$ are constants with $\alpha_{6,1} > 0$. Now, using the above constants in 6.9, we get the following velocity profile solution

$$f(\eta) = \frac{1}{\left(L \left(\frac{\sqrt[3]{a_{6.2}}}{6KL} + \frac{a_{6.3}}{3L\sqrt[3]{a_{6.2}}} - \frac{1}{3L} \right)^2 + \frac{\sqrt[3]{a_{6.2}}}{6KL} + \frac{a_{6.3}}{3L\sqrt[3]{a_{6.2}}} - \frac{1}{3L} \right)} e^{-\left(\frac{\sqrt[3]{a_{6.2}}}{6KL} + \frac{a_{6.3}}{3L\sqrt[3]{a_{6.2}}} - \frac{1}{3L} \right) \eta} - \frac{1}{\left(L \left(\frac{\sqrt[3]{a_{6.2}}}{6KL} + \frac{a_{6.3}}{3L\sqrt[3]{a_{6.2}}} - \frac{1}{3L} \right)^2 + \frac{\sqrt[3]{a_{6.2}}}{6KL} + \frac{a_{6.3}}{3L\sqrt[3]{a_{6.2}}} - \frac{1}{3L} \right)}. \quad (6.13)$$

The mathematical expression for local skin friction is expressed as

$$C_f = \frac{\tau_w}{\rho u_w^2} = \frac{Re_x^{-0.5}}{A_1} f''(0), \quad (6.14)$$

in (6.14), $\tau_w = \mu_{nf} \left(\frac{\partial u}{\partial y} \right)_{y=0}$ is the stress at wall and $Re_x = \frac{xu_w}{\nu}$ the Reynolds number.

6.1.2 Heat Transfer Analysis

In this section, study the heat transport in existence of the thermal radiation and Joule heating phenomenon has been presented. The governing equation is given as [125]:

$$u \frac{\partial T}{\partial x} + v \frac{\partial T}{\partial y} = \alpha_{nf} \frac{\partial^2 T}{\partial y^2} - \frac{1}{(\rho C_p)_{nf}} \frac{\partial q_r}{\partial y} + \frac{\sigma_{nf} B_0^2}{(\rho C_p)_{nf}} u^2, \quad (6.15)$$

where

$$q_r = -\frac{4\sigma^*}{3k^*} \frac{\partial T^4}{\partial y}. \quad (6.16)$$

Here, α_{nf} the thermal diffusivity, T shows the temperature field and specific heat is denoted by $(C_p)_{nf}$. Using (6.16) into (6.15), we get

$$u \frac{\partial T}{\partial x} + v \frac{\partial T}{\partial y} = \alpha_{nf} \frac{\partial^2 T}{\partial y^2} + \frac{1}{3(\rho C_p)_{nf}} \frac{16\sigma^* T_\infty^3}{k^*} \frac{\partial^2 T}{\partial y^2} + \frac{\sigma_{nf} B_0^2}{(\rho C_p)_{nf}} u^2. \quad (6.17)$$

The boundary conditions are

$$\left. \begin{aligned} T = T_w = T_\infty + T_0(x/l)^2 & \quad \text{at} \quad y = 0, \\ T \rightarrow T_\infty & \quad \text{as} \quad y \rightarrow \infty. \end{aligned} \right\} \quad (6.18)$$

Here, T_0 expresses the constant reference temperature, l denotes the characteristic length, T_w is the temperature at sheet and the free stream temperature is represented by T_∞ . The similarity variable is given by [125]:

$$\theta(\eta) = \frac{T - T_\infty}{T_w - T_\infty}. \quad (6.19)$$

The following dimensionless energy equation is found after utilizing the similarity variables defined in (6.5) and (6.19)

$$\Psi\theta'' + Prf\theta' - 2Prf'\theta + \frac{PrM_2}{A_4}Ec f'^2 = 0, \quad (6.20)$$

where

$$Ec = \frac{u^2}{(T_w - T_\infty) Cp}, \quad Pr = \frac{\nu_f}{\alpha_f}, \quad N = \frac{4\sigma^*T_\infty^3}{K^*K_f}, \quad \Psi = \left(A_3 + \frac{4N}{3} \right)$$

$$A_3 = \frac{(k_s + 2k_f) + (-2\phi k_f + 2\phi k_s)}{(k_s + 2k_f) + 2\phi(k_f - k_s)}, \quad A_4 = \left(1 - \phi + \phi \frac{(\rho Cp)_s}{(\rho Cp)_f} \right). \quad (6.21)$$

Here Pr expresses the Prandtl number, Ec the Eckert number and N the radiation parameter. The reduced boundary condition are:

$$\left. \begin{aligned} \theta(\eta) = 1 & \quad \text{at} \quad \eta = 0, \\ \theta(\eta) \rightarrow 0 & \quad \text{as} \quad \eta \rightarrow \infty. \end{aligned} \right\} \quad (6.22)$$

Now, substituting (6.9) in (6.20), one can have

$$\Psi\theta_{\eta\eta} + Pr \left(\chi \left(\frac{1 - e^{-\alpha_{6.1}\eta}}{\alpha_{6.1}} \right) \right) \theta_\eta - 2Pr\chi e^{-\alpha_{6.1}\eta}\theta + \frac{PrM_2}{A_4}Ec (\chi e^{-\alpha_{6.1}\eta})^2 = 0. \quad (6.23)$$

Any linear differential equation of second order can be reduced to Kummer's ordinary differential equation. For this purpose, a new variable

$$\xi_{6.1} = -\frac{Pr \chi e^{-\alpha_{6.1}\eta}}{\Psi \alpha_{6.1}^2}, \quad (6.24)$$

is introduced.

As a result, (6.23) becomes Kummer's ordinary differential equation:

$$\xi_{6.1} \frac{\partial^2 \theta}{\partial \xi_{6.1}^2} + (h - \xi_{6.1}) \frac{\partial \theta}{\partial \xi_{6.1}} - g\theta = -\frac{Pr M_2 \chi}{A_4} Ec (e^{-\alpha_{6.1}\eta})^2, \quad (6.25)$$

where $h = (1 - P)$, $P = \frac{Pr \chi}{\Psi \alpha_{6.1}^2}$, $\chi = \frac{1}{L\alpha_{6.1} + 1}$ and $g = -2$. The boundary conditions are taken as

$$\theta(\xi_{6.1}) = 1, \quad \theta(0) = 0. \quad (6.26)$$

The closed form solution of (6.25) with (6.26) in the form of the Kummer's functions [105] is given as

$$\begin{aligned} \theta(\xi_{6.1}) = & \frac{-(\xi_{6.1} m_1 M_2 Ec, \alpha_{6.1}^2) \Psi}{2 Pr A_4 m_4 m_5} + \frac{\left(-\frac{\xi_{6.1} m_6 \alpha_{6.1}^2 \Psi (L\alpha_{6.1} + 1)}{Pr}\right)^{m_7} m_2 m_9}{2 m_6^{m_7} m_3 \Psi^2 \alpha_{6.1}^4 A_4 m_4 m_5} \\ & + \frac{\xi_{6.1} M_2 Ec \alpha_{6.1}^2 \Psi}{2 Pr A_4}, \end{aligned} \quad (6.27)$$

where

$$\begin{aligned} m_1 = & \left(1 - \frac{Pr}{(L\alpha_{6.1} + 1) \Psi \alpha_{6.1}^2}\right)^2 + (2\xi_{6.1} + 1) \left(1 - \frac{Pr}{(L\alpha_{6.1} + 1) \Psi \alpha_{6.1}^2}\right) \\ & + \xi_{6.1}^2 + 2\xi_{6.1}, \\ m_2 = & M \left(-2 + \frac{Pr}{(L\alpha_{6.1} + 1) \Psi \alpha_{6.1}^2}, 1 + \frac{Pr}{(L\alpha_{6.1} + 1) \Psi \alpha_{6.1}^2}, -\xi_{6.1}\right), \\ m_3 = & M \left(\frac{Pr}{(L\alpha_{6.1} + 1) \Psi \alpha_{6.1}^2} - 2, 1 + \frac{Pr}{(L\alpha_{6.1} + 1) \Psi \alpha_{6.1}^2}, \frac{-Pr}{(L\alpha_{6.1} + 1) \Psi \alpha_{6.1}^2}\right), \\ m_4 = & 1 - \frac{Pr}{(L\alpha_{6.1} + 1) \Psi \alpha_{6.1}^2}, \quad m_5 = 2 - \frac{Pr}{(L\alpha_{6.1} + 1) \Psi \alpha_{6.1}^2}, \\ m_6 = & -\frac{Pr}{(L\alpha_{6.1} + 1) \Psi \alpha_{6.1}^2}, \end{aligned}$$

$$m_7 = \frac{Pr}{(L\alpha_{6.1} + 1) \Psi \alpha_{6.1}^2}, \quad m_8 = \frac{-2 \xi_{6.1} Ec M_2 \alpha_{6.1}^4 \Psi^2 Pr}{(L\alpha_{6.1} + 1) Pr},$$

$$m_9 = 2 \Psi^2 \alpha_{6.1}^4 A_4 m_4^2 + 2 \Psi^2 \alpha_{6.1}^4 A_4 m_4 + m_4 m_8 - m_8 + \frac{\xi_{6.1} Ec M_2 Pr \alpha_{6.1}^2 \Psi}{(L\alpha_{6.1} + 1)^2}.$$

Here, M represents the confluent hypergeometric function of the 1st kind. The solution of 6.23 are defined as follows

$$\theta(\eta) = \frac{m'_1 M_2 Ec e^{-\alpha_{6.1} \eta}}{(2 L\alpha_{6.1} + 2) A_4 m_4 m_5} + \frac{(m_6 e^{-\alpha_{6.1} \eta})^{m_7} m'_2 m'_9}{2 m_6^{m_7} m_3 \Psi^2 \alpha_{6.1}^4 A_4 m_4 m_5} - \frac{Ec M_2 e^{-\alpha_{6.1} \eta}}{(2 L\alpha_{6.1} + 2) A_4}, \quad (6.28)$$

where

$$m'_1 = \left(1 - \frac{Pr}{(L\alpha_{6.1} + 1) \Psi \alpha_{6.1}^2}\right)^2 + \left(2 \frac{Pr e^{-\alpha_{6.1} \eta}}{(L\alpha_{6.1} + 1) \Psi \alpha_{6.1}^2} + 1\right)$$

$$\times \left(1 - \frac{Pr}{(L\alpha_{6.1} + 1) \Psi \alpha_{6.1}^2}\right) + \frac{Pr^2 (e^{-\alpha_{6.1} \eta})^2}{(L\alpha_{6.1} + 1)^2 \Psi^2 \alpha_{6.1}^4} + \frac{2Pr e^{-\alpha_{6.1} \eta}}{(L\alpha_{6.1} + 1) \Psi \alpha_{6.1}^2},$$

$$m'_2 = M \left(-2 + \frac{Pr}{(L\alpha_{6.1} + 1) \Psi \alpha_{6.1}^2}, 1 + \frac{Pr}{(L\alpha_{6.1} + 1) \Psi \alpha_{6.1}^2}, \frac{-Pr e^{-\alpha_{6.1} \eta}}{(L\alpha_{6.1} + 1) \Psi \alpha_{6.1}^2}\right),$$

$$m'_8 = 2 \frac{Ec M_2 e^{-\alpha_{6.1} \eta} \alpha_{6.1}^2 \Psi Pr}{(L\alpha_{6.1} + 1)^2},$$

$$m'_9 = 2 \Psi^2 \alpha_{6.1}^4 A_4 m_4^2 + 2 \Psi^2 \alpha_{6.1}^4 A_4 m_4 + m_4 m'_8 - m'_8 - \frac{Ec M_2 e^{\alpha_{6.1} \eta} Pr^2}{(L\alpha_{6.1} + 1)^3}.$$

$$\theta_\eta(0) = \frac{-C_3 M_2 Ec}{(2 L\alpha_{6.1} + 2) A_4 C_1 C_2} + \frac{C_4 M_2 Ec \alpha_{6.1}}{(2 L\alpha_{6.1} + 2) A_4 C_1 C_2}$$

$$+ \frac{C_5 Pr C_8 C_6}{2 (L\alpha_{6.1} + 1) \Psi^3 \alpha_{6.1}^5 C_5 C_8 A_4 C_1 C_2} - C_{10}, \quad (6.29)$$

where

$$C_1 = 1 - \frac{Pr}{(L\alpha_{6.1} + 1) \Psi \alpha_{6.1}^2}, \quad C_2 = 2 - \frac{Pr}{(L\alpha_{6.1} + 1) \Psi \alpha_{6.1}^2},$$

$$C_3 = \frac{-2prC_1}{\alpha_{6.1} (L\alpha_{6.1} + 1) \Psi} - \frac{2Pr^2}{(L\alpha_{6.1} + 1)^2 \Psi^2 \alpha_{6.1}^3} - \frac{2Pr}{\alpha_{6.1} (L\alpha_{6.1} + 1) \Psi},$$

$$C_4 = C_1^2 + \left(2 \frac{Pr}{(L\alpha_{6.1} + 1) \Psi \alpha_{6.1}^2} + 1\right) C_1 + \frac{Pr^2}{(L\alpha_{6.1} + 1)^2 \Psi^2 \alpha_{6.1}^4}$$

$$\begin{aligned}
& + \frac{2pr}{(L\alpha_{6.1} + 1) \Psi \alpha_{6.1}^2}, \\
C_5 & = \left(-\frac{Pr}{(L\alpha_{6.1} + 1) \Psi \alpha_{6.1}^2} \right)^{1-C_1}, \\
C_6 & = \frac{-2Ec M_2 C_1 \alpha_{6.1}^2 \Psi Pr}{(L\alpha_{6.1} + 1)^2} + 2 \Psi^2 \alpha_{6.1}^4 A_4 C_1^2 - \frac{2Ec M_2 \alpha_{6.1}^2 \Psi Pr}{(L\alpha_{6.1} + 1)^2} \\
& + 2 \Psi^2 \alpha_{6.1}^4 A_4 C_1 - \frac{Ec M_2 Pr^2}{(L\alpha_{6.1} + 1)^3}, \\
C_7 & = 2 \frac{Ec M_2 \alpha_{6.1}^3 C_1 \Psi Pr}{(L\alpha_{6.1} + 1)^2} + 2 \frac{Ec M_2 \alpha_{6.1}^3 \Psi Pr}{(L\alpha_{6.1} + 1)^2} + \frac{Ec M_2 \alpha_{6.1} e Pr^2}{(L\alpha_{6.1} + 1)^3}, \\
C_8 & = M \left(-C_2, 1 + \frac{Pr}{(L\alpha_{6.1} + 1) \Psi \alpha_{6.1}}, C_1 - 1 \right), \\
C_9 & = M \left(-C_1, 2 + \frac{Pr}{(L\alpha_{6.1} + 1) \Psi \alpha_{6.1}^2}, C_1 - 1 \right), \\
C_{10} & = -\frac{C_9 Pr C_6}{\alpha_{6.1}^5 (L\alpha_{6.1} + 1) \Psi^3 C_8 A_4 C_1} \left(2 + 2 \frac{Pr}{(L\alpha_{6.1} + 1) \Psi \alpha_{6.1}^2} \right)^{-1} \\
& - C_7 \frac{1}{2 \Psi^2 \alpha_{6.1}^4 A_4 C_1 C_2}.
\end{aligned}$$

The expression of the local Nusselt number as follows:

$$Nu = \frac{-k_{nf} x \left(\frac{\partial T}{\partial y} \right)_{y=0}}{k_f (T_w - T_\infty)} = -\frac{k_{nf}}{k_f} Re_x^{1/2} \theta_\eta(0). \quad (6.30)$$

In the current study, the local Nusselt number is

$$\frac{k_f}{k_{nf}} Nu_x Re_x^{-1/2} = -\theta_\eta(0). \quad (6.31)$$

6.2 Results and Discussion

The effect of the several physical parameters on the velocity and temperature profiles have been shown in this section in order to examine the behavior of these parameters. Geometrical view of the physical model is depicted in Figure 6.1. Figure 6.2 is prepared to check the trend of the velocity field for ϕ in the presence of the L separately, while keeping M_2 and K constant. It is examined that the velocity field is enhanced by increasing the magnitude of ϕ . Impact of the velocity

slip parameter is illustrated in Figure 6.3. It is observed that the velocity profile reduces with a decrements in the slip parameter is depicted in Figure 6.3. An increase in the M_2 strongly accelerates the velocity profile shown in Figure 6.4. Moreover, it is noted that the velocity profile rises by an increment within M_2 .

Physical insight of the temperature field along with effect of L , K , N , Pr , M_2 and ϕ is plotted in Figures 6.5-6.9 respectively. The temperature profile develops rapidly for ϕ . It is observed that platelets shaped nanoparticles has high temperature profile than the cylinder and brick shaped nanoparticles see in Figure 6.5. In Figure 6.6, the influence of M_2 on the temperature field is discussed. Additionally, it is concluded that an increment into the magnitude of M_2 shows an increasing trend of the temperature filed. It is expressed that the temperature profile enhances due to less heat conduction. Therefore, we can concluded that the heat conduction is comparatively less in platelets nanoparticles than the cylinder and brick shaped nanoparticles. The effect of L on the temperature field is portrayed in Figure 6.7. It is seen that increasing the velocity slip parameter, the temperature field is enhanced. Figure 6.8 portrays the impact of the Prandtl number on the temperature profile. It is seen that the temperature profile decelerates by enhancing the magnitude of Pr . As Pr is inversely proportional to the thermal conductivity of the fluid, therefore heat may diffuse faster from the sheet in case of the low-Prandtl fluid number as compared the case of a fluid having high Pr magnitude. The impact of N is displayed in Figure 6.9. It is noticed that the temperature field accelerates because of an increment in the magnitude of N .

Figure 6.10 expresses the influence of Ec on the non-dimensional temperature gradient $-\theta'(0)$. It can be observed that the non-dimensional temperature gradient enhances by an increment in Ec . Physically, Ec is the ratio of advective transport to heat dissipation potential. Moreover, an increment in the energy transport rate indicates that the heat dissipation is decreases in Ec . Figure 6.11 shows diminishing behavior of the heat transport rate by increasing the magnitude of M_2 . The impact of Pr on the heat transfer rate is reflected in Figure 6.12. It is examined that the value of $-\theta'(0)$ increases by an increase in Pr . Figure 6.13 illustrates the rise in a heat transfer rate for radiation parameter. Additionally, increasing rate of

the local Nusselt number is more high in case of platelets shaped nanoparticles. It is noticed through Figure 6.14 that the local skin friction coefficient is accelerated for an increasing the value of M_2 . In Figure 6.15, the magnitude of $-f''(0)$ reduces gradually by an increment in L . A decrements in $-f''(0)$ by enhancing ϕ is concluded through Figure 6.16. In Figure 6.17, the magnitude of $-f''(0)$ decreases with an increment in the permeability parameter.

Table 6.1, shows the thermal characteristics of engine oil and magnetite are given as [126] and [127]. Table 6.2 displays the nanoparticles shape with their shape factor is given by Timofeeva et al. [115]. The effect of ϕ on Nusselt number are plotted in Figures 6.18-6.20. In Figures 6.21-6.26, the stream lines behavior is shown. The effect of thermal conductivity of cylinders, bricks and platelets shaped nanoparticles are represented in Figure 6.27.

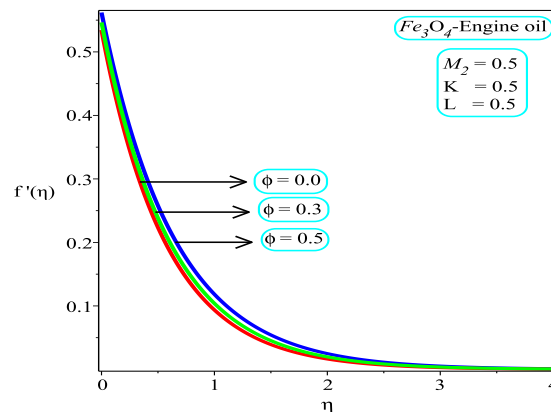


FIGURE 6.2: Impact of variation in ϕ on $f'(\eta)$

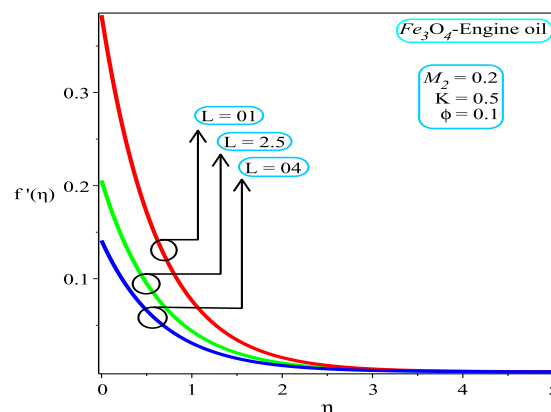


FIGURE 6.3: Impact of variation in L on $f'(\eta)$

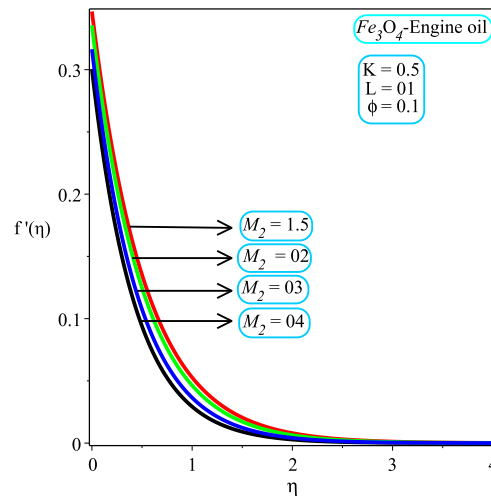


FIGURE 6.4: Impact of variation in M_2 on $f'(\eta)$

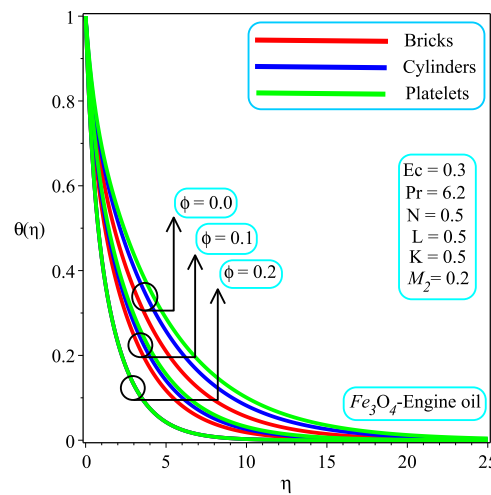


FIGURE 6.5: Impact of variation in ϕ on $\theta(\eta)$

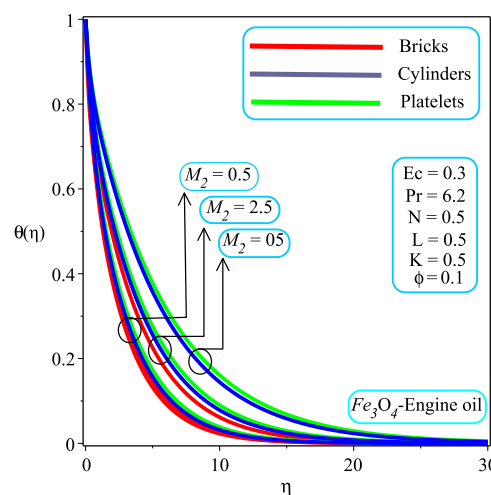


FIGURE 6.6: Impact of variation in M_2 on $\theta(\eta)$

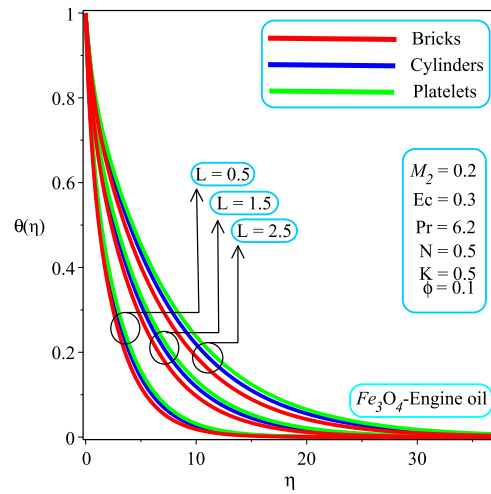


FIGURE 6.7: Impact of variation in L on $\theta(\eta)$

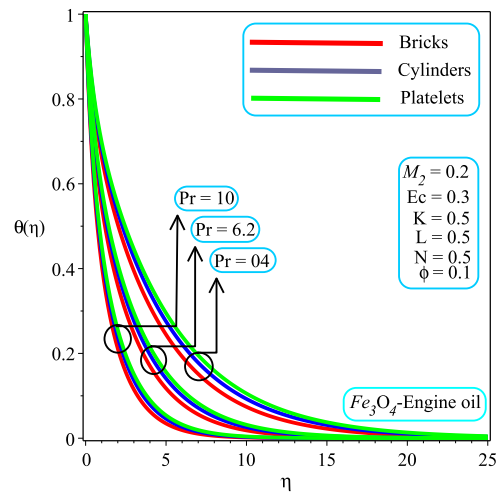


FIGURE 6.8: Impact of variation in Pr on $\theta(\eta)$

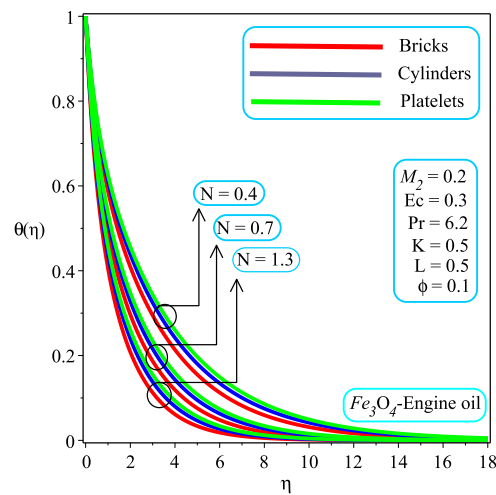


FIGURE 6.9: Impact of variation in N on $\theta(\eta)$

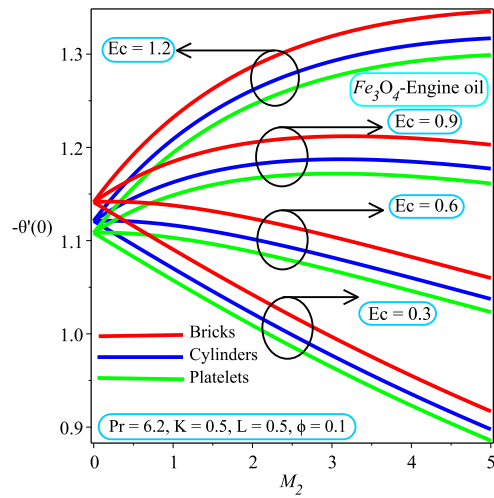


FIGURE 6.10: Impact of variation in Ec on $-\theta'(0)$

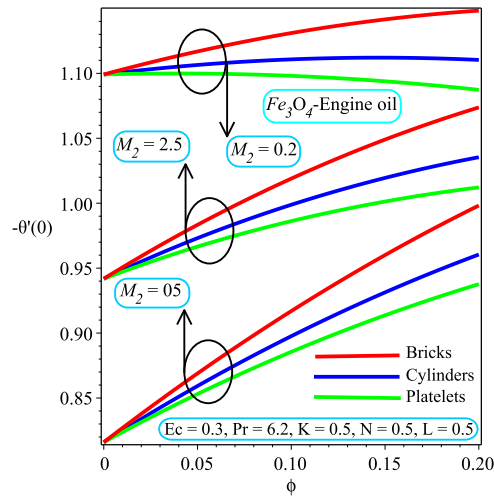


FIGURE 6.11: Impact of variation in M_2 on $-\theta'(0)$

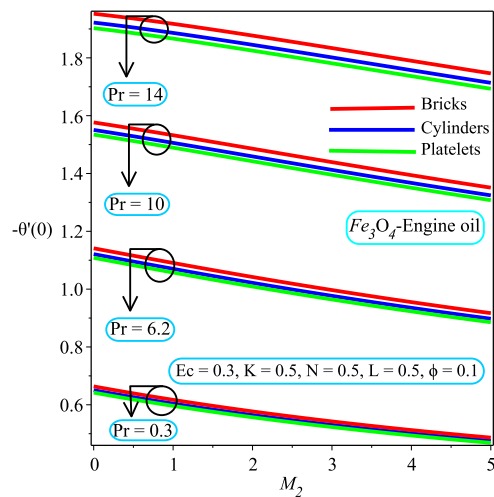


FIGURE 6.12: Impact of variation in Pr on $-\theta'(0)$

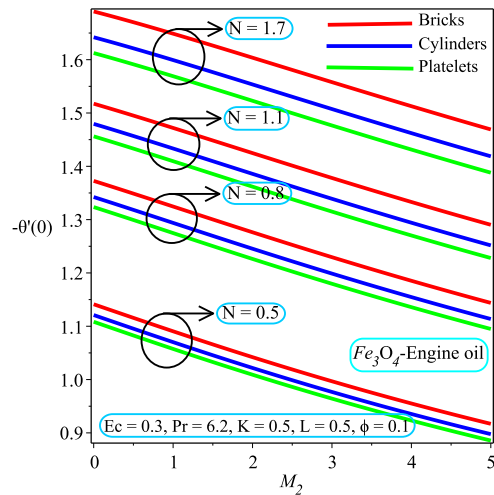


FIGURE 6.13: Impact of variation in N on $-\theta'(0)$

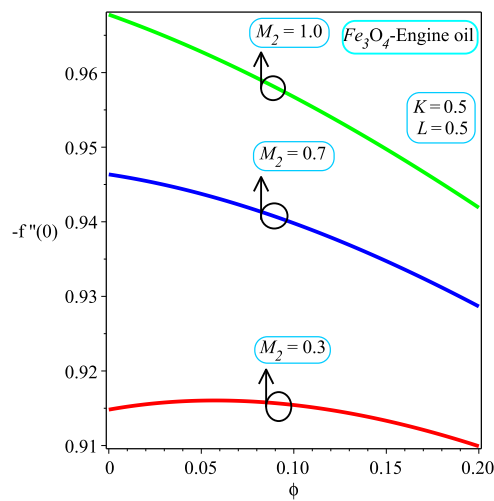


FIGURE 6.14: Impact of variation in M_2 on $-f''(0)$

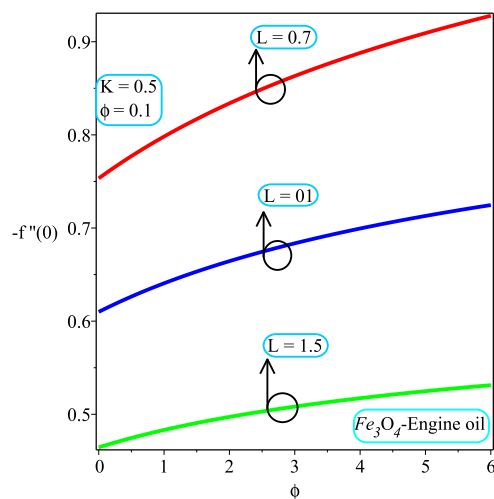


FIGURE 6.15: Impact of variation in L on $-f''(0)$

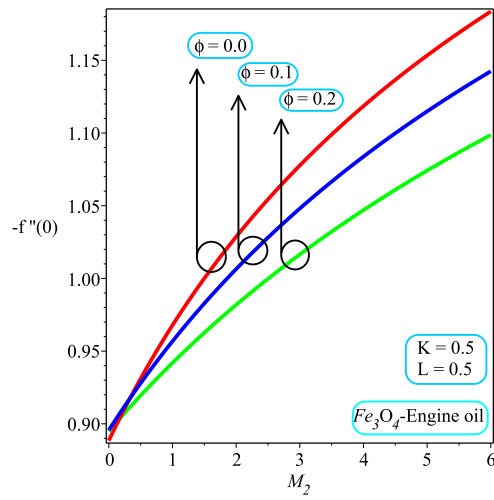


FIGURE 6.16: Impact of variation in ϕ on $-f''(0)$

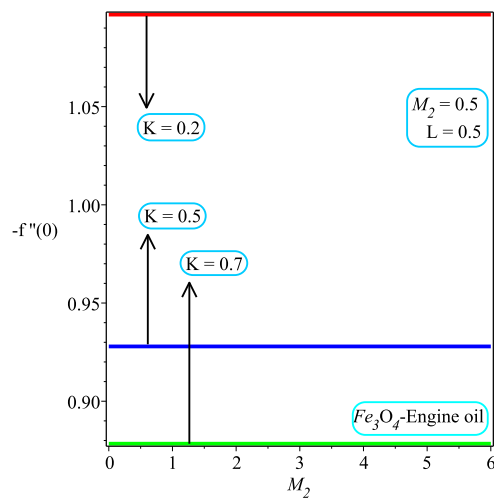


FIGURE 6.17: Impact of variation in K on $-f''(0)$

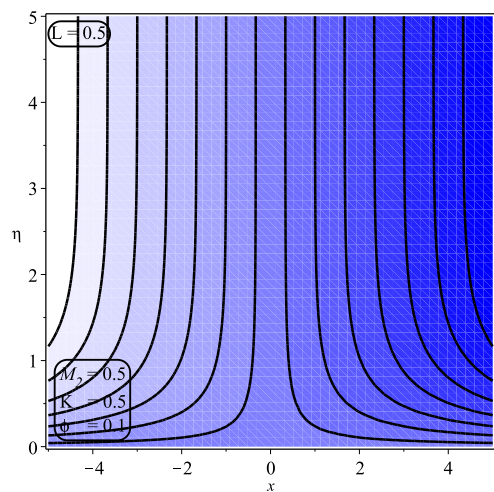
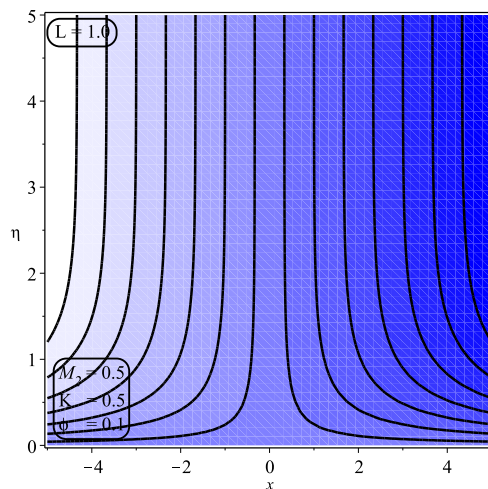
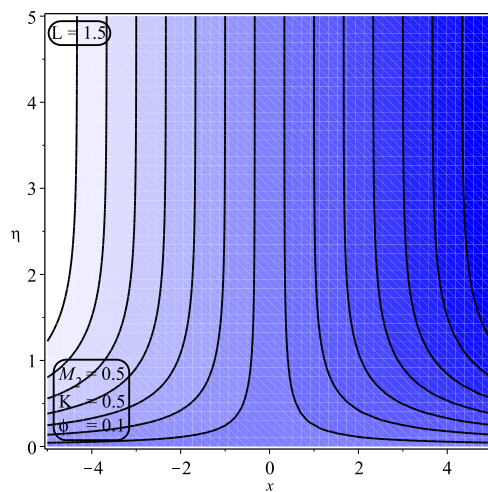
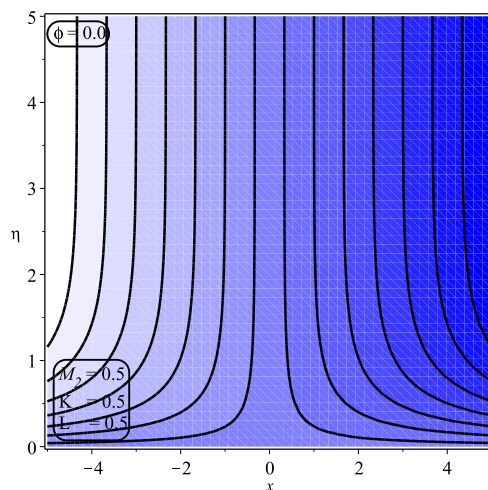


FIGURE 6.18: Contour plot for $L = 0.5$

FIGURE 6.19: Contour plot for $L = 1.0$ FIGURE 6.20: Contour plot for $L = 1.5$ FIGURE 6.21: Contour plot for $\phi = 0.0$

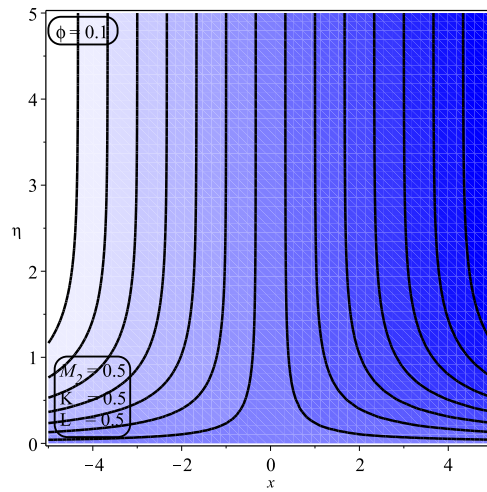


FIGURE 6.22: Contour plot for $\phi = 0.1$

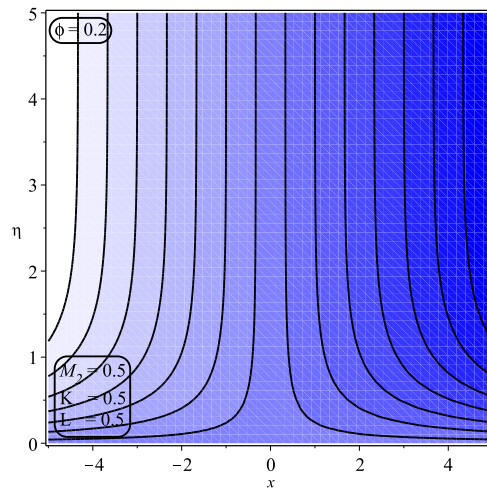


FIGURE 6.23: Contour plot for $\phi = 0.2$

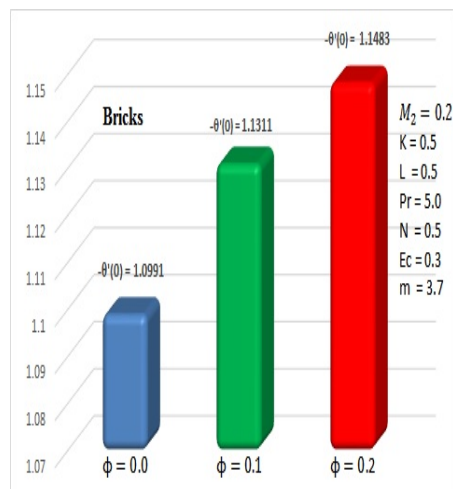


FIGURE 6.24: Impact of variation in ϕ on $-\theta'(0)$, bricks

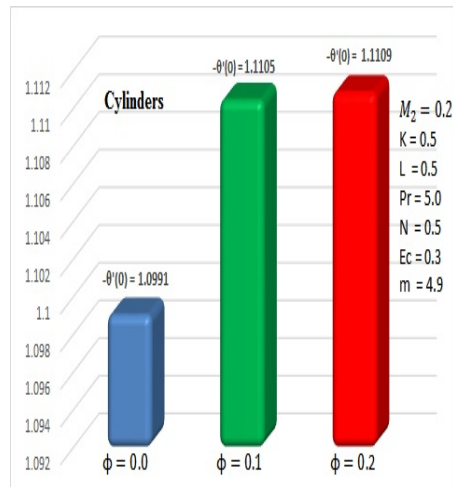


FIGURE 6.25: Impact of variation in ϕ on $-\theta'(0)$, cylinders

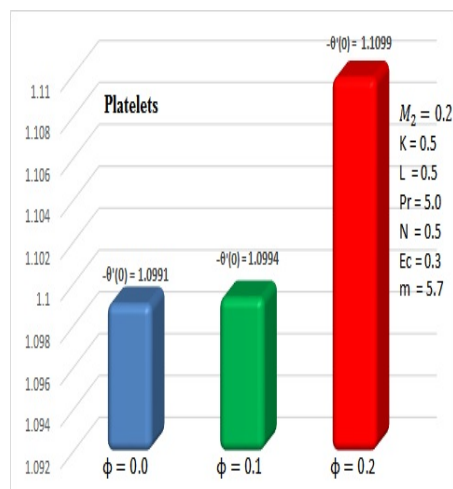


FIGURE 6.26: Impact of variation in ϕ on $-\theta'(0)$, platelets

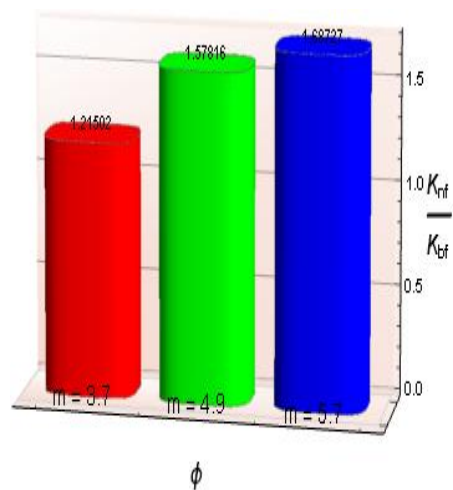





FIGURE 6.27: Impact of variation in thermal conductivity for different shapes

TABLE 6.1: Thermal characteristics of conventional fluid and solid nanoparticles.

Physical characteristics	$\rho(kg m^{-3})$	$c_p(J/kgK)$	$K(W/mk)$
Engine oil	884	1910	0.144
Fe_3O_4	5180	670	9.7

TABLE 6.2: Numerical values of m (shape factor).

Nanoparticles	Shape	m
Bricks		$\frac{370}{100}$
Cylinders		$\frac{490}{100}$
Platelets		$\frac{570}{100}$

6.3 Conclusion

The hydromagnetics nanofluid flow having different shaped nanoparticles with velocity slip, thermal radiation and Ohmic heating impacts over a stretching surface is studied. We concluded the following results:

- The velocity field is a decreasing function of velocity ratio parameter L and the Hartmann number while ϕ has the opposite behavior.
- The temperature field enhances by increasing the value of ϕ , velocity slip parameter and Hartmann number M_2 .

- It is found that Platelets nanoparticles have highest thermal conductivity and cylinders have least.
- It is examined that the temperature profile reduced in case of bricks, cylinders and platelets shaped nanoparticles by increasing the magnitude of Pr and N . Moreover, the decreasing rate in the bricks shaped nanoparticles is faster than the cylinders and platelets shaped nanoparticles.
- An increase in Ec , Pr and N is found responsible for an augmentation in the change of heat transport. The heat transfer rate decreases with an increment in the Hartmann number M_2 .
- The local skin friction coefficient diminishes by increasing the values of the Hartmann number, L , ϕ and permeability parameter K .

Chapter 7

Conclusion and Future Work

The current chapter comprises of the outcomes of this thesis and some future directions.

7.0.1 Conclusion

This thesis examines the importance of fluid flow and heat transport of Newtonian viscous nanofluid over a stretching/shrinking surface. The momentum analysis is carried out with impact of magnetic field, porous medium and stagnation point. The influence of linear thermal radiation and Joule heating are taken for heat transport analysis. The closed form solutions of the considered governing equations are obtained and results are illustrated through graphs and numerical tables. The main outcomes of the present study are:

7.0.1.1 Shrinking Case:

- It is noticed that the velocity field is an increasing function of ϕ and the suction parameter.
- It is examined that the temperature field accelerates effectively by an increment in ϕ and decelerates with N .

- It is illustrated that the local skin friction coefficient is a rising function of the Hartmann number and increasing/decreasing function of ϕ .
- It is seen that an increment in Pr and thermal radiation parameter is found responsible for a gain in the rate of energy transport.
- It is observed that the entropy generation field increases by an increment in the Brinkman number, Re , Hartmann number and behaves oppositely for the temperature difference parameter.
- The irreversibility parameter gains due to an increment in the temperature difference parameter and reduces by an increase in Ec .

7.0.1.2 Stretching Case:

- The velocity profile of nanofluid decreases with an increasing value of ϕ in Cu -water.
- The velocity profile behavior is opposite for Al_2O_3 -water and Fe_3O_4 -engine oil by gaining the magnitude of ϕ .
- It is found that the velocity profile is a diminishing function of velocity slip parameter L and Hartmann number M_2 in Cu -water, Al_2O_3 -water and Fe_3O_4 -engine oil.
- The temperature profile increases for each value of ϕ , M_2 , β and L in case of Cu -water, Al_2O_3 -water and Fe_3O_4 -engine oil.
- It is found that Platelets nanoparticles have highest thermal conductivity and cylinders have least in case of Fe_3O_4 -Engine oil.
- It is seen that the temperature field reduces in case of Cu -water, Al_2O_3 -water and Fe_3O_4 -engine oil by increasing the values Pr and N .
- The local skin friction coefficient increases by enhancing the values of Hartmann number in Cu -water, Al_2O_3 -water and Fe_3O_4 -engine oil.

- It is seen that the value of $-f''(0)$ increasing efficiently by enhancing the magnitude of an aligned angle. Moreover, value of $-f''(0)$ is not affected due to zero inclination.
- The local skin friction coefficient is decreasing function of L , ϕ and K in Fe_3O_4 -engine oil.
- An increase in Ec and Pr is found responsible for an augmentation in the rate of heat transfer.

7.0.1.3 Exponentially Stretching Case:

- The velocity profile is a decreasing function of ϕ , velocity ratio parameter and the mass blowing parameter, whereas it has an opposite behavior for the mass suction parameter.
- The temperature profile accelerates because of an increasing value of the Eckert number and M_2 .
- It is observed that the temperature field reduces with an increase in Pr and velocity ratio parameter.
- An increment in the suction parameter is found responsible for an augmentation in the local Nusselt number.
- The impact of Platelets shaped nanoparticles are greater than that of cylinders and bricks in the temperature field.
- It is examined that the value of $-\theta'(0)$ increases by an increase in Ec , M_2 and K .
- The magnitude of the local skin friction coefficient accelerates by increasing the value of ϕ .

7.0.2 Future work

Fluid are very important in all aspects of life even from morning cup of tea to the

evening bath. The industrial significance of Newtonian fluids flow are discussed in introduction and literature review section. In future, I have plan to study the impact of non-Newtonian fluid models. In short, I would like to proceed in the following possible directions:

- Heat transport analysis of the Casson nanofluid induced by a stretching surface with an inclined MHD.
- Second law analysis of Maxwell nanofluid with porous medium provoked by a stretching sheet.
- Impact of radiation on Jeffery nanofluid past a shrinking surface with Joule heating.
- Analysis of hyperbolic tangent fluid flow with the influence of viscous dissipation under slip condition.

Bibliography

- [1] F. H. Harlow and A. A. Amsden, “Fluid dynamics. A Lasl Monograph.” Los Alamos Scientific Lab., N. Mex., Tech. Rep., 1971.
- [2] K. Das, A. Sarkar, and P. K. Kundu, “Cu-water nanofluid flow induced by a vertical stretching sheet in presence of a magnetic field with convective heat transfer,” *Propulsion and Power Research*, vol. 6, no. 3, pp. 206–213, 2017.
- [3] S. Jahan, H. Sakidin, R. Nazar, and I. Pop, “Analysis of heat transfer in nanofluid past a convectively heated permeable stretching/shrinking sheet with regression and stability analyses,” *Results in Physics*, vol. 10, pp. 395–405, 2018.
- [4] S. Bilal, M. Malik, A. Hussain, and M. Khan, “Effects of temperature dependent conductivity and absorptive/generative heat transfer on MHD three dimensional flow of Williamson fluid due to bidirectional non-linear stretching surface,” *Results in Physics*, vol. 7, pp. 204–212, 2017.
- [5] A. Hafeez, A. S. Alshomrani, and M. Khan, “Multiple physical aspects during the flow and heat transfer analysis of Carreau fluid with nanoparticles,” *Scientific Reports*, vol. 8, no. 1, p. 17402, 2018.
- [6] B. Prasannakumara, B. Gireesha, M. Krishnamurthy, and K. G. Kumar, “MHD flow and nonlinear radiative heat transfer of Sisko nanofluid over a nonlinear stretching sheet,” *Informatics in Medicine Unlocked*, vol. 9, pp. 123–132, 2017.
- [7] D. Ramya, R. S. Raju, J. A. Rao, and A. Chamkha, “Effects of velocity and thermal wall slip on magnetohydrodynamics (MHD) boundary layer viscous

- flow and heat transfer of a nanofluid over a non-linearly-stretching sheet: a numerical study,” *Propulsion and Power Research*, vol. 7, no. 2, pp. 182–195, 2018.
- [8] F. Saba, N. Ahmed, S. Hussain, U. Khan, S. Mohyud-Din, and M. Darus, “Thermal analysis of nanofluid flow over a curved stretching surface suspended by carbon nanotubes with internal heat generation,” *Applied Sciences*, vol. 8, no. 3, p. 395, 2018.
- [9] M. Govindaraju, S. Saranya, A. A. Hakeem, R. Jayaprakash, and B. Ganga, “Analysis of slip MHD nanofluid flow on entropy generation in a stretching sheet,” *Procedia Engineering*, vol. 127, pp. 501–507, 2015.
- [10] R. U. Haq, S. Nadeem, Z. H. Khan, and N. S. Akbar, “Thermal radiation and slip effects on MHD stagnation point flow of nanofluid over a stretching sheet,” *Physica E: Low-dimensional Systems and Nanostructures*, vol. 65, pp. 17–23, 2015.
- [11] F. Mabood and S. Shateyi, “Multiple slip effects on MHD unsteady flow heat and mass transfer impinging on permeable stretching sheet with radiation,” *Modelling and Simulation in Engineering*, 2019.
- [12] M. G. Reddy, “Heat generation and thermal radiation effects over a stretching sheet in a micropolar fluid,” *ISRN Thermodynamics*, 2012.
- [13] A. Dawar, Z. Shah, M. Idrees, W. Khan, S. Islam, and T. Gul, “Impact of thermal radiation and heat source/sink on Eyring–Powell fluid flow over an unsteady oscillatory porous stretching surface,” *Mathematical and Computational Applications*, vol. 23, no. 2, p. 20, 2018.
- [14] K. Singh and M. Kumar, “Effects of thermal radiation on mixed convection flow of a micropolar fluid from an unsteady stretching surface with viscous dissipation and heat generation/absorption,” *International Journal of Chemical Engineering*, 2016.
- [15] N. Dzulkifli, N. Bachok, N. Yacob, N. Md Arifin, and H. Rosali, “Unsteady

- stagnation-point flow and heat transfer over a permeable exponential stretching/shrinking sheet in nanofluid with slip velocity effect: A stability analysis,” *Applied Sciences*, vol. 8, no. 11, p. 2172, 2018.
- [16] N. Ishak, H. Hashim, M. K. A. Mohamed, N. M. Sarif, N. Rosli, and M. Z. Salleh, “Thermal radiation effects on stagnation point flow past a stretching/shrinking sheet in a Maxwell fluid with slip condition,” *Journal of Physics: Conference Series*, vol. 890, no. 1, p. 012021, 2017.
- [17] N. A. A. M. Nasir, A. Ishak, and I. Pop, “Stagnation point flow and heat transfer past a permeable stretching/shrinking Riga plate with velocity slip and radiation effects,” *Journal of Zhejiang University-SCIENCE A*, vol. 20, no. 4, pp. 290–299, 2019.
- [18] S. U. Choi and J. A. Eastman, “Enhancing thermal conductivity of fluids with nanoparticles,” Argonne National Lab., IL (United States), Tech. Rep., 1995.
- [19] J. Eastman, S. U. Choi, S. Li, L. Thompson, and S. Lee, “Enhanced thermal conductivity through the development of nanofluids,” *MRS online Proceedings Library Archive*, vol. 457, 1996.
- [20] Y. Ding, H. Chen, L. Wang, C.-Y. Yang, Y. He, W. Yang, W. P. Lee, L. Zhang, and R. Huo, “Heat transfer intensification using nanofluids,” *KONA Powder and Particle Journal*, vol. 25, pp. 23–38, 2007.
- [21] H. Masuda, A. Ebata, and K. Teramae, “Alteration of thermal conductivity and viscosity of liquid by dispersing ultra-fine particles (dispersion of γ - Al_2O_3 , SiO_2 and TiO_2 ultra-fine particles),” vol. 4, pp. 227–233, 1993.
- [22] M. Hamad, “Analytical solution of natural convection flow of a nanofluid over a linearly stretching sheet in the presence of magnetic field,” *International Communications in Heat and Mass Transfer*, vol. 38, no. 4, pp. 487–492, 2011.
- [23] A. M. Rohni, S. Ahmad, and I. Pop, “Flow and heat transfer over an un-

- steady shrinking sheet with suction in nanofluids,” *International Journal of Heat and Mass Transfer*, vol. 55, no. 7-8, pp. 1888–1895, 2012.
- [24] A. Noghrehabadi, R. Pourrajab, and M. Ghalambaz, “Effect of partial slip boundary condition on the flow and heat transfer of nanofluids past stretching sheet prescribed constant wall temperature,” *International Journal of Thermal Sciences*, vol. 54, pp. 253–261, 2012.
- [25] H. F. Oztop and E. Abu-Nada, “Numerical study of natural convection in partially heated rectangular enclosures filled with nanofluids,” *International Journal of Heat and Fluid Flow*, vol. 29, no. 5, pp. 1326–1336, 2008.
- [26] N. A. Yacob, A. Ishak, I. Pop, and K. Vajravelu, “Boundary layer flow past a stretching/shrinking surface beneath an external uniform shear flow with a convective surface boundary condition in a nanofluid,” *Nanoscale Research Letters*, vol. 6, no. 1, p. 314, 2011.
- [27] W. Khan and I. Pop, “Boundary-layer flow of a nanofluid past a stretching sheet,” *International Journal of Heat and Mass Transfer*, vol. 53, no. 11-12, pp. 2477–2483, 2010.
- [28] A. Ullah, Z. Shah, P. Kumam, M. Ayaz, S. Islam, and M. Jameel, “Viscoelastic MHD nanofluid thin film flow over an unsteady vertical stretching sheet with entropy generation,” *Processes*, vol. 7, no. 5, p. 262, 2019.
- [29] S. Zokri, N. Arifin, M. Salleh, A. Kasim, N. Mohammad, and W. Yusoff, “MHD Jeffrey nanofluid past a stretching sheet with viscous dissipation effect,” *Journal of Physics: Conference Series*, vol. 890, no. 1, p. 012002, 2017.
- [30] M. Chandrasekar and M. Kasiviswanathan, “Analysis of heat and mass transfer on MHD flow of a nanofluid past a stretching sheet,” *Procedia Engineering*, vol. 127, pp. 493–500, 2015.
- [31] M. A. Mjankwi, V. G. Masanja, E. W. Mureithi, and M. N. James, “Unsteady MHD flow of nanofluid with variable properties over a stretching sheet

- in the presence of thermal radiation and chemical reaction,” *International Journal of Mathematics and Mathematical Sciences*, 2019.
- [32] R. Vasanthakumari and P. Pondy, “Mixed convection of silver and titanium dioxide nanofluids along inclined stretching sheet in presence of MHD with heat generation and suction effect,” *Mathematical Modelling of Engineering Problems*, vol. 5, no. 2, pp. 123–129, 2018.
- [33] N. Tarakaramu and P. Narayan, “Unsteady MHD nanofluid flow over a stretching sheet with chemical reaction,” *Materials Science and Engineering Conference Series*, vol. 263, no. 6, p. 062030, 2017.
- [34] P. Suriyakumar and S. A. Devi, “Buongiorno model for hydromagnetic convective flow of nanofluid over an inclined stretching surface with variable stream conditions,” *Journal of Advanced Research in Applied Mechanics & Computational Fluid Dynamics*, vol. 6, no. 1, pp. 1–14, 2019.
- [35] R. S. Saif, T. Hayat, R. Ellahi, T. Muhammad, and A. Alsaedi, “Stagnation-point flow of second grade nanofluid towards a nonlinear stretching surface with variable thickness,” *Results in Physics*, vol. 7, pp. 2821–2830, 2017.
- [36] S. Nadeem and S. Hussain, “Heat transfer analysis of Williamson fluid over exponentially stretching surface,” *Applied Mathematics and Mechanics*, vol. 35, no. 4, pp. 489–502, 2014.
- [37] K. Ahmad, Z. Wahid, and Z. Hanouf, “Heat transfer analysis for Casson fluid flow over stretching sheet with Newtonian heating and viscous dissipation,” vol. 1127, no. 1, p. 012028, 2019.
- [38] B. Sakiadis, “Boundary-layer behavior on continuous solid surfaces. ii. the boundary layer on a continuous flat surface,” *AIChE Journal*, vol. 7, no. 2, pp. 221–225, 1961.
- [39] B. C. Sakiadis, “Boundary-layer behavior on continuous solid surfaces: I. boundary-layer equations for two-dimensional and axisymmetric flow,” *AIChE Journal*, vol. 7, no. 1, pp. 26–28, 1961.

- [40] L. J. Crane, "Flow past a stretching plate," *Zeitschrift für angewandte Mathematik und Physik ZAMP*, vol. 21, no. 4, pp. 645–647, 1970.
- [41] S. Nadeem, R. U. Haq, and C. Lee, "MHD flow of a Casson fluid over an exponentially shrinking sheet," *Scientia Iranica*, vol. 19, no. 6, pp. 1550–1553, 2012.
- [42] S. Nadeem, R. U. Haq, N. S. Akbar, and Z. H. Khan, "MHD three-dimensional Casson fluid flow past a porous linearly stretching sheet," *Alexandria Engineering Journal*, vol. 52, no. 4, pp. 577–582, 2013.
- [43] A. Ishak, "Similarity solutions for flow and heat transfer over a permeable surface with convective boundary condition," *Applied Mathematics and Computation*, vol. 217, no. 2, pp. 837–842, 2010.
- [44] P. D. Ariel, "The three-dimensional flow past a stretching sheet and the homotopy perturbation method," *Computers & Mathematics with Applications*, vol. 54, no. 7-8, pp. 920–925, 2007.
- [45] T. Hayat and M. Qasim, "Effects of thermal radiation on unsteady magnetohydrodynamic flow of a micropolar fluid with heat and mass transfer," *Zeitschrift für Naturforschung A*, vol. 65, no. 11, pp. 950–960, 2010.
- [46] J. Raza, "Thermal radiation and slip effects on magnetohydrodynamic (MHD) stagnation point flow of Casson fluid over a convective stretching sheet," *Propulsion and Power Research*, 2019.
- [47] S. Reza-E-Rabbi, S. Arifuzzaman, T. Sarkar, M. S. Khan, and S. F. Ahmed, "Explicit finite difference analysis of an unsteady mhd flow of a chemically reacting Casson fluid past a stretching sheet with Brownian motion and thermophoresis effects," *Journal of King Saud University-Science*, 2018.
- [48] T. E. Akinbobola and S. S. Okoya, "The flow of second grade fluid over a stretching sheet with variable thermal conductivity and viscosity in the presence of heat source/sink," *Journal of the Nigerian Mathematical Socie-*

- ty, vol. 34, no. 3, pp. 331–342, 2015.
- [49] K. K. Lakshmi, B. Gireesha, R. S. Gorla, and B. Mahanthesh, “Effects of diffusion-thermo and thermo-diffusion on two-phase boundary layer flow past a stretching sheet with fluid-particle suspension and chemical reaction: A numerical study,” *Journal of the Nigerian Mathematical Society*, vol. 35, no. 1, pp. 66–81, 2016.
- [50] F. Mabood and K. Das, “Outlining the impact of melting on MHD Casson fluid flow past a stretching sheet in a porous medium with radiation,” *Heliyon*, vol. 5, no. 2, p. e01216, 2019.
- [51] A. Ali and S. Asghar, “New approach to the exact solution of viscous flow due to stretching (shrinking) and porous sheet,” *Results in Physics*, vol. 7, pp. 1122–1127, 2017.
- [52] I. Rashid, R. U. Haq, Z. Khan, and Q. M. Al-Mdallal, “Flow of water based alumina and copper nanoparticles along a moving surface with variable temperature,” *Journal of Molecular Liquids*, vol. 246, pp. 354–362, 2017.
- [53] R. U. Haq, I. Rashid, and Z. Khan, “Effects of aligned magnetic field and cnts in two different base fluids over a moving slip surface,” *Journal of Molecular Liquids*, vol. 243, pp. 682–688, 2017.
- [54] S. Asghar, A. Ahmad, and A. Alsaedi, “Flow of a viscous fluid over an impermeable shrinking sheet,” *Applied Mathematics Letters*, vol. 26, no. 12, pp. 1165–1168, 2013.
- [55] S. Mishra, I. Khan, Q. Al-Mdallal, and T. Asifa, “Free convective micropolar fluid flow and heat transfer over a shrinking sheet with heat source,” *Case Studies in Thermal Engineering*, vol. 11, pp. 113–119, 2018.
- [56] M. Bhatti, A. Shahid, and M. Rashidi, “Numerical simulation of fluid flow over a shrinking porous sheet by successive linearization method,” *Alexandria Engineering Journal*, vol. 55, no. 1, pp. 51–56, 2016.
- [57] E. Magyari and B. Keller, “Heat and mass transfer in the boundary layers

- on an exponentially stretching continuous surface,” *Journal of Physics D: Applied Physics*, vol. 32, no. 5, p. 577, 1999.
- [58] R. Damseh, “Thermal boundary layer on an exponentially stretching continuous surface in the presence of magnetic field effect,” *Int. J. of Applied Mechanics and engineering*, vol. 11, no. 2, pp. 289–299, 2006.
- [59] I. Ullah, S. Shafie, and I. Khan, “Effects of slip condition and Newtonian heating on MHD flow of Casson fluid over a nonlinearly stretching sheet saturated in a porous medium,” *Journal of King Saud University-Science*, vol. 29, no. 2, pp. 250–259, 2017.
- [60] D. Srinivasacharya and P. Jagadeeshwar, “Cross-diffusion effects on an exponentially stretching sheet in a doubly stratified viscous fluid,” *Engineering Science and Technology, an International Journal*, vol. 20, no. 6, pp. 1571–1578, 2017.
- [61] A. Jafarimoghaddam, “On the homotopy analysis method (HAM) and homotopy perturbation method (HPM) for a nonlinearly stretching sheet flow of Eyring-Powell fluids,” *Engineering Science and Technology, an International Journal*, vol. 22, no. 2, pp. 439–451, 2019.
- [62] S. Bilal, M. Malik, M. Awais, A. Hussain, and I. Khan, “Numerical investigation on 2D viscoelastic fluid due to exponentially stretching surface with magnetic effects: an application of non-Fourier flux theory,” *Neural Computing and Applications*, vol. 30, no. 9, pp. 2749–2758, 2018.
- [63] E. M. Elbashbeshy, T. Emam, and K. Abdelgaber, “Effects of thermal radiation and magnetic field on unsteady mixed convection flow and heat transfer over an exponentially stretching surface with suction in the presence of internal heat generation/absorption,” *Journal of the Egyptian Mathematical Society*, vol. 20, no. 3, pp. 215–222, 2012.
- [64] E. Elbashbeshy, “Heat transfer over an exponentially stretching continuous surface with suction,” *Archives of Mechanics*, vol. 53, no. 6, pp. 643–651, 2001.

- [65] M. Sheikholeslami, M. Gorji-Bandpy, and D. Ganji, "Lattice Boltzmann method for MHD natural convection heat transfer using nanofluid," *Powder Technology*, vol. 254, pp. 82–93, 2014.
- [66] M. Rashidi, N. V. Ganesh, A. A. Hakeem, and B. Ganga, "Buoyancy effect on mhd flow of nanofluid over a stretching sheet in the presence of thermal radiation," *Journal of Molecular Liquids*, vol. 198, pp. 234–238, 2014.
- [67] A. Zeeshan, A. Majeed, and R. Ellahi, "Effect of magnetic dipole on viscous ferro-fluid past a stretching surface with thermal radiation," *Journal of Molecular liquids*, vol. 215, pp. 549–554, 2016.
- [68] T. Hayat, S. Asad, M. Mustafa, and A. Alsaedi, "MHD stagnation-point flow of Jeffrey fluid over a convectively heated stretching sheet," *Computers & Fluids*, vol. 108, pp. 179–185, 2015.
- [69] R. Jat, G. Chand, and D. Rajotia, "MHD heat and mass transfer for viscous flow over nonlinearly stretching sheet in a porous medium," *Thermal Energy and Power Engineering*, vol. 3, pp. 191–197, 2014.
- [70] W. Ibrahim and O. Makinde, "Magnetohydrodynamic stagnation point flow and heat transfer of Casson nanofluid past a stretching sheet with slip and convective boundary condition," *Journal of Aerospace Engineering*, vol. 29, no. 2, p. 04015037, 2015.
- [71] S. Das, H. Mandal, R. Jana, and O. Makinde, "Magneto-nanofluid flow past an impulsively started porous flat plate in a rotating frame," *Journal of Nanofluids*, vol. 4, no. 2, pp. 167–175, 2015.
- [72] G. Ramesh, B. Giresha, T. Hayat, and A. Alsaedi, "MHD flow of Maxwell fluid over a stretching sheet in the presence of nanoparticles, thermal radiation and chemical reaction: a numerical study," *Journal of Nanofluids*, vol. 4, no. 1, pp. 100–106, 2015.
- [73] B. Mahanthesh, B. Giresha, I. Animasaun, T. Muhammad, and N. Shashikumar, "MHD flow of SWCNT and MWCNT nanoliquids past

- a rotating stretchable disk with thermal and exponential space dependent heat source,” *Physica Scripta*, vol. 94, no. 8, p. 085214, 2019.
- [74] I. M. Alarifi, A. G. Abokhalil, M. Osman, L. A. Lund, M. B. Ayed, H. Belmabrouk, and I. Tlili, “MHD flow and heat transfer over vertical stretching sheet with heat sink or source effect,” *Symmetry*, vol. 11, no. 3, p. 297, 2019.
- [75] T. Kunnegowda, B. Mahanthesh, G. Lorenzini, and I. L. Animasaun, “Significance of induced magnetic field and exponential space dependent heat source on quadratic convective flow of Casson fluid in a micro-channel via HPM,” *Symmetry*, vol. 6, no. 3, pp. 369–384, 2019.
- [76] F. Mebarek-oudina and R. Bessaïh, “Numerical modeling of MHD stability in a cylindrical configuration,” *Journal of the Franklin Institute*, vol. 351, no. 2, pp. 667–681, 2014.
- [77] A. Bejan, “A study of entropy generation in fundamental convective heat transfer,” *Journal of Heat Transfer*, vol. 101, no. 4, pp. 718–725, 1979.
- [78] M. Afridi, M. Qasim, I. Khan, and I. Tlili, “Entropy generation in MHD mixed convection stagnation-point flow in the presence of Joule and frictional heating,” *Case studies in thermal engineering*, vol. 12, pp. 292–300, 2018.
- [79] H. Sithole, H. Mondal, and P. Sibanda, “Entropy generation in a second grade magnetohydrodynamic nanofluid flow over a convectively heated stretching sheet with nonlinear thermal radiation and viscous dissipation,” *Results in Physics*, vol. 9, pp. 1077–1085, 2018.
- [80] M. M. Bhatti, T. Abbas, and M. M. Rashidi, “Entropy generation as a practical tool of optimisation for non-Newtonian nanofluid flow through a permeable stretching surface using SLM,” *Journal of Computational Design and Engineering*, vol. 4, no. 1, pp. 21–28, 2017.
- [81] A. Noghrehabadi, M. R. Saffarian, R. Pourrajab, and M. Ghalambaz, “Entropy analysis for nanofluid flow over a stretching sheet in the presence of

- heat generation/absorption and partial slip,” *Journal of Mechanical Science and Technology*, vol. 27, no. 3, pp. 927–937, 2013.
- [82] M. Abd El-Aziz and A. A. Afify, “MHD Casson fluid flow over a stretching sheet with entropy generation analysis and Hall influence,” *Entropy*, vol. 21, no. 6, p. 592, 2019.
- [83] W. A. Khan and I. M. Pop, “Boundary layer flow past a stretching surface in a porous medium saturated by a nanofluid: Brinkman-Forchheimer model,” *PloS one*, vol. 7, no. 10, p. e47031, 2012.
- [84] R. Barik, G. Dash, and P. Rath, “Heat and mass transfer on MHD flow through a porous medium over a stretching surface with heat source,” *Mathematical Theory and Modeling*, vol. 2, no. 7, pp. 49–59, 2012.
- [85] C. J. Etwire, I. Y. Seini, and R. Musah, “Effects of oil-based nanofluid on a stretching surface with variable suction and thermal conductivity,” *Diffusion Foundations*, vol. 11, pp. 99–109, 2017.
- [86] S. Mukhopadhyay, “Analysis of boundary layer flow over a porous nonlinearly stretching sheet with partial slip at the boundary,” *Alexandria Engineering Journal*, vol. 52, no. 4, pp. 563–569, 2013.
- [87] P. Singh, N. S. Tomer, S. Kumar, and D. Sinha, “Effect of radiation and porosity parameter on magnetohydrodynamic flow due to stretching sheet in porous media,” *Thermal Science*, vol. 15, no. 2, pp. 517–526, 2011.
- [88] A. Khan, D. Khan, I. Khan, F. Ali, F. ul Karim, and M. Imran, “Mhd flow of sodium alginate-based Casson type nanofluid passing through a porous medium with Newtonian heating,” *Scientific Reports*, vol. 8, no. 1, p. 8645, 2018.
- [89] Y. Cengel and J. Cimbala, *Fluid Mechanics—Fundamentals and Applications*. McGraw-Hill Internat. Ed., 2006.
- [90] F. M. White and I. Corfield, *Viscous Fluid Flow (McGraw-Hill Mechanical Engineering)*. McGraw-Hill New York, 2006.

- [91] R. Bansal, *A Textbook of Fluid Mechanics and Hydraulic Machines*. Laxmi Publications, 2004.
- [92] Y. A. Cengel, S. Klein, and W. Beckman, *Heat Transfer: a Practical Approach*. McGraw-Hill New York, 1998.
- [93] W. Yu and H. Xie, “A review on nanofluids: preparation, stability mechanisms, and applications,” *Journal of Nanomaterials*, p. 1, 2012.
- [94] H. Gupta, G. Agrawal, and J. Mathur, “An overview of nanofluids: A new media towards green environment,” *International Journal of Environmental sciences*, vol. 3, no. 1, pp. 433–440, 2012.
- [95] O. Maj, “A mathematical introduction to magnetohydrodynamics,” in *Vorlesung (SS 2017)*, 2017.
- [96] D. Halliday, J. Walker, and R. Resnick, *Fundamentals of Physics*. John Wiley & Sons, 2013.
- [97] J. Kunes, *Dimensionless Physical Quantities in Science and Engineering*. Elsevier, 2012.
- [98] M. Fakour, A. Rahbari, E. Khodabandeh, and D. D. Ganji, “Nanofluid thin film flow and heat transfer over an unsteady stretching elastic sheet by LSM,” *Journal of Mechanical Science and Technology*, vol. 32, no. 1, pp. 177–183, 2018.
- [99] E. H. Aly, “Existence of the multiple exact solutions for nanofluid flow over a stretching/shrinking sheet embedded in a porous medium at the presence of magnetic field with electrical conductivity and thermal radiation effects,” *Powder Technology*, vol. 301, pp. 760–781, 2016.
- [100] M. Kumari, H. S. Takhar, and G. Nath, “MHD flow and heat transfer over a stretching surface with prescribed wall temperature or heat flux,” *Wärme- und Stoffübertragung*, vol. 25, no. 6, pp. 331–336, 1990.
- [101] A. Chakrabarti and A. Gupta, “Hydromagnetic flow and heat transfer over

- a stretching sheet,” *Quarterly of Applied Mathematics*, vol. 37, no. 1, pp. 73–78, 1979.
- [102] K. Bhattacharyya, M. Uddin, and G. Layek, “Exact solution for thermal boundary layer in Casson fluid flow over permeable shrinking sheet with variable wall temperature and thermal radiation,” *Alexandria Engineering Journal*, vol. 55, no. 2, pp. 1703–1712, 2016.
- [103] M. S. Abel, N. Mahesha, and J. Tawade, “Heat transfer in a liquid film over an unsteady stretching surface with viscous dissipation in presence of external magnetic field,” *Applied Mathematical Modelling*, vol. 33, no. 8, pp. 3430–3441, 2009.
- [104] H. Dessie and N. Kishan, “MHD effects on heat transfer over stretching sheet embedded in porous medium with variable viscosity, viscous dissipation and heat source/sink,” *Ain Shams Engineering Journal*, vol. 5, no. 3, pp. 967–977, 2014.
- [105] M. Abramowitz and I. A. Stegun, “Handbook of Mathematical Functions with Formulas, Graphs, and Mathematical Tables,” *National Bureau of Standards Applied Mathematics Series*, no. 55, 1972.
- [106] C. Sulochana and N. Sandeep, “Stagnation point flow and heat transfer behavior of Cu -water nanofluid towards horizontal and exponentially stretching/shrinking cylinders,” *Applied Nanoscience*, vol. 6, no. 3, pp. 451–459, 2016.
- [107] N. Dzulkiifi, N. Bachok, I. Pop, N. Yacob, N. Arifin, and H. Rosali, “Unsteady stagnation-point flow and heat transfer over an exponential stretching sheet in copper-water nanofluid with slip velocity effect,” *Journal of Physics: Conference Series*, vol. 1132, no. 1, p. 012029, 2018.
- [108] E. A.-H. Tora and T. Moustafa, “Numerical simulation of an $Al_2O_3 - H_2O$ nanofluid as a heat transfer agent for a flat-plate solar collector,” *International Journal of Scientific and Engineering Research*, vol. 4, no. 5, pp.

- 562–573, 2013.
- [109] S. Chaudhary and K. Kanika, “Viscous dissipation and Joule heating in MHD Marangoni boundary layer flow and radiation heat transfer of Cu–water nanofluid along particle shapes over an exponential temperature,” *International Journal of Computer Mathematics*, pp. 1–16, 2019.
- [110] M. A. Yousif, H. F. Ismael, T. Abbas, and R. Ellahi, “Numerical study of momentum and heat transfer of MHD Carreau nanofluid over an exponentially stretched plate with internal heat source/sink and radiation,” *Heat Transfer Research*, vol. 50, no. 7, pp. 649–658, 2019.
- [111] D. Rollins and K. Vajravelu, “Heat transfer in an electrically conducting fluid over a stretching surface,” *Intl. J. Non-linear Mechanics*, vol. 27, pp. 265–277, 1992.
- [112] R. Cortell, “Fluid flow and radiative nonlinear heat transfer over a stretching sheet,” *Journal of King Saud University-Science*, vol. 26, no. 2, pp. 161–167, 2014.
- [113] K. Das, “Cu-water nanofluid flow and heat transfer over a shrinking sheet,” *Journal of Mechanical Science and Technology*, vol. 28, no. 12, pp. 5089–5094, 2014.
- [114] M. Imtiaz, F. Shahid, T. Hayat, and A. Alsaedi, “Melting heat transfer in Cu-water and Ag-water nanofluids flow with homogeneous-heterogeneous reactions,” *Applied Mathematics and Mechanics*, vol. 40, no. 4, pp. 465–480, 2019.
- [115] E. V. Timofeeva, J. L. Routbort, and D. Singh, “Particle shape effects on thermophysical properties of alumina nanofluids,” *Journal of Applied Physics*, vol. 106, no. 1, p. 014304, 2009.
- [116] P. Kumar, U. Mahabaleshwar, P. Sakanaka, and G. Lorenzini, “An MHD effect on a Newtonian fluid flow due to a superlinear stretching sheet,” *Journal of Engineering Thermophysics*, vol. 27, no. 4, pp. 501–506, 2018.

- [117] R. K. Tiwari and M. K. Das, “Heat transfer augmentation in a two-sided lid-driven differentially heated square cavity utilizing nanofluids,” *International Journal of Heat and Mass Transfer*, vol. 50, no. 9-10, pp. 2002–2018, 2007.
- [118] T. Fang, J. Zhang, and S. Yao, “Slip MHD viscous flow over a stretching sheet—an exact solution,” *Communications in Nonlinear Science and Numerical Simulation*, vol. 14, no. 11, pp. 3731–3737, 2009.
- [119] A. A. Hakeem, P. Renuka, N. V. Ganesh, R. Kalaivanan, and B. Ganga, “Influence of inclined Lorentz forces on boundary layer flow of Casson fluid over an impermeable stretching sheet with heat transfer,” *Journal of Magnetism and Magnetic Materials*, vol. 401, pp. 354–361, 2016.
- [120] N. Freidoonimehr and A. B. Rahimi, “Exact-solution of entropy generation for MHD nanofluid flow induced by a stretching/shrinking sheet with transpiration: Dual solution,” *Advanced Powder Technology*, vol. 28, no. 2, pp. 671–685, 2017.
- [121] N. Bachok, A. Ishak, R. Nazar, and N. Senu, “Stagnation-point flow over a permeable stretching/shrinking sheet in a copper-water nanofluid,” *Boundary Value Problems*, vol. 2013, no. 1, p. 39, 2013.
- [122] S. Anjali Devi and P. Suriyakumar, “Effect of magnetic field on Blasius and Sakiadis flow of nanofluids past an inclined plate,” *Journal of Taibah University for Science*, vol. 11, no. 6, pp. 1275–1288, 2017.
- [123] A. Gul, I. Khan, S. Shafie, A. Khalid, and A. Khan, “Heat transfer in MHD mixed convection flow of a ferrofluid along a vertical channel,” *PloS one*, vol. 10, no. 11, p. e0141213, 2015.
- [124] N. A. Khan and S. Khan, “Dual solution of Casson fluid over a porous medium: Exact solutions with extra boundary condition,” *ACTA Universitatis Cibiniensis*, vol. 68, no. 1, pp. 35–49, 2016.
- [125] M. M. Rashidi and E. Erfani, “A new analytical study of MHD stagnation-point flow in porous media with heat transfer,” *Computers & Fluids*, vol.

- 40, no. 1, pp. 172–178, 2011.
- [126] B. Jalili, S. Sadighi, P. Jalili, and D. D. Ganji, “Characteristics of ferrofluid flow over a stretching sheet with suction and injection,” *Case Studies in Thermal Engineering*, p. 100470, 2019.
- [127] M. Mustafa, A. Mushtaq, T. Hayat, and A. Alsaedi, “Rotating flow of magnetite-water nanofluid over a stretching surface inspired by non-linear thermal radiation,” *PloS one*, vol. 11, no. 2, p. e0149304, 2016.